

### 3. EXPLANATORY NOTES<sup>1</sup>

Shipboard Scientific Party<sup>2</sup>

## INTRODUCTION

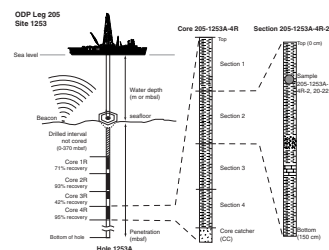
This chapter includes information on shipboard methods that will help the reader understand the basis for our preliminary interpretations and also help the interested investigator select samples for further analysis. Coring techniques and core handling, including the numbering of sites, holes, cores, sections, and samples (Fig. F1), are the same as those reported in previous *Initial Reports* volumes of the *Proceedings of the Ocean Drilling Program* (ODP) and are only briefly summarized.

### Authorship of Site Chapters

The separate sections of the site chapters were written by the following shipboard scientists (authors are listed in alphabetical order; no seniority is implied):

Principal Results: Shipboard Scientific Party  
Background and Objectives: Morris, Villinger  
Operations: Klaus, Pettigrew  
Lithostratigraphy: Cardace, Clift, Strasser  
Igneous and Metamorphic Petrology: Chavagnac, Morris, Schramm  
Structural Geology: Saffer, Vannucchi  
Physical Properties: Pfender, Saffer, Screaton  
Paleomagnetism: Hisamitsu  
Inorganic Geochemistry: Kastner, Solomon  
Organic Geochemistry: Haeckel  
Microbiology: Cardace, Santelli  
Downhole Measurements: Pfender, Saffer, Screaton, Villinger  
Downhole Logging: Pfender, Screaton, Thu

F1. Core, section, and sample numbering, p. 46.



<sup>1</sup>Examples of how to reference the whole or part of this volume.  
<sup>2</sup>Shipboard Scientific Party addresses.

## Reference Depths

Seafloor depths and cored intervals below seafloor (meters below seafloor [mbsf]) are determined by drill pipe measurement.

## Numbering of Sites, Holes, Cores, Sections, and Samples

Drill sites are numbered consecutively from the first site drilled by the *Glomar Challenger* in 1968. A site refers to one or more holes drilled while the ship was positioned over a single acoustic beacon. The first hole drilled at a given site is assigned the site number modified by the suffix "A," the second hole takes the site number and suffix "B," and so forth. These suffixes are assigned regardless of recovery, as long as penetration takes place.

Each cored interval is generally 9.5 m long, which is the length of a core barrel. Coring intervals may be shorter and may not necessarily be adjacent if separated by intervals drilled but not cored. The depth interval assigned to an individual core begins with the depth below the seafloor at which the coring operation began and extends to the depth that the coring operation ended for that core.

A recovered core is typically divided into 1.5-m-long sections that are numbered serially from 1 through 7 (or less if partial recovery) beginning at the top. When the recovered core is shorter than the cored interval, the top of the core is equated with the top of the cored interval by convention in order to achieve consistency in handling analytical data derived from the cores. Also by convention, material recovered from the core catcher is placed in a separate section during the core description, labeled core catcher (CC), and placed below the last (bottom) section recovered in the liner. The core catcher is placed at the top of the cored interval in cases where material is only recovered in the core catcher.

Samples removed from a core section are designated by distance measured in centimeters from the top of the section to the top and bottom of each sample removed from that section. A full identification number for a sample consists of the following information: leg, site, hole, core number, core type, section number, and top to bottom interval in centimeters measured from the top of section. For example, a sample identification of "205-1253A-4R-2, 20–22 cm" represents a sample removed from the interval between 20 and 22 cm below the top of Section 2. Core 4R designates that this core was taken during rotary core barrel coring of Hole 1253A from Leg 205.

All ODP core identifiers indicate core type. The following abbreviations are used:

- H = advanced hydraulic piston corer (APC).
- X = extended core barrel (XCB).
- R = rotary core barrel (RCB).

## Core Handling

As soon as a core is retrieved on deck, the core liner with the core inside is marked into section lengths, each section is labeled, and the core is cut into sections. If a whole-round sample is to be taken, the desired interval is identified and cut out of the core, and then the section is cut. When possible, these samples are taken from the bottom of sections.

During Leg 205, whole-round samples were taken for interstitial water analyses, organic geochemistry, and microbiology as well as for post-cruise permeability and consolidation/strength measurements. For safety monitoring, small (~5 cm<sup>3</sup>) plugs of sediment are taken from the end of one section per core for headspace gas analysis. If pockets of gas are present, a vacutainer gas sample is taken through the core liner.

Each section is then sealed at the top and bottom using acetone to seal color-coded plastic caps to the plastic core liner. A blue end cap marks the top of a section, a clear cap marks the bottom, and a yellow cap marks the end of a section from which a whole-round sample has been removed. The sample code (e.g., IW for interstitial water) is written on the yellow cap. The core sections are then carried into the laboratory, and the length of the core sections (recovery) and any samples taken are logged into the shipboard database.

After the core sections equilibrate to ambient laboratory temperature (~2–4 hr), they are run through the multisensor track (MST). For soft sediments, thermal conductivity measurements are then made (see “**Physical Properties**,” p. 19). Cores are subsequently split lengthwise into working and archive halves. The archive half is used for non-destructive measurements: visual core description, digital core imaging, paleomagnetism, magnetic susceptibility, and color reflectance. Samples are taken from the working half for shipboard physical property measurements (see “**Physical Properties**,” p. 19) before being sampled for additional shipboard and postcruise studies. The archive halves were photographed a whole core at a time, and close-up photographs were taken as requested. Finally, the core sections were put into labeled plastic tubes, sealed, and transferred to cold-storage space aboard the drilling vessel. Following the cruise, the cores were transported to ODP’s Gulf Coast Repository in College Station, Texas. We did not sail a shipboard micropaleontologist during Leg 205. Samples were taken for post-cruise biostratigraphy and will be integrated into the *Scientific Results* volume.

### **Igneous and Metamorphic Rocks**

Igneous rock cores are handled differently from sedimentary cores. To minimize contamination of cores with platinum-group elements and gold, we requested that scientists and technicians remove all jewelry from their hands and wrists before handling the core on the core-receiving platform and wear latex gloves to minimize microbial contamination. Once on deck, samples for microbiological studies are taken immediately to minimize contamination. Then, the core catcher sample is placed at the bottom of the core liner, and total core recovery is calculated by pushing the rock pieces together and measuring the total length to the nearest centimeter. This information is logged into the shipboard CORELOG database program. Then the core is cut into 1.5-m-long sections and transferred to the laboratory.

The contents of each section are transferred into 1.5-m-long sections of split-core liner, where the bottoms of oriented pieces (i.e., pieces that clearly could not have rotated top to bottom about a horizontal axis in the liner) are marked with a red wax pencil. This ensures that orientation is not lost during splitting and labeling. Important primary features of the cores are recorded at this time. The core then is split into archive and working halves. A plastic spacer separates individual pieces and/or reconstructed groups of pieces in the core liner. These spacers may represent a substantial interval of no recovery. Each piece is num-

bered sequentially from the top of each section, beginning with number 1; reconstructed pieces are all assigned the same number but with a consecutive suffix letter (e.g., Piece 1A, 1B, etc.). Pieces are labeled only on the outer cylindrical surfaces of the core. If the piece is oriented, an arrow pointing to the top of the section is added to the label. Because pieces are free to rotate about a vertical axis during drilling, relative azimuthal orientation during Leg 205 was possible only by using paleomagnetic data. Prior to splitting the core, it is run through the MST system.

In splitting the core, every effort is made to ensure that important features are represented in both halves. The archive half is described visually. Most archive sections are run through the cryogenic magnetometer, except for cores with pieces that are too short or disrupted. The archive halves are then photographed with both black-and-white and color film, one core at a time. Nondestructive physical property measurements, such as magnetic susceptibility, are also performed on the archive half of the core. The working half is sampled for shipboard physical property measurements, paleomagnetic studies, inductively coupled plasma–atomic emission spectroscopy (ICP-AES), X-ray diffraction, and thin section studies. Once the macroscopic description and shipboard analyses are fully integrated, the working half of the hard rock core is sampled for shore-based laboratory studies. After samples are taken, both halves of the core are shrink-wrapped in plastic to prevent rock pieces from vibrating out of sequence during transit, placed into labeled plastic tubes, sealed, and transferred to cold-storage space aboard the drilling vessel. As with the other Leg 205 cores, they are housed at ODP’s Gulf Coast Repository at Texas A&M University.

## LITHOSTRATIGRAPHY

The description of sedimentary units recovered during ODP Leg 205 included estimates of sediment composition based on smear slides, thin sections, carbonate measurements, ICP-AES, and X-ray diffraction, documentation of sedimentary and deformational structures, drilling disturbance, presence and type of fossils, bioturbation intensity, induration, diagenetic alteration, and color.

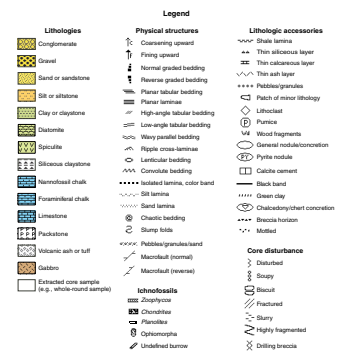
### Barrel Sheet Data

Information from the cores was entered into AppleCORE (version 8.1m) software, which generated a one-page graphical log of each core (“barrel sheet”). A wide variety of features, such as sediment lithology, primary sedimentary structures, bioturbation, soft-sediment deformation, and core disturbance is indicated by patterns and symbols in the graphic logs. A key to the full set of patterns and symbols used on the barrel sheets is shown in Figure F2. The symbols are schematic, but they are placed as close as possible to their proper stratigraphic position, or arrows indicate the interval for which the symbol applies. The columns on the barrel sheets are as follows.

### Lithology

Sediment lithologies are represented by patterns in the “Graphic Lithology” column. This column may consist of up to three vertical strips, depending on the number of the major end-member constitu-

F2. Barrel sheet patterns for lithologies, p. 47.



ents present in the sediment mixture. Sediments with only one major component group (i.e., all other component groups are <10% each) are represented by one strip. Sediment nomenclature follows the scheme shown in Figure F3 in the case of sediment comprising a mixture of carbonate, clastic, and volcanoclastic components. For clastic and volcanoclastic sediments, the sediments are further classified on the basis of grain size and the relative proportion of different grains sizes in the total. A ternary diagram (Fig. F4) shows the naming scheme for sediment composed of a mixture of clay, silt, and sand. Because of the limitations of the AppleCORE software, intervals <20 cm thick cannot be adequately displayed at the scale used for the barrel sheets, but they are described in the "Description" columns of the barrel sheets where appropriate.

**Physical Structures, Accessories, and Ichnofossils**

Depositional structures were noted with regard to large-scale patterns seen in the sediment and the rocks. They may include laminations, massive rip-up clasts, cross-bedding, cross-laminations, and erosional structures. Most clay-rich sediments recovered during ODP Leg 205 were either parallel laminated or heavily bioturbated. Primary structures were often impossible to identify where bioturbation was common.

**Core Disturbance**

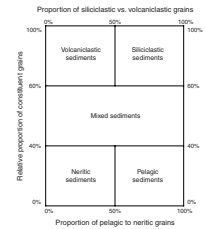
Natural structures (physical or biological) can be difficult to distinguish from disturbances created by the coring process. Deformation and disturbance of sediment that resulted from the coring process are illustrated in the "Drilling Disturbance" column with the symbols shown in Figure F2. Blank regions indicate the absence of drilling disturbance. The degree of drilling disturbance for soft sediments was described using the following categories:

- Slightly disturbed = bedding contacts slightly bent.
- Moderately disturbed = bedding contacts bowed.
- Highly disturbed = bedding hardly discernible, sometimes showing flow structures.
- Soupy = water-saturated intervals that have lost all original structure.

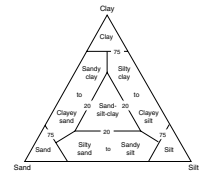
Fragmentation in indurated sediments and rock was described using the following categories:

- Slightly fragmented = core pieces in place with little drilling slurry or brecciation.
- Moderately fragmented = core pieces in place or partly displaced but original orientation preserved or recognizable (drilling slurry may surround fragments).
- Highly fragmented = core pieces are from the interval cored and are probably in correct stratigraphic sequence (although they may not represent the entire section), but the original orientation is completely lost.
- Drilling breccia = core pieces have lost their original orientation and stratigraphic position and may have been mixed with drilling slurry.

**F3.** Classification scheme for sediments, p. 48.



**F4.** Naming clastic and volcanoclastic sediments, p. 49.



## **Sample Types**

The stratigraphic position of samples taken for shipboard analysis and the location of close-up photographs is indicated in the "Samples" column of the barrel sheet according to the following codes:

- SS = smear slide.
- THS = thin section.
- WRP = whole-round physical properties.
- ICP = inductively coupled plasma (ICP) analysis.
- IW = interstitial water.
- WRB = whole-round microbiology.
- Pmag = Paleomagnetic analysis.

## **Fractures (Deformation Structures)**

Any disruptions or faults in evidence during examination of the core were recorded in this section, as were brecciation and textures associated with deformation. Veins and their infillings were noted with as much detail as possible.

## **Description**

The written description for each core, located under the "Description" column on the barrel sheets, contains a brief overview of both major and minor lithologies present, color gradation, grain-size gradation, and fossils. Sediment color was determined using a Minolta CM-2002 spectrophotometer mounted on the archive-half multisensor track (AMST). The spectrophotometer measures reflectance in thirty-one 10-nm-wide bands of the visible spectrum (400–700 nm) on the archive half of each core section. Spectrophotometer readings were taken after covering the surface of each core section with clear plastic film. Calibration for the color scanner did not include a correction for the plastic film because the effect is minor even with very brightly colored lithologies. The area measured is a circle 8 mm in diameter, and the spectrophotometer integrates the sensed color over this area. The AMST was not programmed to avoid taking measurements in intervals with a depressed core surface or in disturbed areas of core with drilling slurry or biscuits. The color data are a part of the ODP Janus database. Additional information about measurement and interpretation of spectral data with the Minolta spectrophotometer can be found in Balsam et al. (1997, 1998) and Balsam and Damuth (2000). To describe the relationship between two units that are in contact with one another within a core section, sharp and gradational (denoted with S or G, respectively) contacts were noted.

The size of grains was assessed based on Wentworth's (1922) classification. Size grading refers to the change in grain size within an individual unit. Normal grading refers to the grains becoming finer upward. Reverse grading refers to the grains becoming coarser upward. The word "Normal" or "Reverse" was included in the description to denote the type of grading observed, if any.

## **Smear Slides**

Grain size and composition of sediments were determined using smear slides. These were prepared according to the procedures described

in the handbook for shipboard sedimentologists (Mazzullo et al., 1988). Identification in terms of general components was undertaken in accordance with Rothwell (1989). For semiquantitative visual estimation of sediment textures and determination of major components, we used the Comparison Chart for Visual Percentage Estimation determined by Terry and Chilingar (1955). In the case of smear slides, however, the percentage had to be corrected to compensate for the degree of dispersion of the grains in the smear slide. Quantitative estimate of grain size and composition are made in the tables located in the site summary. We did not follow the system used by the ODP Leg 170 Scientific Party at Sites 1039 and 1040 in which they distinguished whether components were abundant, common, or present in trace amounts. Because Leg 170 scientists did not specify percentages for their categories, a direct comparison is difficult, although >30% is considered to be abundant, 10%–30% to be common, and <10% to be trace.

Smear slides provide only rough estimates of the relative abundances of detrital constituents. This is the result of some fundamental limits:

1. The mineral identification of fine silt- to clay-sized particles is difficult using only a petrographic microscope.
2. Sand-sized grains tend to be underestimated because it is difficult to incorporate them in the smear slide. Care must also be taken to correct for the area taken on the smear by the mounting medium.

### **Thin Sections of Sediments**

We examined thin sections from the core intervals noted on the barrel sheets to complement and refine the hand-specimen observations. The same terminology was used for thin section descriptions as for the visual core descriptions (VCDs). In sediments, the proportions of lithic, crystal, and vitric components as well as the finer-grained matrix were estimated. The textural terms that we used are defined in MacKenzie et al. (1982). Tables summarizing data from thin sections and smear slides are included (see the “[Core Descriptions](#)” contents list). These tables include information about the locations of samples in the core and an estimate of the abundance of different grain sizes and different grain types where appropriate.

### **Lithologic Units**

We subdivided the core into consecutively numbered lithologic units, under the “Lithologic Unit” column, on the basis of changes in grain size, mineral presence, and abundance. Where appropriate, the stratigraphic units defined by earlier drilling during ODP Leg 170 were employed to assist in correlation.

### **Sediment Classification**

We employed the ODP standard sediment classification scheme of Mazzullo et al. (1988). Sediment names consist of a principal name relating to the dominant composition of the sediment (e.g., claystone, marl, or chert) and one or two modifiers that precede the principal name (e.g., ash-bearing siliceous clay). Principal names may be preceded by a major modifier (e.g., diatomaceous) that relates to a component group that is common or abundant but not dominant. As an ex-

ample, diatomaceous claystone describes a hard sediment that contains >50% siliciclastic clay and >30% diatoms. Minor modifiers were used to specify a common component group (i.e., <30%, but >10% of the sediment). Minor modifiers are used with the suffix “-bearing” and precede the major modifiers. Thus, a soft sediment with dominant radiolarians, abundant calcareous nannofossils, and common volcanic ash would be called a nannofossil-rich radiolarian ooze with volcanic ash. Besides composition, principal names vary according to the grain size and the induration of the sediment. Principal sediment names are as follows:

1. Calcareous sediments: the calcareous end-member of our classification includes sediments made up of all kinds of calcareous fossil shells or tests, resedimented and diagenetic carbonate grains, and cements. Sediments that contain more than ~70% calcareous components, the majority of which were secreted by pelagic organisms (planktonic foraminifers and calcareous nannofossils) are called ooze if they are soft, chalk if they are firm, and limestone if they are hard. These names may be preceded by the dominant calcareous microfossil.
2. Siliceous sediments: the siliceous end-member of our classification includes sediments rich in siliceous microfossils, as well as the diagenetic modifications of these sediments and silica-rich hydrothermal precipitates. Sediments dominated by siliceous microfossils and indeterminate silica that contains <30% carbonate are called radiolarian, diatom, or siliceous ooze if they are soft, porcellanite if they are firm to hard, and chert if they are hard enough not to be scratched by a stainless steel probe. In addition to this field classification, the terms porcellanite and chert bear a strong compositional notion. Thus, porcellanite is typically composed of opal-CT (christobalite-tridymite), but it may also contain diagenetic quartz, carbonate, and silicates (mostly clay minerals). Chert is usually dominated by quartz and tends to be a purer silica but may also contain clay minerals and carbonate. Soft, friable sediments dominated by radiolarians are called radiolarian ooze or radiolarian marl, depending on their carbonate content. The more indurated forms of this sediment are called radiolarite or radiolarian chert depending on the degree of induration.
3. Silicate sediments: sediments dominated by nonbiogenic, mostly detrital, silicate components are further subdivided based on the relative proportion of siliciclastic and volcanoclastic sediments. If the majority of the detrital components are siliciclastic, the sediment is called sand if the average grain size is between 63  $\mu\text{m}$  and 2 mm, silt (2–63  $\mu\text{m}$ ), or clay (<2  $\mu\text{m}$ ). Mixtures of sand, silt, and clay are named according to the classification of Shepard (1954). The suffix “-stone” is added if the sediment is indurated. The principal name for sediments dominated by volcanoclastic components is volcanic silt or volcanic sand if they are redeposited and volcanic ash if they are primary air fall deposits.

### **X-Ray Diffraction**

Routine samples for shipboard X-ray diffraction (XRD) analysis were taken primarily from the squeeze cake residues of interstitial water whole rounds. Additional samples were collected periodically from minor lithologies such as carbonate-cemented claystone and volcanic ash.



Samples were freeze-dried, crushed either by hand with agate mortar and pestle or with a ball mill, and mounted as random bulk powders. The XRD laboratory aboard the *JOIDES Resolution* is equipped with a Philips PW-1825 programmable X-ray generator and a Philips PW-1710/00 diffraction control unit with a PW-1770 automatic sample changer. Machine settings for calibration standards and all samples for all sites were as follows:

Generator tension = 40 kv.  
Generator current = 35 mA.  
Tube anode = Cu.  
Wavelength = 1.54184 Å (CuK<sub>α</sub>).  
Intensity ratio = 0.5.  
Focus = LFF (long fine focus).  
Irradiated length = 12 mm.  
Divergence slit = automatic.  
Receiving slit = 0.2 mm.  
Step size = 0.02°2θ.  
Count time per step = 1 s.  
Scanning rate = 2°2θ/min.  
Ratemeter constant = 0.2 s.  
Spinner = off.  
Monochromometer = on.  
Scanning range = 2°2θ to 70°2θ.

The software used for XRD data reduction is MacDiff (version 4.1.1). This shareware application for Macintosh supports digital data processing and measurement of peak geometry. Peak intensity (counts per step) and peak area (total counts) were recorded after creating a baseline (200 iterations for all °2θ values) and smoothing the counts (17-term filter of standard weighted means).

Normalization factors for shipboard conversion of integrated peak areas to semiquantitative relative abundances of dominant minerals were used previously during ODP Leg 190, when matrix singular value decomposition was used to solve for reliable normalization factors using the method of Fisher and Underwood (1995). Peak areas were recorded for the (101) quartz, (104) calcite, (002) plagioclase, (100) quartz, (101) cristobalite, and composite clay peak at  $d = 4.5 \text{ \AA}$ . Calibration depends upon the analysis of known weight percent mixtures of mineral standards that are fair matches for the natural sediments encountered along the Middle America Trench. All XRD-determined abundances were normalized to 100%. It is imperative that the normalization factors presented in Table T1 be used only to reduce data gathered on the Philips XRD instrument currently in use on the *JOIDES Resolution*, and only when operating parameters match those presented above (Table T1). The inherent problems of analyzing mixtures of highly crystalline minerals (quartz and plagioclase) and randomly oriented phyllosilicates (clay minerals) prevent use of the bulk-powder data in characterizing abundance of individual clay minerals. Although it would be premature at this time to assign relative abundance values to the minerals tracked by shipboard XRD, postcruise biogenic silica assessment will make it possible to evaluate calculated relative abundance of dominant minerals with depth. The normalization factors presented here will be crucial in that next step.

Error associated with calculating relative mineral abundance is expressed in Table T2 for each standard. The difference between the

---

T1. Normalization factors for bulk-powder samples, p. 67.

---

---

T2. Abundances of minerals, p. 68.

---

known weight percentage of a given mineral and the calculated, normalized weight percentage of that mineral is provided. The maximum difference encountered (for plagioclase) was 6.07 wt%. Relative percent error, calculated as [(normalized weight percentage – measured weight percentage)/measured weight percentage]×100 average <3%, although errors are significantly higher than the average where mineral abundances are low.

Beyond routine semiquantitative assessment of relative mineral abundance, we also used XRD to characterize representative samples of volcanic ash. Because of the variability of crystal content, amorphous glass content, and alteration products in such samples, we simply recorded the intensity and area of representative peaks generated by common minerals (e.g., clays, zeolites, quartz, plagioclase, cristobalite, calcite, amphibole, pyroxene, pyrite, and halite). A final parameter to measure is the ratio of peak areas for (100) quartz ( $d = 4.257 \text{ \AA}$ ) to (101) cristobalite ( $d = 4.0397 \text{ \AA}$ ). The accuracy of this ratio suffers from interference between the highest-intensity cristobalite peak and a secondary plagioclase peak at  $\sim 22^\circ 2\theta$ .

Whereas samples for bulk XRD were taken at intervals at every site, clay fraction XRD analyses were carried out only when the clay fraction was of specific geological interest. Approximately 5 cm<sup>3</sup> of freeze-dried sediment was set into a 600-mL glass beaker and broken into small (gravel-sized) pieces if the sample was considerably indurated. Enough 3% H<sub>2</sub>O<sub>2</sub> was poured over the sample to cover it completely in order to remove organic material, and the beaker was covered with a watch glass until the reaction was complete,  $\sim 24$  hr in most cases. At this stage for carbonate samples, 10% acetic acid was added to remove the carbonate and the mixture was well stirred and left for 12 hr then spun down completely using the 21K Marathon centrifuge. Acetic acid was decanted, and the sample was twice washed with deionized water (DI). All washes were accomplished by spinning the centrifuge tubes until all solids had settled to the bottom of the centrifuge tube. Approximately 175 mL of dispersant (Calgon: 4 g/1000 mL DI) was added to the sample, and the mixture was well stirred and left overnight. Throughout these solution baths, occasional stirring maintained the sample suspension and an ultrasonic bath was used to help disaggregate stubborn samples. Following disaggregation, we washed samples in 50-mL centrifuge tubes three times to generate a washed bulk sample.

The sonic dismembrator disaggregated the sample thoroughly in preparation for making the clay split; the dismembrator was not used for >3 min duration to avoid clay grain damage. In centrifuge tubes, the washed bulk sample was run at 1000 rotations per minute for 3.2 min to settle the >2- $\mu\text{m}$  fraction. A 10-mL aliquot of the suspension was drawn into a large syringe and emptied slowly into the funnel of a Millipore suction filtration apparatus using 0.45- $\mu\text{m}$  Millipore filters (4.5 cm in diameter). After the water passed through and before the clay caught on the filter dried, the filter was removed from the apparatus and laid carefully on a slide, transferring the clay layer to the slide surface. Each slide was analyzed unaltered and again after 24 hr in a room-temperature glycol chamber. The XRD instrument operating parameters were the same as for bulk XRD except step size was  $0.010^\circ 2\theta$ , and the scan was from  $2^\circ 2\theta$  to  $35^\circ 2\theta$ .



## Visual Core Descriptions

VCD forms (Fig. F6) were used to document each section of the igneous rock cores. From left to right on the VCD form the following are displayed: (1) a photograph of the archive half of the core, (2) a scale from 0 to 150 cm, (3) the piece numbers, (4) a graphical representation of the pieces and their relationships to each other, (5) the orientation of pieces, (6) the location of shipboard analyses, (7) the lithologic units and any boundaries between, (8) the observed deformation structures (see “**Structural Geology**,” p. 17), (9) the percentage of phenocrysts, (10) the grain size, (11) the proportion of vesicles, (12) the degree of alteration, and (13) the presence of mineralization. To the right are more detailed descriptions of selected hand samples.

In the graphic representation, a horizontal line across the entire width of this column denotes a plastic spacer. Vertically oriented pieces are indicated on the form by an upward-pointing arrow to the right of the appropriate piece.

The location of samples selected for shipboard studies is indicated in the column headed “Shipboard studies,” using the following notation:

- XRD = X-ray diffraction analysis.
- ICP = inductively coupled plasma–atomic emission spectroscopy.
- TSB = petrographic thin section.
- PP = physical property analysis.
- MBIO = microbiology analysis.
- Pmag = paleomagnetic analysis.

The VCD forms also display the number of the lithologic unit and the location of the unit boundaries. Units were defined based on major changes in lithology, texture, structure, and mineralogy. After we made lithologic descriptions, we attempted to integrate the observations to define unit boundaries. The boundaries often reflect major physical changes in the core (e.g., pillowed vs. massive or cumulate vs. massive) that were also observed in the physical property and downhole measurements.

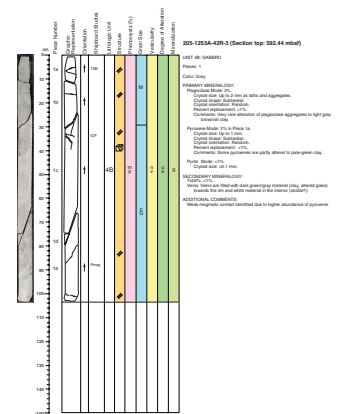
The VCD entry for structure refers to whether the unit is cumulate, massive, pillowed, hyaloclastic, banded, brecciated, scoriaceous, or tuffaceous but also refers to all structural features such as normal fault, reverse fault, veins, fractures, and voids. Symbols used to describe deformation features are defined in “**Structural Geology**,” p. 17. For veins and fractures, we described their abundance, width, orientation, and mineral linings and fillings. Where possible, the minerals filling the veins were identified in the “voids” portion of the VCD.

In the phenocryst column, we present the types of minerals visible with a hand lens or binocular microscope, their distribution within the unit, and, for each phase, their abundance (volume percent) and size range (millimeters) with further comments as appropriate. The classification is described as follows:

- a = aphyric (<1% phenocrysts).
- sp = sparsely phyric (1%–2% phenocrysts).
- mp = moderately phyric (2%–10% phenocrysts).
- hp = highly phyric (>10% phenocrysts).

This is intended to more accurately define the name of the rock by the types of phenocrysts present (e.g., sparsely plagioclase-olivine phyric, in

F6. Example of igneous rock VCD, p. 51.



which the amount of plagioclase exceeds the amount of olivine or, in the case of gabbro, pyroxene-plagioclase phyrlic, where the percentage of pyroxene is higher than that of plagioclase).

Groundmass grain size was identified as medium grained (MG) if the average grain size was 1 mm or greater, fine grained (FG) if the grains could be identified and were <1 mm, microcrystalline (M) if the groundmass crystals could be seen but were too fine to identify, cryptocrystalline (C) if crystals could not be distinguished, hypocrySTALLINE (HY) if glass was present with crystals and crystal abundance exceeded glass abundance, and hypohyaline (HH) if glass abundance exceeded crystals. The same terminology was used to describe the groundmass of gabbro. Mineral morphology was indicated as anhedral (an), subhedral (su), or euhedral (eu).

Vesicularity was described as vesicle abundance (visual estimates of the volume fraction of vesicles were supplemented by observations using a binocular microscope), size, shape (sphericity and angularity), and also whether the vesicles are empty or filled and the nature of the filling. We use the following classification:

- nv = nonvesicular (vesicle content <1%).
- spv = sparsely vesicular (vesicle content 1%–5%).
- mov = moderately vesicular (vesicle content 5%–20%).
- hiv = highly vesicular (vesicle content >20%).
- GI = unaltered glass.
- AGI = altered glass.

We graded the degree of alteration as

- ua = unaltered (<2% of alteration products by volume).
- s = slight (2%–10%).
- m = moderate (10%–40%).
- h = high (40%–80%).
- vh = very high (80%–95%).
- c = complete (95%–100%).

Changes of alteration through a section or a unit were also noted. Where possible, we identified the secondary minerals such as carbonate, clay, zeolite, or iron oxide.

Finally, we also documented the presence of mineralization and described its abundance, size, orientations, shape, and mineral linings.

Each section of core was examined separately by two describers for igneous and metamorphic characteristics. The boundaries of the lithologic units were drawn on the VCD form, and for Hole 1253A the units were numbered continuously from the end of Leg 170, starting with Unit 4 (gabbro). Units were divided into subunits (A, B, etc.) on structural and mineralogical grounds; subunits were further subdivided on the basis of detailed observations discussed in “**Petrology,**” p. 26, in the “**Site 1253**” chapter. The VCDs also contain a text description of each section of core that includes the (1) leg, site, hole, core number, core type, section number; (2) depth of the top of the section in meters below seafloor; (3) unit number (consecutive downhole), number of pieces in the unit in the section, and rock name; and (4) groundmass, grain size, Munsell color, vesicle abundance and size, structure, nature of the alteration, information about abundance and filling of fractures, and additional comments. The legend for the VCDs is shown in Figure F7.

**F7. Igneous texture/structure definitions and abbreviations, p. 52.**

Igneous texture/structure definitions and abbreviations	
Structure	a s m h Anhedral (1-2%) Sparsely phyrlic (1%-5%) Moderately phyrlic (5%-10%) Highly phyrlic (1-15%)
Phenocryst	G a p F M C Glass Anhedral (1-2 mm) Fine grained (1-2 mm) Medium grained (2-5 mm) Microcrystalline groundmass Crystalline groundmass
Grain size	n s m h Nonvesicular (1-1%) Sparsely vesicular (1%-5%) Moderately vesicular (5%-20%) Highly vesicular (20%)
Vesicularity	u s m h vh c Unaltered (<2%) Slight (2%-10%) Moderate (10%-40%) High (40%-80%) Very high (80%-95%) Complete (95%-100%)
Degree of alteration	u s m h vh c Unaltered (<2%) Slight (2%-10%) Moderate (10%-40%) High (40%-80%) Very high (80%-95%) Complete (95%-100%)
Mineralization	P Pyrite in the groundmass

## Thin Sections

Thin sections of igneous rocks were studied in transmitted light to complete and refine the hand-specimen observations and are summarized in the format shown in Figure F8. Observations included textural features that were not identified in hand specimen; precise determination of grain size of phenocrysts and groundmass; the mineralogy, abundance, and kind of aggregates (glomerocrysts); the presence of inclusions within phenocrysts; and the presence of spinel, oxides, and sulfides. Crystal sizes of all primary phases were measured. In addition, mineral morphologies, grain sizes, and textural features were described. The terms heterogranular (different crystal sizes), seriate (continuous range in grain size), porphyritic (indicating presence of phenocrysts), aggregate (containing clusters of crystals), hypocrystalline (100% crystals) to hypohyaline (100% glass), and intergranular (olivine and/or pyroxene grains between plagioclase laths) were used to describe the textures of the groundmass. The same terminology was used for thin section descriptions and the megascopic descriptions.

In addition to macroscopic description of alteration, alteration as observed in thin sections is presented in the thin section log (Figure F8), where we present the amount of secondary minerals, their size if measurable, and any further information on their occurrence (e.g., Fe oxides replacing glass). We also provided a description of voids in term of abundance, location, size, morphology, and filling.

All information gathered on the primary minerals and their alteration products are summarized within the comment section to highlight all specific features. Digital photomicrographs are used to illustrate representative characteristics. We provide a photomicrograph of the entire thin section and then close-up pictures of specific features. Each digital photomicrograph is numbered according to the thin section number and the close-up number (e.g., picture of thin section 1 with three close-up photographs are numbered 1-A, 1-B, and 1-C). The location of the close-up pictures is shown in the photomicrograph of the entire thin section.

## Inductively Coupled Plasma–Atomic Emission Spectroscopy Analyses

Chemical analyses of basalt and gabbro were determined during Leg 205 using ICP-AES. We selected representative samples of gabbro from Hole 1253A for shipboard ICP-AES analysis. Large whole-rock pieces were first cut with a diamond-impregnated saw blade and ground on a diamond wheel to remove surface contamination. Samples were washed in an ultrasonic bath containing methanol for ~10 min, followed by three consecutive ~10-min washes in an ultrasonic bath containing nanopure deionized water, and then dried for ~12 hr in an oven at 110°C. The cleaned whole-rock samples (~20 cm<sup>3</sup>) were reduced to fragments <1 cm in diameter by crushing between two disks of Delrin plastic in a hydraulic press and ground for ~5 min in a Spex 8510 shatterbox with a tungsten carbide barrel. The sample powders were weighed on a Scientech balance and ignited to determine weight loss on ignition.

We weighed 100 ± 2-mg aliquots of the ignited whole-rock powders and mixed them with 400 ± 0.4 mg of lithium metaborate (LiBO<sub>2</sub>) flux that had been preweighed on shore. Standard rock powders and full procedural blanks were included with the unknowns for each sample

F8. Thin section description form, p. 53.

run. All samples and standards were weighed on the Cahn Electro balance. Weighing errors are conservatively estimated to be  $\pm 0.01$  mg.

Mixtures of flux and rock powders were fused in Pt-Au crucibles at 1050°C for 10–12 min in a Bead Sampler NT-2100. A total of 10  $\mu$ L of 0.172-mM aqueous lithium bromide (LiBr) solution was added to the mixture, before fusion, as an antiwetting agent to prevent the cooled bead from sticking to the crucible. Cooled beads were transferred to 125-mL polypropylene bottles and dissolved in 50 mL of 2.3-M HNO<sub>3</sub> by shaking with a Burrell wrist-action bottle shaker for an hour. After digestion of the glass bead, all of the solution was filtered to 0.45  $\mu$ m into a clean 60-mL widemouthed polypropylene bottle. Next, 2.5 mL of this solution was transferred to a plastic vial and diluted with 17.5 mL of 2.3-M HNO<sub>3</sub> to bring the total volume to 20 mL. The solution-to-sample dilution factor for this procedure is ~4000. Dilutions were conducted using a Brinkmann Instruments dispensette (0–25 mL).

Major and minor (Si, Ti, Al, Fe, Mn, Mg, Ca, Na, K, and P) and trace (Zr, Y, Sr, Ba, Ni, Cr, Sc, and V) element concentrations of powder samples were determined with the JY2000 Ultracore ICP-AES. The JY2000 sequentially measures characteristic emission intensities (with wavelengths between ~100 and 800 nm). Murray et al. (2000) developed protocols for dissolution and ICP-AES analysis of rock powders (see also Shipboard Scientific Party, 2001). The JY2000 plasma was ignited 30 min before each run to allow the instrument to warm up and stabilize. After the warm-up period, a zero-order search was performed to check the mechanical zero of the diffraction grating. After the zero-order search, the mechanical step positions of emission lines were tuned by automatically searching with a 0.002-nm window across each emission peak using a U.S. Geological Survey (USGS) Basalt Hawaiian Volcano Observatory standard (BHVO-2) or Basalt Columbia River (BCR-2) prepared in 2.3-M HNO<sub>3</sub>, analogous to sample preparation for unknowns. The only exception is P, which was automatically searched by using a single-element standard. During the initial setup, an emission profile was collected for each peak, using BHVO-2, to determine peak-to-background intensities and to set the locations of background points for each element. The JY2000 software uses these background locations to calculate the net intensity for each emission line. The photomultiplier voltage was optimized by automatically adjusting the gain for each element using the standard (BHVO-2 or BCR-2) (see Gladney et al., 1990; Gladney and Roetlands, 1988) with the highest concentration for that element. Before each run, a profile of BHVO-2 was collected to assess the performance of the instrument from day to day.

All ICP-AES data presented in the site reports were acquired using the Gaussian analytical mode of the Windows 5 JY2000 software. This mode fits a Gaussian curve to a variable number of points across a peak and then integrates to determine the area under the curve. Each sample and standard was run as an unknown at least twice, nonsequentially, in all sample runs, and labeled as A and B.

A typical ICP-AES run included (1) a set of five certified rock standards of which four are basaltic (BHVO-2, BIR-1 [USGS Icelandic (Reykjanes) basalt], BCR-2 [USGS], and JB-2 [Geological Survey of Japan (GSJ)]) and one is gabbroic (Jgb-1 [GSJ]), run at the beginning, middle, and end of the sample run; (2) up to eleven unknown samples; (3) a drift-correcting sample (BHVO-2 or BCR-2 standard) analyzed every fifth sample position and at the beginning and end of each run; and (4) a blank solution run near the beginning, middle, and end of each run.

A 2.3-M HNO<sub>3</sub> wash solution was run for a minimum of 90 s between each of the samples and standards.

Following each sample run, the raw intensities were transferred to an Excel data file, and data reduction was completed using Kaleidagraph software. The enhanced plotting functions in Kaleidagraph allowed quick assessment of drift, the repeatability of standards and the blank, and identification of occasional discordant measurements. This ensured proper control over standardization and drift correction. Once transferred, a drift correction was then applied to each element and to the blank by linear interpolation between drift-monitoring solutions run before and after a particular batch of samples, assuming that the time between measurements during autosampling was constant. The drift correction was applied to the blank after noticing for some elements a substantial systematic drift for the blank itself, consistent with the trend of the BHVO-2 or BCR-2 drift monitor. The average of the three drift-corrected procedural blank measurements was then deducted from the drift-corrected intensities of all samples. Following drift correction and blank subtraction, concentrations for each sample were calculated from linear regressions using the average intensity per unit concentration for the five standards measured, each one being measured twice during the run. The blank was also included in the regression with both its intensity and concentration set at zero. This calibration is based on several standards rather than normalization to a single standard, such as BHVO-2 only. The regression technique gave excellent correlation coefficients (>0.99) for most oxides and trace elements (except Ni and P at ~0.8, and Si and Al at 0.95). It also revealed either important discrepancies between standards or problems with sample preparation in the cases of Cu and Zn, which accordingly are not reported in the site chapters. In addition, concentration variations of Si, Al, and Ca are also observed from time to time between duplicate analyses of some samples and standards. The cause of these variations remains unclear.

Estimates of accuracy and precision for major and trace element analyses were based on fits to the regressions for BHVO-2, BIR-1, JB-2, BCR-2, and JGb-1, the results of which are presented in Table T3. To assess the reproducibility, all standards were run as an unknown and the measured values were compared to the certified values. In general, run-to-run relative precision by ICP-AES was better than 3% for the major elements. Run-to-run relative precision for trace elements was generally <5%. Exceptions typically occurred when the element in question was near the detection limit of the instrument.

### **X-Ray Diffraction**

Identifications of secondary minerals, such as vein and void fillings, were determined by XRD using a Philips PW1729 X-ray diffractometer. Samples were taken from altered bulk rock and small spots in veins or cavity fillings to identify materials with distinctive visual characteristics. The samples were freeze-dried overnight and crushed to fine grain size using a mortar and pestle, and the powders were mixed in water slurries on glass slides. Detailed setups for XRD are described in “**X-Ray Diffraction**,” p. 8, in “Lithostratigraphy.”

---

T3. Major and trace element concentrations, p. 69.

---



## STRUCTURAL GEOLOGY

Study of the sedimentary cover and oceanic basement of the subducting Pacific plate and the décollement zone in the overriding Middle American plate during Leg 205 focused on the interaction between deformation and fluid processes at convergent margins. Differences in recovery of hard rock at Site 1253 and sediment at Site 1254 required integration of two different approaches for the description of deformation features. Procedures for documenting the structural geology of Leg 205 cores closely followed those used during previous drilling of the Costa Rica convergent margin during Leg 170 (Kimura, Silver, Blum, et al., 1997), which in turn is based on the approach first developed at the Nankai Trough during Leg 131 (Taira, Hill, Firth, et al., 1991). Techniques for hard rock description were those used during Leg 185 (Plank, Ludden, Escutia, et al., 2000) and Leg 187 (Christie, Pedersen, Miller, et al., 2001).

Each structural feature observed in cores was annotated on the Visual Structural Description forms, using the structural geology symbols shown in Figure F9 (e.g., Lundberg and Moore, 1986). Structural features were then manually sketched on a separate structural geology description sheet (Fig. F10). A Structural Description Sheet (SDS) was used to document more detailed description of the structural information, such as the apparent and true orientations of veins and fractures and crosscutting relationships (Fig. F11).

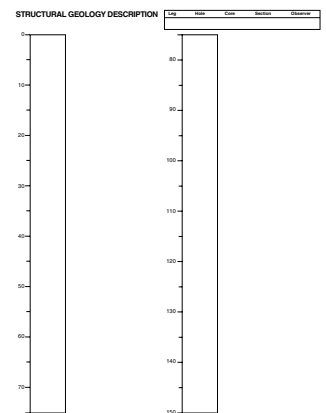
For structures observed in hard rock cores or in broken sections of sediment cores, the piece number was recorded on the SDS. Recording the piece number, even in sediments, preserves the information needed during paleomagnetic reorientation. Features such as horizontal bedding planes are located by using two identical interval depth values, whereas inclined structures, such as fault zones, are located by an interval top and bottom. The thickness of a dipping structure differs from the length of the interval over which it occurs and is therefore documented in a separate column titled "Thickness."

The orientations of structural features were measured using the protractor-goniometer method pictured in Figure F12 and explained in detail in the "Explanatory Notes" chapter of the Leg 131 *Initial Reports* volume (Taira, Hill, Firth, et al., 1991). For linear features, such as those seen on broken surfaces within the core, a direct measurement of plunge and trend was usually possible, although it was often more convenient in practice to measure the orientation of a toothpick inserted into the core and aligned with the linear structure in order to avoid additional cutting of the spilt core to measure in the third dimension. In most instances, determining the orientation of planar structures required the measurement of two apparent dips: the intersection of the structure with the core face and a second intersection, commonly that seen in a surface cut perpendicular to the core face. Again, it was helpful in practice to measure the orientation of a toothpick inserted in line with this second intersection. The true spatial orientation was then derived, using a stereographic projection program (STEREONET version 4.25 by R.W. Allmendinger), by finding the great circle that fit the two apparent dips. The two apparent measurements were recorded in columns 7–10 of the SDS (Fig. F11). Fault planes with striations were recorded with the trend and plunge of the lineation and the sense of movement ("+" = reverse; "-" = normal) and a confidence level that in-

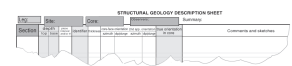
F9. Visual description sheet symbols, p. 54.



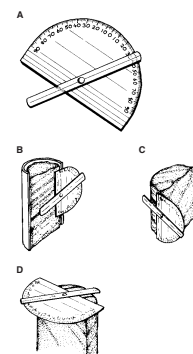
F10. Structural geology visual description sheet, p. 55.



F11. Layout of the structural description sheet, p. 56.



F12. Protractor-goniometer, p. 57.



dicates the quality of this determination (high confidence; very probable; possible, but not certain; or no indication).

The explicit reference to orientation within the core is necessary because the actual geographic orientation of most cores is not known, having been broken into pieces and differentially rotated during RCB drilling. The length of the core was taken to represent the vertical; therefore, the direction at right angles to the core axis was the horizontal, relative to which dip angles and plunges were measured (Fig. F13). All structural data are reported using the double line at the back of the working half of the core as a reference azimuth at 000°; the back of the archive half, therefore, represents the 180° azimuth.

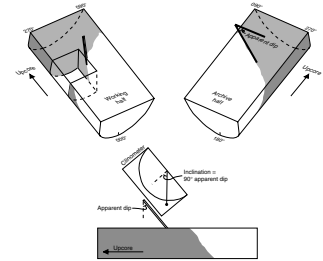
Data and some commentary were extracted from the SDS and entered into a structural spreadsheet, as necessary for statistical manipulation, and to produce graphical representations of the structural geology presented in the site reports. We placed particular importance on attempting to restore the orientations of structures in the cores to their unrotated positions before drilling, using paleomagnetic data.

Reorientation to true north in the geographic reference frame was remarkably successful during Nankai Leg 190, when most of the reorientations in RCB cores were carried out using paleomagnetic records (Moore, Taira, Klaus, et al., 2001). Because RCB drilling rotates individual core segments differentially relative to one another, magnetic declination of natural remanent magnetism (NRM) were used to reorient the individual pieces of core back to their in situ orientation (Taira, Hill, Firth, et al., 1991, p. 44, table 6). However, rather than passing individual pieces of core through the cryogenic magnetometer specifically for this purpose, we used the paleomagnetic declination and inclination data (after removing the drilling-induced overprint) that are now readily accessible in the ODP Janus database (see “Paleomagnetism,” p. 21).

We initially recorded the interval of an intact segment of rotated core (or several adjacent and clearly similarly oriented pieces) in which a structure of interest occurred as a “piece interval” on the SDS. Two or more NRM declination measurements per piece (taken from the ODP Janus paleomagnetic database) are needed to give reliable results. Because the routine measurements were made at 5-cm intervals, viable segments must be at least ~7 cm in length. Moreover, only those pieces where the paleomagnetic declinations were reasonably consistent, normally <10° difference between two measurements, were considered as suitable. A check on the integrity of this procedure was performed during Leg 190 on several APC cores by making both Tensor tool and NRM corrections on the same structural data (Moore, Taira, Klaus, et al., 2001); the results were found to be very consistent, generally to within 10° and in most cases to <2°. The relevant declination value was entered into our structural spreadsheet. A simple algorithm based on the steps given in Taira, Hill, Firth, et al. (1991, p. 44, table 6) was used to determine the true geographic orientation of each structure.

As during all legs, a persistent problem in describing structural features in the cores was the distinction between natural structures and those induced or modified by the drilling process. Core disturbance is not reported here unless it reflected original structure or sediment rheology. Also following the practice of previous legs, steeply inclined fractures, especially those lacking strongly and regularly developed slickensides, were generally considered to be drilling induced.

F13. Core reference system, p. 58.



## PHYSICAL PROPERTIES

Physical properties were measured on unsplit cores and on the undisturbed parts of split cores. The MST was used for nondestructive measurements of wet bulk density, electrical resistivity, magnetic susceptibility, and natural gamma radiation in unsplit cores. Thermal conductivity measurements were also conducted on unsplit and split sediment cores and split rock cores. Compressional wave velocities were measured on both soft and lithified sediment and rock cores. Portions of split cores that were undisturbed by drilling and sampling, gas expansion, bioturbation, cracking, and large voids were used to obtain specimens for moisture and density measurements and calculations (wet bulk density, grain density, dry bulk density, water content, void ratio, and porosity).

Physical property measurements were conducted after the cores had at least 2–4 hr to equilibrate to near-ambient room temperature (i.e., 21°–24°C), except where noted. Many of the measurements can vary with core temperature and should be obtained in a stable temperature environment for best results. A summary of each of the physical property measurement procedures for Leg 205 is outlined below and described in more detail by Blum (1997).

### Multisensor Track Measurements

Cores were first run through the MST, which combines five sensors on an automated track to measure magnetic susceptibility, bulk density, electrical resistivity, and natural gamma ray emission on whole-core sections. The respective sensors are the magnetic susceptibility meter, the gamma ray attenuation (GRA) densiometer, the noncontact electrical resistivity (NCR) sensor, and the natural gamma ray (NGR) detector. MST measurement of *P*-wave velocities was not conducted because measured MST *P*-wave velocities on XCB and RCB cores are usually of poor quality as a result of the small core diameter and loss of coupling between the liner and the core. MST data were sampled at discrete intervals, with the sampling rate chosen to optimize the resolution and quality of the data.

### Magnetic Susceptibility

Magnetic susceptibility was measured with a Bartington meter MS2 using an 80-mm internal diameter sensor loop (88-mm coil diameter) operating at a frequency of 565 Hz and an alternating field of 80 A/m (0.1 mT). The sensitivity range was set to the low sensitivity setting (1.0 Hz). The sample period and interval were set to 2 s and 4 cm, respectively. The raw mean value of the measurements was calculated and stored automatically. The quality of these results degrades in XCB and RCB sections, where the core may be undersized and/or disturbed. Nevertheless, the general downhole trends can be useful for stratigraphic correlations, and peaks may help to identify discrete ash layers. The MS2 meter measures relative susceptibilities, which have not been corrected for the differences between core and coil diameters.

### Gamma Ray Attenuation Bulk Density

Bulk density was measured for unsplit core sections as they passed through the GRA densiometer, using a sampling period of 2 s every 4

cm on the MST. The gamma ray source was  $^{137}\text{Cs}$ . For each site, the GRA bulk densities and the bulk densities measured on discrete samples were compared.

### **Noncontact Resistivity**

The relatively new Geotek NCR system was installed for trial purposes during Leg 204 (Shipboard Scientific Party, 2003). The NCR technique operates by inducing a high-frequency magnetic field in the core from a transmitter coil, which in turn induces electrical currents in the core that are inversely proportional to the resistivity. A receiver coil measures very small magnetic fields that are regenerated by the electrical current. To measure these very small magnetic fields accurately, a difference technique has been developed that compares the readings generated from the measuring coils to the readings from an identical set of coils operating in air. This technique provides the requisite accuracy and stability. Resistivities between 0.1 and 10  $\Omega\text{m}$  can be measured at spatial resolutions along the core of ~2–4 cm. In cores from Leg 205, measurements were taken every 4 cm.

Calibration was achieved by filling short lengths of core liner (~25 cm each) with water of known concentrations of NaCl (Shipboard Scientific Party, 2003). This provides a series of calibration samples with known resistivities that are then placed on the MST and logged. Averaged measurements for the samples were then plotted against the known resistivity to define a power law calibration equation.

### **Natural Gamma Ray Emissions**

NGR emissions are a function of the random and discrete decay of radioactive atoms and are measured through scintillation detectors as outlined by Hoppie et al. (1994). During Leg 205, NGR emissions were measured for 20 s per each 10 cm length of core, except where noted. NGR calibration was performed at the beginning of the leg, and sample standards were measured at the end of every site.

### **Thermal Conductivity**

Thermal conductivity was measured using the TK04 system described by Blum (1997). This system employs a single-needle probe (Von Herzen and Maxwell, 1959) heated continuously in full-space configuration for soft sediments and in half-space configuration for lithified sediments and igneous rock cores. Under conditions of moderate to full recovery, thermal conductivity measurements were conducted at a frequency of at least two per core.

Thermal conductivity was measured for full-core unconsolidated sediment sections using a full-space single-probe TeKa (Berlin) TK04 unit. A hole was drilled in the outer core liner, and the 2-mm temperature probe was inserted into the working half of the core section. For igneous rock samples, a smooth surface was prepared on a ~5-cm split-core specimen that had been placed in a water bath for a minimum of 15 min. The half-space needle probe was secured onto the flat surface of the half core. At the beginning of each half-space and full-space measurement, temperatures in the samples were monitored automatically, without applying a heater current, until the background thermal drift was determined to be  $<0.04^\circ\text{C}/\text{min}$ . The heating was then started, and the temperature increase in the probe was recorded.

The reported thermal conductivity measurement for each sample was the average of three repeated measurements for the full-space method and four measurements for the half-space method. Data are reported in watts per meter Kelvin with a stated error of ~5%. Assessment of thermal stability is automatic with the TK04 meter, which does not require shipboard calibration.

### **Moisture and Density Measurements**

Moisture and density (MAD) measurements were determined by measuring wet mass, dry mass, and dry volume of specimens from the split cores. Samples for MAD measurements were collected at a frequency of two per complete section in sediment and one per section in igneous rock. Where whole-round samples were taken from a section, one of the two MAD samples was taken adjacent to it. Care was taken to sample undisturbed parts of the core and to avoid drilling slurry.

Immediately after the samples were collected, wet sediment mass ( $M_{\text{wet}}$ ) was measured. Dry sediment mass ( $M_{\text{dry}}$ ) and dry sediment volume ( $V_{\text{dry}}$ ) were determined after the samples had dried in a convection oven for 24 hr at a temperature of  $105 \pm 5^\circ\text{C}$ . Wet and dry masses were determined using electronic balances that compensate for the ship's motion, and dry volume was measured using a gas pycnometer.

Moisture content, grain density, bulk density, and porosity were calculated from the measured wet mass, dry mass, and dry volume as described by Blum (1997). Corrections were made for the mass and volume of evaporated seawater using a seawater density of  $1.024 \text{ g/cm}^3$  and a salt density of  $2.20 \text{ g/cm}^3$ .

### **P-Wave Velocities on Split Cores**

The method for measurement of compressional wave velocity ( $V_p$ ) was dependent on the degree of sediment consolidation. The velocity meter was calibrated by measuring  $V_p$  in water.

For the hard rock and semilithified or lithified sediments sampled during Leg 205, only the PWS3 contact probe system, described by Boyce (1976), could be employed. The PWS3 system calculates velocity using measured traveltime and sample thickness measured with a digital micrometer. If core recovery permitted, one set of velocity measurements was conducted per section, with additional measurements taken in sections characterized by varying lithology.

## **PALEOMAGNETISM**

Paleomagnetic investigations during Leg 205 had two major purposes: to investigate diagenetic dissolution of magnetic minerals in sediment and igneous rocks and to investigate microfabrics related to deformation processes in the subduction zone. These investigations need a large number of discrete samples; therefore, one or two minicore samples were taken from each section of a core. On the ship, NRM of all minicore samples, thermal demagnetization, and isothermal remanent magnetization (IRM) tests for some pilot samples were carried out as an initial approach to magnetic studies during Leg 205. These rock magnetic data will be combined with postcruise studies of anisotropy of magnetic susceptibility (AMS). In addition, postdepositional remanent magnetization of the archive half of the core was routinely measured to

identify age boundaries of magnetic chrons recorded in the sediments and constrained to previous paleomagnetic polarities reported from ODP Leg 170 (Kimura, Silver, Blum, et al., 1997). The results of these measurements were used for core orientation correction and magnetostratigraphy.

### Laboratory Facilities

Two magnetometers are installed in the paleomagnetic laboratory on the *JOIDES Resolution* for measurements of halved long cores and for discrete samples. A 2G Enterprises pass-through cryogenic direct-current superconducting quantum interference device rock magnetometer (model 760-R) measures the magnetic intensity of samples and can routinely demagnetize the samples up to 80 mT with a 200-Hz frequency in-line alternating-field (AF) demagnetizer (model 2G600). The cryogenic magnetometer and the AF demagnetizer are interfaced to a PC-compatible computer and are controlled by a 2G Long Core software program by Core Logic. The sensing coils in the cryogenic magnetometer can also measure seven discrete samples at 10-cm intervals. Background noise at the sensor of the cryogenic magnetometer shows  $2.20 \times 10^{-10}$  Am<sup>2</sup> averaged over 10 min. Magnetic fields were also measured at the sensing point of the magnetometer by a fluxgate magnetometer (model APS 520), and fields of  $2.24 \times 10^{-5}$  mT,  $3.94 \times 10^{-5}$  mT, and  $1.31 \times 10^{-4}$  mT were observed on the +x-, +y-, and +z-axes, respectively. For the paleomagnetic measurement and rock magnetic tests of discrete samples, a Molspin spinner magnetometer is also available on the ship. Additional instruments used for demagnetization of samples include a DTECH AF demagnetizer (model D-2000) capable of demagnetization up to 200 mT and a Schonstedt thermal demagnetizer (model TSD-1) capable of demagnetization up to 800°C. For a test of partial anhysteretic remanent magnetization (pARM), the D-2000 is equipped with a pARM-2 system, consisting of two parallel coils mounted outside and on-axis with the AF coil of the GSD-1 demagnetizer.

Magnetic susceptibility was initially measured for all whole-core sections with the MST system (see “**Physical Properties**,” p. 19). The susceptibility loop sensor on the MST system operates at a frequency of 565 Hz and AF intensity of 80 A/m (= 0.1 mT). The resolution of the loop is  $2 \times 10^{-6}$  SI on the 0.1 range. The susceptibilities should be multiplied by a correction factor to account for the volume of material that passed through the coils. The standard correction factor for ODP core is ~0.66. The magnetic susceptibility of the archive-half core was also measured using a point susceptibility sensor on the AMST (see “**Barrel Sheet Data**,” p. 4, in “Lithostratigraphy”). The AMST and MST units have the same type of susceptibility meter (Bartington Instruments model MS2C), but the sensor range is different. The susceptibility loop sensor for the MST system is 80 mm in diameter and has a ~5-cm-wide sensor range designed for passing through a whole-round core. The point susceptibility meter on the AMST is designed for sensitive measurement of magnetic susceptibility of archive-half cores and has a sensor range of ~1 cm. The point sensor operates at a frequency of 2 kHz and has the same resolution ( $2 \times 10^{-6}$  SI on 0.1 range). A Geofyzika Brno Kappabridge KLY-2 magnetic susceptibility meter produces an opportunity to measure magnetic susceptibility as well as AMS of a discrete sample.

To investigate the magnetic mineralogy of discrete samples, experiments of the acquisition of IRM were carried out using an Analysis Ser-

vices Company impulse magnetizer model IM-10 capable of applying magnetic fields from 0.02 to 1.35 T.

### Paleomagnetic and Rock Magnetic Measurements

ODP core orientation designates the positive x-axis direction as the horizontal direction (“geomagnetic north” in a global coordinate reference frame) from the center of the core to the median line between a pair of lines inscribed lengthwise on the working half of each core liner (Fig. F14). Continuous measurements of NRM and remanence were made on the archive half of the core using the pass-through cryogenic magnetometer. Remanence measurements were made at demagnetization steps of 10, 20, and 30 mT at intervals of 5–10 cm.

Rock magnetic experiments were conducted on selected discrete samples to identify the magnetic minerals in sediments. Thermal demagnetization of multicomponent isothermal remanent magnetization (Lowrie, 1990) was used as the primary means of identifying the magnetic composition of magnetic minerals. For these experiments, orthogonally applied fields of 1.0, 0.3, and 0.1 T were used to generate the IRM components. The samples were then demagnetized using 15 thermal steps from 50° to 650°C.

### Discrete Sample Acquisition

For the study, one to two discrete oriented samples were acquired from each section of the working half of the core. Plastic cubes (8 cm<sup>3</sup> and 1 cm<sup>3</sup>) were used for soft sediments, and 10-cm<sup>3</sup> minicores were cut from sections of crystalline and igneous rock. Paleomagnetic measurement of some core samples was also conducted for azimuth reorientation of structure observed in the cores.

### Core Orientation

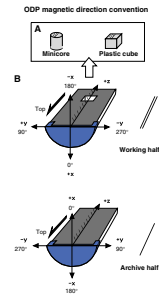
During Leg 205, only RCB coring was performed. Reorientation of the rotated portions, caused by RCB drilling, was accomplished by using paleomagnetic results on the archive half of the core. Core orientation was also performed using discrete samples from the working half of the core. Characteristic inclination and declination directions were isolated by stepwise AF demagnetization. The core orientations were rotated to 180° when reversed polarity was observed in the samples.

Some discrete samples need additional reorientation after the paleomagnetic measurement. When the discrete samples are set on the tray of the cryogenic magnetometer upside down, the system control program cannot work to correct their direction even though the program has a reorientation command. In this case, measured +x- and +y-axes must be changed into -x- and -y-axes, respectively. Otherwise, magnetic declination of the samples shows the opposite direction. The discrete samples taken from the working half should be set on the tray following the basic coordinate system for the archive-half core (Fig. F14) to prevent direction troubles caused by program errors.

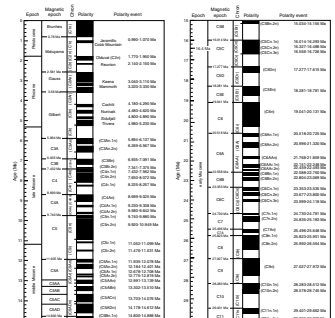
### Magnetostratigraphy

The magnetic polarity timescale of Berggren et al. (1995a, 1995b) was used when interpreting observed polarity boundaries (Fig. F15). Additional geomagnetic short events (subchrons) that may prove to be use-

F14. ODP coordinate systems, p. 59.



F15. Magnetostratigraphic time-table, p. 60.



ful stratigraphic markers are short reversals within long-period geomagnetic chrons such as the Brunhes (0.0–0.78 Ma)–Matuyama (0.78–2.581 Ma) polarity chrons. Because of difficulty in identifying the polarity timescale without shipboard micropaleontological data, observed polarity boundaries on this cruise were simply compared with previous paleomagnetic results from Leg 170 for confirmation of polarity age.

## **INORGANIC GEOCHEMISTRY**

### **Pore Fluid Sampling and Chemical Analyses**

Shipboard pore fluid analyses were performed on fluids squeezed from 15- to 45-cm-long whole-round sections that were cut and capped immediately after the core retrieval on deck. One to two whole-round samples per core were obtained from the section of the core with little to no apparent drilling disturbance. The sediment was immediately removed from the core liner, and the outer layer, which mostly consists of sediments permeated by drill water (surface seawater) spiked with perfluoro(methylcyclohexane) (C<sub>7</sub>F<sub>13</sub>) and fluorescent latex microspheres, was carefully trimmed to remove any potential contaminants. The cleaned pieces of sediment were placed into a titanium squeezer (modified after Manheim and Sayles, 1974) between one or two Whatman number 1 filters that were previously rinsed in high-purity water to remove processing acids. The hydraulic press was operated up to a maximum pressure of ~30,000 psi (205 MPa). The sediment sample remained under pressure until most of the squeezable water was removed. Pore fluid was collected into prewashed 10- to 50-cm<sup>3</sup> plastic syringes and filtered through disposable 0.45- $\mu$ m Gelman polysulfone filters. Samples were stored in acid-cleaned plastic vials pending shipboard analyses. Aliquots for future shore-based isotopic analyses were placed in glass ampoules and heat sealed, and aliquots for future trace metal and elemental analyses were placed in three acid-washed plastic vials and acidified to 10% with Optima-grade nitric acid. Samples for future dissolved inorganic carbon analyses were poisoned with a saturated mercuric chloride solution, and sulfide was precipitated with a 50% CdNO<sub>3</sub> solution.

Pore water samples were routinely analyzed for salinity and total dissolved solids with a Goldberg optical handheld refractometer (Reichert) and for pH and alkalinity by Gran titration with a Brinkmann Instruments pH electrode and a Metrohm autotitrator. Chloride concentration was determined by titration with AgNO<sub>3</sub>. Calcium and magnesium concentrations were analyzed by ethylene-bis(oxyethylenitrilo)tetraacetic acid and disodium ethylenediamine tetraacetic acid titrations, respectively. Silica and ammonium determinations were carried out by colorimetry using a Milton Roy Spectronic 301 spectrophotometer and a Milton Roy Mr. Sipper introduction system (Gieskes et al., 1991). Pore fluids were not analyzed for phosphate because of the low (~1  $\mu$ M) and constant concentration observed during Leg 170 within the intervals cored during Leg 205.

International Association of Physical Sciences Organizations (IAPSO) standard seawater was used for calibrating all techniques. The reproducibility of these analyses, expressed as percent precision calculated from multiple determinations of IAPSO standard seawater or of a standard are alkalinity,  $\leq 3\%$ ; chloride,  $\leq 0.15\%$ ; calcium,  $\leq 1\%$ ; magnesium,  $\leq 1\%$ ; silica,  $\leq 2\%$ ; and ammonium, 4%; and the accuracy for silica is  $\leq 4\%$ . At



all sites, sodium was determined using charge balance calculations, where  $\Sigma(\text{cation charge}) = \Sigma(\text{anion charge})$ , as well as by ICP-AES.

Sulfate was analyzed by ion chromatography (ICr) using the Dionex DX-120. The reproducibility of the sulfate analyses, expressed as percent precision calculated from multiple determinations of IAPSO standard seawater or of a standard is  $\leq 2\%$ . Potassium, calcium, and magnesium concentrations were not determined by ICr because of an unidentified problem that persisted even after exchanging the cation column and the suppressor. These elements were analyzed by ICP-AES, which provides better precision than the ICr.

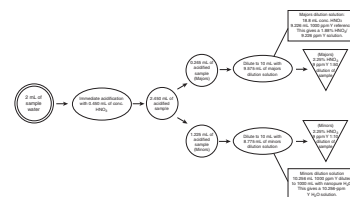
The major cations and the minor elements: lithium, boron, strontium, barium, rubidium, manganese, iron, and silica were determined by using the Jobin-Yvon Ultrace ICP-AES following the general procedure outlined by Murray et al. (2000) and modified by M. Delaney. The shipboard "master" ICP standard (Murray et al., 2000; modified by M. Delaney) was expanded so that Si concentrations could be determined. In addition, a special external standard was prepared for rubidium because of the element's high detection limit ( $\sim 50$  ppm) on the ICP-AES. In preparation for analysis by ICP-AES, aliquots of interstitial waters were acidified with nitric acid ( $\text{HNO}_3$ ) and diluted tenfold (2.25%  $\text{HNO}_3$  and 9 ppm Y) with nanopure water for the minor elements and diluted fifty times (2.25%  $\text{HNO}_3$  and 9 ppm Y) for the major elements. Analytical blanks were prepared identically by analyzing nanopure water, which was acidified to matrix levels, and Y was added to match the samples. A detailed flow chart for preparation of pore fluid samples for ICP-AES analyses is available in Figure F16. At all sites, sodium was also determined using charge balance calculations.

The reproducibility of the major and minor element analyses, expressed as percent precision calculated from multiple determinations of IAPSO standard seawater or of standards and samples are sodium,  $\leq 0.1\%$ ; magnesium,  $\leq 0.2\%$ ; potassium,  $\leq 0.4\%$ ; calcium,  $\leq 0.3\%$ ; boron, lithium, and barium,  $\leq 2\%$ ; iron and manganese,  $\leq 3\%$ ; Si and Sr,  $\leq 1\%$ . Accuracies of the ICP-AES analyses for these elements, as determined by standards run as unknowns, are sodium,  $< 0.5\%$ ; magnesium,  $< 1\%$ ; potassium,  $< 4\%$ ; calcium,  $< 0.5\%$ ; boron,  $\sim 8\%$ ; barium,  $< 3\%$ ; iron,  $< 5\%$ ; lithium,  $\sim 4\%$ ; manganese,  $\sim 6\%$ ; silica,  $< 4\%$ ; and strontium,  $< 6\%$ . Rubidium concentrations were lower than the detection limit of this ICP-AES.

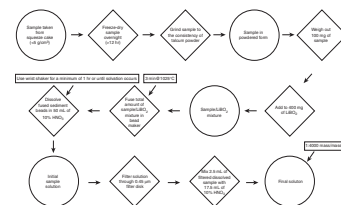
### Sediment Sampling and Chemical Analyses

Bulk sediment samples were analyzed routinely during Leg 205. Samples for bulk sediments were taken from interstitial water squeezed cakes and from select sediment horizons chosen by the sedimentologists. Bulk samples were prepared according to the method of Murray et al. (2000). Samples were first freeze-dried and powdered. Samples and standards (0.1 g) were mixed with  $\text{LiBO}_2$  flux (0.4 g). Analytical blanks were prepared using 0.4-g  $\text{LiBO}_2$  flux to ensure matrix matching. A solution of 0.172-mM LiBr wetting agent (10  $\mu\text{L}$ ) was added to the samples, standards, and blanks. This mixture was fused for 3 min at  $1025^\circ\text{C}$  in an NT-2100 Bead Sampler prior to dissolution in 50 mL of 10%  $\text{HNO}_3$ . A 5-mL aliquot of the resulting solutions was filtered (0.45  $\mu\text{m}$ ) and diluted with 35 mL of 10%  $\text{HNO}_3$ , resulting in a 4000-fold dilution of the original powders (refer to Fig. F17). Na, Mg, K, Ca, Sr, Ba, Fe, Mn, Cu, Al, Ti, Si, P, Cr, Zr, Y, and V concentrations were determined using a Jobin-

F16. ICP interstitial water sample preparation, p. 61.



F17. ICP sediment sample preparation, p. 62.



Yvon Ultrace ICP-AES using a Type-C Meinhard concentric nebulizer following the general procedure outlined by Murray et al. (2000).

For these analyses, the certified standards SGR-1 (Green River shale), MAG-1 (marine mud), SCO-1 (Cody shale), NBS-1c (argillaceous limestone), NBS-99a (sodium plagioclase), BIR-1 (Icelandic basalt), and BHVO-2 (Hawaiian basalt) were used to develop a seven-point calibration curve for the major and most minor and trace elements. The precision and accuracy of SGR-1 were consistently inadequate; therefore, this standard was omitted from the calibration curve and subsequent batches of analyses. NBS-1c and NBS-99a do not have certified analyses of the minor and trace elements; Washington University minor and trace element chemistry for the NBS-1c was used instead. These standards were chosen because they are most representative of the lithologies present at Sites 1253 and 1254 as determined by careful inspection of X-ray fluorescence major, minor, and trace element data generated during Leg 170. MAG-1 was chosen as a drift standard because it has higher concentrations of elements analyzed during Leg 205 than the other four standards. One drift standard was run for every four samples (two standards followed by two samples), and one standard was run as an unknown every five samples. The drift and standard samples were also analyzed at the beginning and end of each ICP-AES batch of analyses. Each sample was run six times, and two LiBO<sub>2</sub> flux blanks were run per batch of analyses.

The reproducibility of these analyses, expressed as percent precision calculated from multiple determinations of standards and samples are Al and Sr, <2%; Na, Mg, V, and Si, <3%; Ba, Ca, and Mn, <4%; Fe and K, <5%; Ti and Cr, <6%; Zr, <10%. Y reproducibility, except for three sediment samples, was <8%. The reproducibility for P was low (<25%), and Nb, Ni, Cu, and Zn reproducibilities and/or accuracies were deemed unacceptable (25%).

## **ORGANIC GEOCHEMISTRY**

The shipboard organic geochemistry program for Leg 205 included (1) real-time monitoring of volatile hydrocarbon gases; (2) measurement of the inorganic carbon concentration to determine the amount of carbonate in the sediments; (3) elemental analyses of total organic carbon, total sulfur, and total nitrogen; and (4) characterization of organic matter. All instruments and methods used during Leg 205 are described below. Additional details are summarized in Pimmel and Claypool (2001) as well as Emeis and Kvenvolden (1986). These analyses were performed as part of the routine shipboard safety requirements. The sediment samples needed were usually taken from the end of a core section close to the interstitial water sample, whenever possible.

### **Hydrocarbon Gases**

During Leg 205, the composition and concentration of hydrocarbons and other gases in the sediments were analyzed, usually at intervals of one per core. Two different methods, headspace and vacutainer, were used.

In the headspace method, gases released from the sediments after core recovery were analyzed by gas chromatography (GC). Immediately after retrieval on deck, a calibrated cork borer was used to obtain a defined volume of sediment from the core. Usually an ~5-cm<sup>3</sup> sediment

sample was placed in a 20-cm<sup>3</sup> glass vial that was sealed with a Teflon septum and a metal crimp cap. When consolidated or lithified sediments were encountered, chips of this material were placed in the glass vial and sealed. The vial was then heated for 30 min at a constant temperature of 60°C. A 5-cm<sup>3</sup> volume of the headspace gas in the vial was extracted through the septum with a standard glass syringe for analysis by GC. The vacutainer method of gas collection was used where gas pockets or expansion voids were visible in the core when it was still in the core liner. A special piercing tool was used to penetrate the core liner; an attached 50-mL syringe equipped with a small three-way stop-cock valve was employed to sample the gas.

Headspace and vacutainer gas samples were analyzed using the GC3, a Hewlett Packard 6890 gas chromatograph equipped with a stainless steel column, packed with HayeSep R porous polymer (80/100 mesh), and a flame ionization detector (FID). The GC3 measured the concentrations of methane, ethane, ethene, propane, and propene. Either the headspace syringe or the vacutainer was directly injected into the GC using a 0.25-cm<sup>3</sup> sample loop. Helium was used as the carrier gas at a flow rate of 30 mL/min, increased to 80 mL/min after 3 min, and the GC oven was initially held at 100°C for 5.5 min and then heated up to 140°C. When higher concentrations of propane and higher hydrocarbons were suspected, gas samples were analyzed by the Natural Gas Analyzer (NGA), which measures hydrocarbons from methane to decane as well as N<sub>2</sub>, O<sub>2</sub>, CO<sub>2</sub>, H<sub>2</sub>S, and CS<sub>2</sub>. The NGA is a Hewlett Packard 6890 flame ionization multivalve, multicolumn gas chromatograph equipped with both a thermal conductivity detector (TCD) and an FID. Four columns were used sequentially to provide rapid partitioning and measurement of the gases. The sample was injected onto the entire set of columns using three sample loops. Helium was used as the carrier gas.

The data from both methods were collected and evaluated with a Hewlett Packard Chemstation data acquisition and analysis system. Chromatographic responses were calibrated against preanalyzed standards. On both GCs, the detection limit for hydrocarbons was 1–3 ppmv and the relative measurement accuracy was 3%–8%.

### **Elemental Analysis**

Three 2-cm<sup>3</sup> sediment samples were routinely taken from each core for analysis of total carbon (TC), carbonate carbon (IC), total organic carbon (TOC), total sulfur (TS), and total nitrogen (TN).

Carbonate carbon concentrations of the samples were measured using a Coulometrics 5030 carbonate-carbon analyzer. An ~10-mg sample of freeze-dried, ground material was acidified with 2-N HCl in a glass tube. The liberated CO<sub>2</sub> was carried through a scrubber to remove SO<sub>2</sub> and then into the coulometer cell, where it was absorbed and reacted with monoethanolamine, a colorimetric indicator, causing the blue color to fade. The color change in the solution was measured by a photodetector cell. A program using Labview software read the titration results and provided the concentrations for IC and CaCO<sub>3</sub> (in weight percent). The measurement accuracy is ~1%, and the detection limit is ~0.5 wt%.

TC, TS, and TN were determined using a Carlo Erba NA 1500 CHNS analyzer. About 5 mg of freeze-dried, ground sediment or rock was mixed with V<sub>2</sub>O<sub>5</sub> and combusted in a reactor at 1000°C in an oxygen at-

mosphere. The combustion products  $\text{SO}_2$ ,  $\text{CO}_2$ , and  $\text{NO}_2$  are carried by helium gas through a column packed with  $\text{WO}_3$  and Cu at  $1000^\circ\text{C}$  to reduce  $\text{NO}_2$  to  $\text{N}_2$ . The gases were then separated by a GC (Poropak Q/S 50/80 mesh) and quantified with a TCD. TOC contents were calculated as the difference between TC and IC. For carbon, the measurement precision is  $\sim 0.06$  wt% (accuracy is  $\sim 2\%$ ) and the detection limit is  $\sim 0.3$  wt%, whereas nitrogen and sulfur measurements show low accuracy of  $\sim 20\%$ , and for both, the detection limits are  $\sim 0.02$  wt%.

### Organic Matter Type

The type of organic matter was evaluated in a selected set of samples (based on the  $\text{C}_1/\text{C}_2$  hydrocarbon ratio) by pyrolysis using a Delsi Nermag Rock-Eval II Plus TOC system. The method is based on a whole-rock pyrolysis technique that is designed to identify the type and maturity of organic matter and to detect the petroleum potential of the sediments (Tissot and Welte, 1984; Espitalié et al., 1986). The Rock-Eval system involves a temperature program that first releases volatile hydrocarbons ( $\text{S}_1$ ) at  $300^\circ\text{C}$  for 3 min. Hydrocarbons are then released by thermal cracking of kerogen ( $\text{S}_2$ ) as the temperature is increased from  $300^\circ$  to  $550^\circ\text{C}$  at  $25^\circ\text{C}/\text{min}$ .  $\text{S}_1$  and  $\text{S}_2$  hydrocarbons are measured by an FID. The temperature at which the kerogen releases the maximum amount of  $\text{S}_2$  hydrocarbons provides  $T_{\text{max}}$ , a parameter used to assess the maturity of organic matter. Between  $300^\circ$  and  $390^\circ\text{C}$  of the stepped pyrolysis,  $\text{CO}_2$  that was released from the thermal cracking of organic matter ( $\text{S}_3$ ) is trapped and measured by a TCD. For the characterization of organic matter, the following parameters can be calculated:

$$\text{Hydrogen index (HI)} = 100 (\text{S}_2/\text{TOC}),$$

$$\text{Oxygen index (OI)} = 100 (\text{S}_3/\text{TOC}),$$

$$\text{Pyrolizable carbon (PC)} = 0.083 (\text{S}_1/\text{S}_2), \text{ and}$$

$$\text{Production index (PI)} = \text{S}_1/(\text{S}_1 + \text{S}_2).$$

## MICROBIOLOGY

Recent progress in exploring the deep seafloor biosphere has revealed that microbial populations are consistently present in core samples recovered from the deep oceanic subsurface (Parkes et al., 1994; Wellsbury et al., 1997). Calculations suggest that the subsurface biosphere, extending deep into the crust (Fisk et al., 1998; Furnes and Staudigel, 1999; Furnes et al., 1999), is the largest reservoir of biomass on Earth (Whitman et al., 1998). However, the structure, diversity, and function of subsurface microbial communities remains poorly understood.

The primary shipboard microbiology objective was to obtain sediment and oceanic basalt samples while ensuring the use of sterile techniques at all times of sampling, sample handling, and storage. Little-altered microcrystalline to fine-grained gabbro recovered at Site 1253 was different from the heavily veined and altered thin basalt flows and pillow basalts expected. However, rock samples were taken from the lower part of Subunit 4B for the purposes stated below. Potential con-

tamination will be monitored using chemical tracers at Site 1253 and particulate tracer tests at all shipboard sites. We will begin extraction of deoxyribonucleic acid (DNA) from sediment and rock samples for genetic analyses to quantify bacterial abundance and diversity. We will relate these molecular-based microbial identifications to fluid and solid chemistry in the sediments and to alteration textures and chemical maps of altered crust and analyze the isotopic carbon fractionation of the glass postcruise. This information will allow for better assessment of the microbial community in the deep biosphere, as well as the role that microorganisms play in the alteration of basalts. It will also provide us with more accurate estimates of the microbial role in important geochemical processes such as the evolution of crustal composition and the cycling of elements in the ocean.

## **Core Handling and Sampling**

### **Sediment Sampling**

Syringe plugs were too difficult to obtain from cut core sections on the catwalk because the sediments were very indurated, especially at Site 1253. Instead, a 5-cm<sup>3</sup> whole round was selected for microbiological sampling adjacent to interstitial water whole rounds and it was rapidly transported to the microbiology laboratory for paring and sampling. A sterile spatula was used to free ~0.5 cm<sup>3</sup> of sediment from the most central part of the core. This 0.5-cm<sup>3</sup> sample was scraped into a sterile 2-mL Eppendorf tube containing 1.5-mL 2% formalin solution to fix cells for postcruise cell counting. A ~5-cm<sup>3</sup> plug was excised using a 5-cm<sup>3</sup> autoclaved, cut-off syringe; this specimen was expelled from the syringe immediately into a sterile, 15-mL Falcon tube, capped tightly, and frozen at -80°C for adenosine triphosphate quantification as a means of calibrating cell counts. In the same fashion, a second 5-cm<sup>3</sup> plug was taken, sealed likewise in a sterile Falcon tube, and frozen at -80°C for postcruise microbial community assessment. Samples of drilling fluid were also obtained, caught in 50-mL sterile Falcon tubes as the fluid ran out of the top of the core liner on the catwalk; drilling fluid samples were immediately frozen at -80°C and will be processed similarly to the sediment samples postcruise. Sampling for contamination tests is described below. Taking microbiological samples where interstitial fluid and squeeze cake geochemical analyses are planned increases the future compatibility of geochemical and microbiological results.

### **Igneous Rock Sampling**

Upon core retrieval, samples of drilling fluids were taken in sterile Falcon tubes to determine the microbial populations that naturally occur in these fluids ("background contamination"), then the liner was cut open without disturbing the rock fragments. Pieces indicating some degree of low-temperature alteration were picked with sterile forceps, placed on sterile foil, and immediately transferred from the splitting room to the anaerobic glove box and put on ice to maintain core temperature at or below the in situ temperature.

Working within the glove box, samples were rinsed of unwanted debris with an N<sub>2</sub>-flushed marine salts solution (23.5 g NaCl and 10.8 mg MgCl<sub>2</sub>·6H<sub>2</sub>O per liter). An initial core segment was cut using a hydraulic press under aseptic and anoxic conditions, and any unused portions were immediately returned to the core. All materials, including core

cutters, storage vials, and so on, were sterilized by autoclave or ethanol. Digital images were taken of the core piece prior to and after initial microbial sampling. Images were also taken of the sample used for further microbial work. The images serve as a record for complete core descriptions. The sampled core section was then crushed into several pieces to be used for different investigations. Crushing was done by wrapping the rock in sterile aluminum foil and breaking it into several pieces with a sterile chisel and hammer or mortar and pestle.

A glove bag (Coy, Grass Lake Michigan) containing a nitrogen atmosphere with 5% CO<sub>2</sub> and >2% H<sub>2</sub> was used for anaerobic handling of the core. Sections were brought into the glove bag and insulated on blue ice, and work was performed quickly to minimize warming. Hydrogen is present to combine with residual oxygen in a reaction catalyzed by palladium pellets maintained within the bag. Several hours before each use, the bag was flushed with a gas mixture. As an additional precaution to minimize oxygen contamination, tools and glassware to be used for manipulation and storage of samples for strict anaerobe work were stored within the glove bag.

Although cores were processed as quickly and as carefully as possible, shipboard handling should not be simply accepted as aseptic. We recommend that investigators receiving samples treat them as potentially contaminated and subsample accordingly whenever possible.

### **Igneous Core Section Subsampling**

The crushed rock samples were partitioned into five different parts. One portion was put aside for future fluorescent in situ hybridization analyses. Rock fragments were fixed in 4% paraformaldehyde (Table T4) in sterile Falcon tubes for 4–24 hr. The samples were then washed and stored in a 1:1 mixture of phosphate buffered saline:100% ethanol at –20°C. A second portion was set aside for shore-based microscopic observations. The samples were placed in 10- or 50-mL sterile Falcon tubes depending on sample size. They were then fixed in 2% glutaraldehyde for 4–24 hr before being washed and stored in 0.25% glutaraldehyde at 4°C. A third sample was stored in sterile sample bags at –80°C for shore-based chemical analyses. A fourth sample was immediately stored in sterile 2-mL Eppendorf tubes at –80°C for future DNA extractions and genetic analyses. Finally, a fifth sample was set aside and put on ice to inoculate growth media.

---

T4. Gabbro sample preparation for fluorescent in situ hybridization analysis, p. 71.

---

## **Shipboard Microbiological Procedures and Protocols**

### **Contamination Tests**

The greatest challenge for subsurface microbiological investigations is verification that observed populations and activities are authigenic and not the result of introduced contaminants. Chemical (perfluorocarbon) and particulate (latex microsphere) tracers were used during microbiological coring to check for the potential intrusion of drill water and confirm the suitability of the core material for microbiological research. The presence or absence of these two tracers also acts as a quality assurance check on core handling methods. These tracer techniques were used during several legs and are described in ODP *Technical Note* 28 (Smith et al., 2000a). Samples of the drilling fluids were also collected upon core retrieval to determine the “background contamination.” Note, however, that these methods were developed for APC cor-

ing methods. In the absence of other protocols, Leg 205 scientists used these approaches for RCB coring, with limited success.

### **Perfluorocarbon Tracer**

Perfluorocarbon tracer (PFT) was continuously fed to the drill water at a concentration close to the limit of solubility (1  $\mu\text{g/g}$ ) and well above the detection limit for gas chromatographic analysis (1  $\text{pg/g}$ ). Samples for PFT analysis were taken from all cores intended for microbiological studies. In the sediments, 3-cm<sup>3</sup> syringe subcores were taken from the interior (to monitor intrusion) and exterior (to verify delivery) of a freshly broken core or biscuit surface, extruded into headspace vials, and sealed with Teflon septa. Upon recovery of Subunit 4B, the core liner was split to observe and sample the core. To verify delivery of the PFT, the interior of the liner was wiped with a sterile cotton ball, which was placed in a headspace vial and sealed with a Teflon septum. A small rock fragment was taken from the interior of the core (to monitor tracer intrusion) and stored in a similar fashion as the cotton swab. Air samples were occasionally taken on the catwalk and in the glove box to monitor the background (blank) level of PFT. Samples were analyzed by GC. To avoid high background contamination levels of PFT in the laboratories, PFT containers should be opened on the helideck.

### **Particulate Tracer**

Latex fluorescent microspheres (Polysciences, Inc., Warrington, Pennsylvania; 0.5- $\mu\text{m}$  diameter; YG) were used as a particulate tracer complementary to the volatile PFT. A 2-mL aliquot of microsphere stock (2.69% solids) was diluted with 40 mL of distilled water, sonicated for 2 min, and heat-sealed into a 4-oz Whirl-Pak bag. The bag was then attached with thread to the core catcher, a slight modification from procedures as described in Smith et al. (2000a, 2000b). The bag was positioned to rupture upon impact of the core tube with bottom sediments or rock, mixing the microspheres with seawater and coating the outside of the core as it is pushed into the liner.

During core processing, subsamples of sediments were collected from outer and inner layers for microscopic examination. Weighed samples were mixed with saturated sodium chloride solution and mixed thoroughly to extract microspheres. The slurry was then centrifuged to separate the liquid phase (Marathon 21K; 3 min; 2000 rotations per minute). The uppermost 10 mL of supernatant was filtered onto a black polycarbonate filter (0.2- $\mu\text{m}$  pore size; Millipore), and the filter was mounted on a clean slide for microscopic examination. The usable filter area was  $\sim 1.98 \times 10^8 \mu\text{m}^2$  as determined by the inner diameter of the filtration tower (15.64 mm). Microspheres in slide preparations were counted using a Zeiss Axioplan fluorescence microscope equipped with the Zeiss number 9 filter set (BP 450–490; LP 520), and the number of spheres observed was used to quantify contamination in spheres per gram (sediments) or milliliter (gabbro) of sample. The 100 $\times$  objective was used for detecting cells, where the area for one entire field of view was  $\sim 3.14 \times 10^4 \mu\text{m}^2$  (the diameter for one field of view = 200  $\mu\text{m}$ ). A total of 50 fields of view were analyzed for each sample.

Given the RCB coring during Leg 205, an additional method may be used. Intact biscuits, pared aseptically shipboard, were taken contiguous with interstitial water whole rounds. At Sites 1254 and 1255, elevated sulfate concentrations are indicative of seawater contamination

of biscuit interiors (see “[Inorganic Geochemistry](#),” p. 27, in the “Site 1254” chapter and “[Inorganic Geochemistry](#),” p. 14, in the “Site 1255” chapter).

Samples of the exterior gabbro core for microsphere analyses were taken by washing the core sample with sterile N<sub>2</sub>-flushed marine salts solution and collecting the fluids in a syringe to be transferred to Falcon tubes for storage. Interior gabbro samples were crushed with a steel mortar and pestle, mixed with the marine salts solution, and collected in Eppendorf tubes. Prior to filtering, the samples were vortexed and allowed ~5 min each for settling of the larger particulates. A 5-mL aliquot was taken from each sample and filtered. Samples were visualized and counted as stated previously. Given the indurated and often fractured nature of the igneous rock, these methods are not optimal; all igneous microbiology samples are assumed to have been in contact with seawater.

### Cultivation of Microorganisms

To enrich microorganisms, different media, which were prepared prior to the cruise and are described in Table T5, were inoculated with a slurry from the cold gabbro subsamples set aside for culturing work. The slurry was prepared by first crushing the rock fragment into very small pieces (<2 mm) by wrapping the pieces in sterile foil and smashing with a hammer or with a mortar and pestle. Next the finely crushed pieces were placed into sterile beakers with anoxic (N<sub>2</sub>-flushed) minimal salts solution used for initial rinsing of the core. The beakers were shaken and vortexed to remove microorganisms attached to the rock fragments. Sterile syringes flushed with nitrogen were used to transfer the slurry into capped 5-mL serum vials or into gradient tubes. A sterile needle was used each time to inoculate the various media.

---

T5. Media used for cultivation of microorganisms, p. 72.

---

### Genetic Analysis

Genetic analysis of gabbro samples will allow more detailed identification of microorganisms inhabiting the samples. Following collection of samples, DNA will be extracted following the protocol in Table T6. DNA will then be purified from the samples, following the protocols of Edwards et al. (2000). The 16S ribosomal ribonucleic acid genes will be amplified by polymerase chain reaction using universal primers. Cloning and sequencing (University of Maine sequencing facility) will take place on shore. Determining the phylogenetic relationships of the microbial community will provide more information regarding whether organisms obtained from the samples are contamination artifacts (phylogenies similar those of organisms commonly found in surficial environments or drilling fluids) or if they truly live in gabbro (phylogenies match those of organisms found in subsurface environments).

---

T6. DNA extractions from gabbro samples, p. 74.

---

## DOWNHOLE TOOLS

### The Davis-Villinger Temperature-Pressure Probe

During Leg 205, a combined temperature and pressure tool was employed to determine in situ temperature and pore pressure. The Davis-Villinger Temperature-Pressure Probe (DVTPP) is a modification of the original Davis-Villinger Temperature Probe (DVTP), which is described



in detail by Davis et al. (1997) and summarized by Pribnow et al. (2000) and Graber et al. (2002). The tip is of conical shape, is 1.1 m long, and has a diameter of 8 mm at the lowermost end. In the original version, two thermistors were mounted in the probe, the first located 1 cm above the tip, the second 10 cm above the lower thermistor. A third thermistor, referred to as the internal thermistor, was located in the electronics package. The temperature measurement range is  $-5^{\circ}$  to  $160^{\circ}\text{C}$  with a temperature resolution of 1 mK at ambient deep-sea temperatures, increasing to 10 mK at  $120^{\circ}\text{C}$ . The thermistors are calibrated using the temperature vs. resistance tables provided by the manufacturer and, in addition, adjusted for offset by using bottom water temperatures from oceanographic data and mudline records. Additionally, the probe contains an accelerometer with a total range of  $\pm 2$  g and a resolution of 0.01 g. Both peak and mean acceleration are recorded by the logger. The accelerometer data are used to track vertical disturbances to the instrument package during the equilibration interval.

The DVTTP allows simultaneous measurement of both formation temperature and pressure. The upper thermistor was removed, and ports on the sidewalls of the tip allow hydraulic transmission of formation fluid pressures to a precision pressure gauge inside. The dimensions of the probe tip have not been changed in order to not affect the thermal response. The Paroscientific Digiquartz transducer pressure gauge provides a resolution of 4 Pa over a range of 70 MPa. The tool tip is shown in Figure F18.

The tool is typically deployed by lowering it by wireline to the mudline and pausing for 10 min to collect data. Subsequently, the tool is lowered to the base of the hole and latched in at the bottom of the drill string with the end of the tool extending 1.1 m below the drill bit. The extended probe is pushed into the sediment below the bottom of the hole, and pressure is recorded for  $\sim 30$  min. If smooth pressure decay curves are recorded after penetration, extrapolations to in situ pore pressures are possible.

### Thermal and Pressure Data Reduction

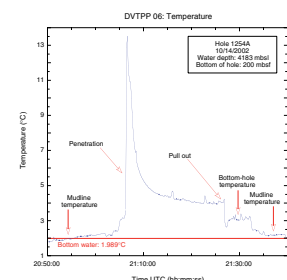
The transient thermal decay curves recorded by the thermistor of the DVTTP are a function of the geometry of the tool and the thermal properties of probe and sediments (Bullard, 1954; Horai and Von Herzen, 1985). Data analysis requires fitting the measurements to temperature decay curves based on probe geometry and thermal properties of the sediment. Pribnow et al. (2000) discuss data analysis procedures and uncertainties. The software used for temperature data processing is CONEFIT, developed by Davis et al. (1997). Resulting uncertainties in the in situ temperature estimates are caused by several factors: (1) the fact the probe does not reach thermal equilibrium during the penetration period and derived temperatures must be extrapolated; (2) contrary to ideal theory, the frictional pulse upon insertion is not instantaneous; (3) temperature data are sampled at discrete intervals so that the exact time of penetration is uncertain; and (4) the in situ thermal conductivity of the sediments is imperfectly known.

Figure F19 shows a typical temperature history recorded by the DVTTP. Various stages in the tool deployment history are marked. Mudline temperature is determined from the time the tool is held near the seafloor prior to penetration of the DVTTP. In this example, the mudline temperature is not yet stable because of the pumping, which is stopped exactly when reaching the mudline. Initial penetration is

F18. View of the DVTTP tip, p. 63.



F19. Typical data from a DVTTP deployment, p. 64.



marked by a temperature pulse due to frictional heating. A second pulse is observed when the tool is extracted from the sediment. In the example shown in Figure F19, we also took bottom-hole and mudline temperatures after the penetration. The best-fitting time of penetration and in situ temperature are calculated by the shipboard analyst. The estimated uncertainty of the derived in situ temperature for good-quality measurements is 0.1°C (Pribnow et al., 2000), although the uncertainty may be considerably larger for poor-quality measurements. Temperature gradients may be better resolved than absolute values of temperature, provided the same tool is used to make all measurements at a given site. In order to calculate heat flow, the thermal conductivity of the sediment must also be specified. Thermal conductivities measured from the core interval closest to the DVTPP measurement were used (see “Physical Properties,” p. 19).

The pressure response of the DVTPP is qualitatively similar to, but slower than, the thermal response. The decay time is a function of the sediment diffusivity and the magnitude of the initial pulse, which is a function of the taper angle and diameter of the tool (Whittle et al., 2001; Heesemann, 2002). Shipboard extrapolations to estimate formation pressures are preliminary estimates. A more complete analysis will be done postcruise.

### Miniaturized Temperature Data Logger

Miniaturized temperature data loggers (MTLs) have been deployed inside the OsmoSamplers for long-term monitoring of fluid temperature fluctuations inside boreholes (see Jannasch et al., this volume). Moreover, they were used to measure high-resolution temperature profiles in the boreholes simultaneous to the wireline logging and to determine the bottom water temperature, which is used for calibration of the DVTPP.

The MTL (Pfender and Villinger, 2002) consists of a 140-mm-long cylindrical body with an outside diameter of 15 mm, housing the electronics, and a thin-walled tip (20 mm long with an outer diameter of 4 mm) containing the temperature sensor. The pressure housing consists of high-strength corrosion-resistant steel and withstands a pressure equivalent of 6000 m water depth. The logger is shown in Figure F20. Programming of the logger and downloading the data are performed without opening the pressure case. A readout unit contacts the logger’s tip and end cap with a voltage delivered by an RS232 interface from a PC, and a high-strength plastic isolator between the tip and main body maintains the voltage so that the communication unit works as a two-point connection for data transfer.

The electronics of the logger consist of a microprocessor, a 16-bit analog-to-digital (A/D) converter, a real-time clock, and nonvolatile memory for up to 64,800 measurements. The sample interval can be varied from 1 s to 255 min, which allows up to 18 hr of logging at a 1-s interval or a longest theoretical recording time of ~33 yr. The complete system is powered by a standard small-sized 3-V lithium battery. We use a thermistor with interchangeability of 0.1 K as a sensing element in order to achieve a resolution of 1 mK at typical deep-sea temperatures of 2°C. The temperature measurement range extends from -5° to 60°C. The absolute accuracy of the logger after calibration with a high-precision thermometer in a well-stirred water bath is <5 mK, which is adequate to resolve expected temperature fluctuations in the boreholes. The design of this temperature sensor in a thin-walled tip satisfies the

F20. View of an MTL, p. 65.



need for a fast-response sensor. The thermal time constant of the system is ~2 s.

## **DOWNHOLE LOGGING**

Downhole logging began in the 1920s as “electrical coring” (Schlumberger et al., 1934), which measured the spontaneous potential (SP) between the surface and the sonde at depth, and it now encompasses a wide range of sensors. It is a method of measurements performed in a drill hole to determine the in situ physical, chemical, and structural properties of formations penetrated by the hole. Logs can be acquired after the hole is drilled (wireline logging) or while/after drilling (logging while drilling [LWD] or measurement while drilling). Wireline logging is most effective in stable formations and where the hole is nearly vertical, whereas LWD can be performed while drilling where formations are unstable or after drilling where the hole has deviated far from the vertical. Wireline logging was used during ODP Leg 205, whereas LWD was done in the area during Leg 170 in 1996 (Kimura, Silver, Blum, et al., 1997).

The combinations of wireline logs on the *JOIDES Resolution* are collected at a speed of 250–300 m/hr, using a variety of instruments that make continuous in situ measurements as a function of depth. The sampling interval of log data ranges from 2.5 mm to 15 cm in depth. The data are rapidly collected, quasicontinuous with depth, and measured in situ; they can be interpreted in terms of the stratigraphy, lithology, mineralogy, and geochemical composition of the penetrated formation. Where core recovery is incomplete or disturbed, log data may provide the only way to characterize the borehole section; where core recovery is good, log and core data complement one another and may be interpreted jointly. Downhole logs are sensitive to formation properties on a scale that is intermediate between those obtained from laboratory measurements on core samples and geophysical surveys. They are useful in calibrating the interpretation of geophysical survey data (e.g., through the use of synthetic seismograms) and provide a necessary link for the integrated understanding of physical properties on all scales. After processing, logs are typically displayed as curves or images of physical and chemical properties of the formations intersected by the borehole. Image logs, in particular, serve to illustrate the physical shape and state of the hole and the character of the formations penetrated. Log data have been used for an ever-growing number and range of applications, such as characterizing formation fluids and measuring the in situ temperature and stress conditions.

Log data quality is largely determined by the state of the borehole wall and individual logging tools. There is also a small but significant difference between drill pipe depth and logging depth that should be taken into account when using the logs for correlation with core and log measurements. In addition, logs from different wireline tool strings may have slight depth mismatches. Therefore, after data acquisition, basic hole condition correction and depth match are generally required. With further processing, log data are combined with core and seismic data to achieve integrated characterization, analysis, and interpretation of both formation fluids and subsurface environments.

## Logging Tool Strings and Operations

During ODP Leg 205, Hole 1253A was drilled, cored, and logged. The logs were acquired using a variety of Schlumberger and Lamont-Doherty Earth Observatory–Borehole Research Group (LDEO-BRG) logging tools that are combined into two “tool strings.” These tool strings are listed as follows:

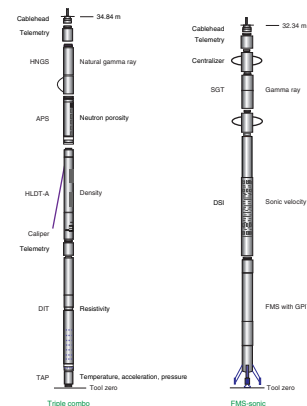
1. The triple combination (triple combo) tool string (resistivity, density, and porosity) (see Fig. F21) consists of the Accelerator Porosity Sonde (APS), the Hostile Environment Litho-Density Tool (HLDT), and the Dual Induction Tool (DIT). The Hostile Environment Gamma Ray Sonde (HNGS) is included at the top of the string, and the LDEO-BRG Temperature/Acceleration/Pressure (TAP) tool is at the bottom.
2. The Formation MicroScanner (FMS)-sonic tool string (Fig. F21) consists of the FMS with the General Purpose Inclinerometer Tool (GPIT) at the bottom, the Dipole Sonic Imager (DSI) in the middle, and the Scintillation Gamma Ray Tool (SGT) and telemetry at the top.

Each tool string also contains a telemetry cartridge facilitating communication from the tools along a double-armored seven-conductor wireline cable to the Schlumberger’s Minimum Configuration Maxis (MCM) computer van on the drill ship. The 9000-m-long logging cable connects the MCM to the tool string through the logging winch and LDEO-BRG wireline heave compensator (WHC).

The WHC is employed to minimize the effect of the ship’s heave on the tool position in the borehole. The logging winch is located aft of the pipe racker. The 160-m-long logging cable fairlead runs from the winch forward to the drill floor, through a sheave back to the heave compensator located alongside the logging winch, then forward to another sheave on the rig floor, up to the crown block on the top of the derrick, and then down into the drill string. As the ship heaves in the swell, an accelerometer located near the ship’s center of gravity measures the movement and feeds the data, in real time, to the WHC. The WHC responds to the ship’s heave by hydraulically moving the compensator sheave to decouple the movement of the ship from the desired movement of the tool string in the borehole (Goldberg, 1990).

In preparation for logging, the boreholes are usually flushed of debris by circulating a “pill” of viscous drilling fluid (sepiolite mud mixed with seawater; approximate weight = 8.8 lb/gal or 1.11 g/cm<sup>3</sup>) through the drill pipe to the bottom of the hole. The bottom-hole assembly (BHA) is pulled up to a depth between 50 and 100 mbsf then run down to the bottom of the hole again to ream borehole irregularities. The hole is subsequently filled with more sepiolite mud, and the pipe is raised to ~50–70 mbsf and kept there to prevent hole collapse during logging. The tool strings are then lowered downhole during sequential runs. During each logging run, incoming data are recorded and monitored in real time on the MCM computer. The tool strings are then pulled up at constant speed to provide continuous measurements as a function of depth of several properties simultaneously. After the logs are acquired, the data are transferred to the downhole measurements laboratory (DHML) and also to LDEO-BRG for processing using a high-speed satellite data link. The LDEO-BRG TAP tool is usually deployed as

F21. Wireline tool strings used during Leg 205, p. 66.



a memory tool. Its preparation and data processing of the LDEO-BRG TAP tool are done in the DHML using a specialized acquisition system.

### Tool Measurement Principles and Applications

The measurement principles and applications of the logging tools are described below. The acronyms and measurement units can be found in Table T7, and principles, applications, and approximate vertical resolution of the tools are summarized in Table T8. More detailed information on individual tools and their geological applications may be found in Ellis (1987), Goldberg (1997), Lovell et al. (1998), Rider (1996), Schlumberger (1989, 1994), Serra (1984, 1986, 1989), and the LDEO-BRG Wireline Logging Services Guide (LDEO-BRG, 2000).

---

T7. Logging tool measurement units and acronyms, p. 75.

---

---

T8. Logging tool specifications, p. 76.

---

### Natural Radioactivity

Two spectral gamma ray tools are usually used to measure and classify natural radioactivity in the formation: the SGT and the HNGS. The SGT uses a sodium iodide scintillation detector and five-window spectroscopy to determine concentrations of potassium (K, in weight percent), thorium (Th, in parts per million), and uranium (U, in parts per million), the three elements whose isotopes dominate the natural radiation spectrum. High K and Th values indicate greater clay concentrations, and increased U values often indicate the presence of organic matter. The HNGS is similar to the SGT, but it uses two bismuth germanate scintillation detectors for a significantly improved tool precision.

The SGT response is sensitive to the borehole diameter, and these diameter effects are corrected during postcruise processing.

### Density

Formation density is determined from the density of electrons in the formation, which is measured with the HLDT. The tool contains a radioactive cesium ( $^{137}\text{Cs}$ ) gamma ray source (622 keV) and far and near gamma ray detectors mounted on a shielded skid, which is pressed against the borehole. Gamma rays emitted by the source undergo Compton scattering, which involves the transfer of energy from gamma rays to the electrons in the formation via elastic collisions. The number of scattered gamma rays that reach the detectors is directly related to the density of electrons in the formation, which is in turn related to bulk density. Porosity may also be derived from this bulk density if the matrix (grain) density is known.

The HLDT also measures the photoelectric effect factor (PEF) caused by absorption of low-energy gamma rays. Photoelectric absorption occurs when gamma rays reach <150 keV after being repeatedly scattered by electrons in the formation. Because PEF depends on the atomic number of the elements in the formation, it varies according to the chemical composition and is essentially independent of porosity. For example, the PEF of pure calcite = 5.08 b/e<sup>-</sup>; illite = 3.03 b/e<sup>-</sup>; quartz = 1.81 b/e<sup>-</sup>; and kaolinite = 1.49 b/e<sup>-</sup>. PEF values can be used in combination with SGT curves to identify different types of clay minerals. Coupling between the tool and borehole wall is essential for good HLDT logs. Poor contact results in underestimation of density values. Poor contact may occur when the borehole diameter is greater than the length of the caliper (e.g., for borehole diameters >48 cm).

The depth of investigation into the formation of the lithodensity tool is of the order of tens of centimeters, depending on the density of the rock.

### **Porosity**

Formation porosity, usually called neutron porosity, is measured with the APS. The sonde incorporates a minitron neutron generator that produces fast neutrons (14.4 MeV) and five neutron detectors (four epithermal and one thermal) positioned at differing intervals from the minitron. The measurement principle involves counting neutrons that arrive at the detectors after being slowed by neutron absorbers surrounding the tool. The highest energy loss occurs when neutrons collide with hydrogen nuclei, which have practically the same mass as the neutron (the neutrons simply bounce off heavier elements without losing much energy). If the hydrogen (i.e., water) concentration is small, as in low-porosity formations, neutrons can travel farther before being captured and the count rates increase at the detector. The opposite effect occurs when the water content is high. However, because hydrogen bound in minerals such as clays or in hydrocarbons also contributes to the measurement, the raw porosity value is often an overestimate.

Upon reaching thermal energies (0.025 eV), the neutrons are captured by the nuclei of Cl, Si, B, and other elements, resulting in a gamma ray emission. This neutron capture cross section ( $\Sigma f$ ) is also measured by the tool.

### **Electrical Resistivity**

The DIT, a conductivity-sensitive device, is most accurate in low- to medium-resistivity formations and is commonly used to measure the formation electrical resistivity.

The DIT has a deep-reading induction device (IDPH), a medium-reading induction device (IMPH), a spherically focused log device (SFLU), and an SP device. The two induction devices transmit high-frequency alternating currents through transmitter coils, creating time-varying magnetic fields that induce currents in the formation. These induced currents create, again, a magnetic field that induces new currents in the receiver coils producing a voltage. These induced currents are proportional to the conductivity of the formation so the voltage is proportional to the resistivity of the formation. The SFLU is a shallow-penetration galvanic device that measures the current necessary to maintain a constant voltage drop across a fixed interval of the formation. In high-resistivity formations ( $>100 \Omega\text{m}$ ), both inductive IDPH and IMPH measurements may be erroneous but the error can be greatly reduced by downhole calibration if a massive formation exists of exceedingly high resistivity.

SPs can originate from a variety of causes: electrochemical, electrothermal, electrokinetic streaming potentials, and membrane potentials because of differences in the mobility of ions in the pore and drilling fluids. SP may be useful to infer fluid flow zones and formation permeability.

### **Temperature, Acceleration, and Pressure**

Downhole temperature, acceleration, and pressure are measured with the LDEO TAP tool. When attached to the bottom of the triple combo

tool string, the LDEO TAP tool is run in an autonomous mode, with data stored in built-in memory. Two thermistors are mounted near the bottom of the tool to detect borehole fluid temperatures at different rates. A thin fast-response thermistor is able to detect small abrupt changes in temperature. A thicker slow-response thermistor is used to estimate temperature gradients and thermal regimes more accurately. The pressure transducer is included to activate the tool at a specified depth. A three-axis accelerometer measures tool movement downhole, providing data for analyzing the effects of heave on a deployed tool string, which should eventually lead to a finer adjustment of the wireline heave compensator.

The borehole temperature record provides information on the thermal regime of the surrounding formation. The vertical heat flow can be estimated from the vertical temperature gradient combined with measurements of the thermal conductivity from core samples.

The temperature record must be interpreted with caution, as the amount of time elapsed between the end of drilling and the logging operation is generally not sufficient to allow the borehole to recover thermally from the influence of drilling fluid circulations. The data recorded under such circumstances may differ significantly from the thermal equilibrium of that environment. Nevertheless, from the spatial temperature gradient it is possible to identify abrupt temperature changes that may represent localized fluid flow into the borehole, indicative of fluid pathways and fracturing and/or breaks in the temperature gradient that may correspond to contrasts in permeability at lithologic boundaries.

### **Acoustic Velocity**

The DSI tool employs a combination of monopole and dipole transducers to make accurate measurements of sonic wave propagation in a wide variety of formations (Shipboard Scientific Party, 1998). In addition to a robust and high-quality measurement of compressional wave velocity, the DSI excites a flexural mode in the borehole that can be used to estimate shear wave velocity even in highly unconsolidated formations. When the formation shear velocity is less than the borehole fluid velocity, particularly in unconsolidated sediments, the flexural wave travels at the shear wave velocity and is the most reliable way to estimate a shear velocity log. Meanwhile, the omnidirectional source generates compressional, shear, and Stoneley waves into hard formations. The configuration of the DSI also allows recording of both in-line and cross-line dipole waveforms. In many cases, the dipole sources could also result in estimates of shear wave velocity in hard rocks better than or equivalent to the monopole source. These combined modes can be used to estimate shear wave splitting caused by preferred mineral and/or structural orientation in consolidated formations. A low-frequency (80 Hz) source enables Stoneley waveforms to be acquired as well.

The DSI measures the transit times between sonic transmitters and an array of eight receiver groups with 15-cm spacing, each consisting of four orthogonal elements that are aligned with the dipole transmitters. During acquisition, the output from these 32 individual elements are differenced or summed appropriately to produce in-line and cross-line dipole signals or monopole-equivalent (compressional and Stoneley) waveforms, depending on the operation modes. The detailed descrip-

tion of tool configuration and data processing are described in the Leg 174B *Initial Reports* volume (Shipboard Scientific Party, 1998).

### **Formation MicroScanner**

The FMS provides high-resolution electrical resistivity-derived images of borehole walls. The tool has four orthogonal arms with pads, each containing 16 button electrodes that are pressed against the borehole wall during the recording. The electrodes are arranged in two diagonally offset rows of eight electrodes each and are spaced ~2.5 mm apart. A focused current is emitted from the four pads into the formation, with a return electrode near the top of the tool. Array buttons on each of the pads measure the current intensity variations. Processing transforms these measurements of the resistivity variations of the formation into continuous, spatially oriented high-resolution images that mimic geologic structures behind the borehole walls. Further processing can provide measurements of dip and direction (azimuth) of planar features in the formation. FMS images are particularly useful for mapping structural features, dip determination, detailed core-log correlation, positioning of core sections with poor recovery, and analysis of depositional environments and stress distribution.

The FMS image is sensitive to structures within ~25 cm beyond the borehole wall and has a maximum vertical resolution of 5 mm with the coverage of 25% of borehole wall for a borehole diameter of 9 $\frac{7}{8}$  in (i.e., RCB bit size). FMS logging commonly includes two passes, the images of which are merged to improve the borehole wall coverage. To produce reliable FMS images, however, the pads must be firmly pressed against the borehole wall. The maximum borehole deviation where good data can be recorded with this tool is 10°. Irregular borehole walls will also adversely affect the images because contact with the wall is poor.

### **Accelerometry and Magnetic Field Measurement**

Three-component acceleration and magnetic field measurements are made with the GPIT. The primary purpose of this tool, which incorporates a three-component accelerometer and a three-component magnetometer, is to determine the acceleration and orientation of the FMS-sonic tool string during logging. The acceleration data allow more precise determination of log depths than is possible on the basis of cable length alone, as the wireline is subject to both stretching and ship heave. This provides a means of correcting the FMS images for irregular tool motion, allowing the true dip and direction (azimuth) of structures to be determined.

## **Log Data Quality, Processing, and Analysis**

### **Log Data Quality**

The quality of several types of log data may be degraded by excessively wide sections of the borehole or by rapid changes in the hole diameter. If it is irregular, wide, or there are many washouts, there may be problems with those tools that require good contact with the wall (density, porosity, and FMS). Deep investigation measurements such as resistivity and sonic velocity are least sensitive to borehole conditions. Corrections can be applied to the original data to reduce the effects of these



conditions and other departures from the conditions under which the tool has been calibrated.

### **Log Depth Scales**

The depth of the wireline logging measurements is determined from the length of the logging cable played out at the winch on the ship. The seafloor is identified on the natural gamma log by the abrupt reduction in gamma ray count at the water/sediment boundary (mudline). The coring depth (drillers depth) is determined from the known length of the BHA and pipe stands.

Discrepancies between the drillers depth and the wireline log depth occur because of core expansion, incomplete core recovery, drill pipe stretch in the case of drill pipe depth, cable stretch (~1 m/km), and cable slip in the case of log depth. Tidal changes in sea level, up to 1 m in the open ocean, will also have an effect. Precise core-log depth matching is difficult in zones where core recovery is low because of the inherent ambiguity of placing the recovered section within the cored interval.

Logs from different tool strings may also have depth mismatches, caused by either cable stretch or incomplete heave compensation during recording. Distinctive features recorded by the Natural Gamma Ray Spectrometry Tool, run on every tool string, provide relative depth offsets and thus a means of depth shifting for correlation between logging runs.

### **Data Recording and Processing**

Data for each logging run were recorded, stored digitally, and monitored in real time using the MCM software. On completion of logging, data are loaded to the Schlumberger GeoFrame software system in the DHML for onboard preliminary interpretation. Basic processing is carried out postcruise to provide a quality-controlled downhole logging data set that can be used for comparison, integration, and correlation with other data collected during each ODP leg. The processing includes depth adjustments to remove depth offsets between data from different logging runs; corrections specific to certain tools and logs; documentation for the logs (with an assessment of log quality); and conversion of the data to a widely accessible format (ASCII for the conventional logs and GIF for the FMS images). Schlumberger's GeoFrame software package is used for most of the processing.

Processed acoustic, caliper, density, gamma ray, magnetic, neutron porosity, resistivity, and temperature data in are available in ASCII.

## REFERENCES

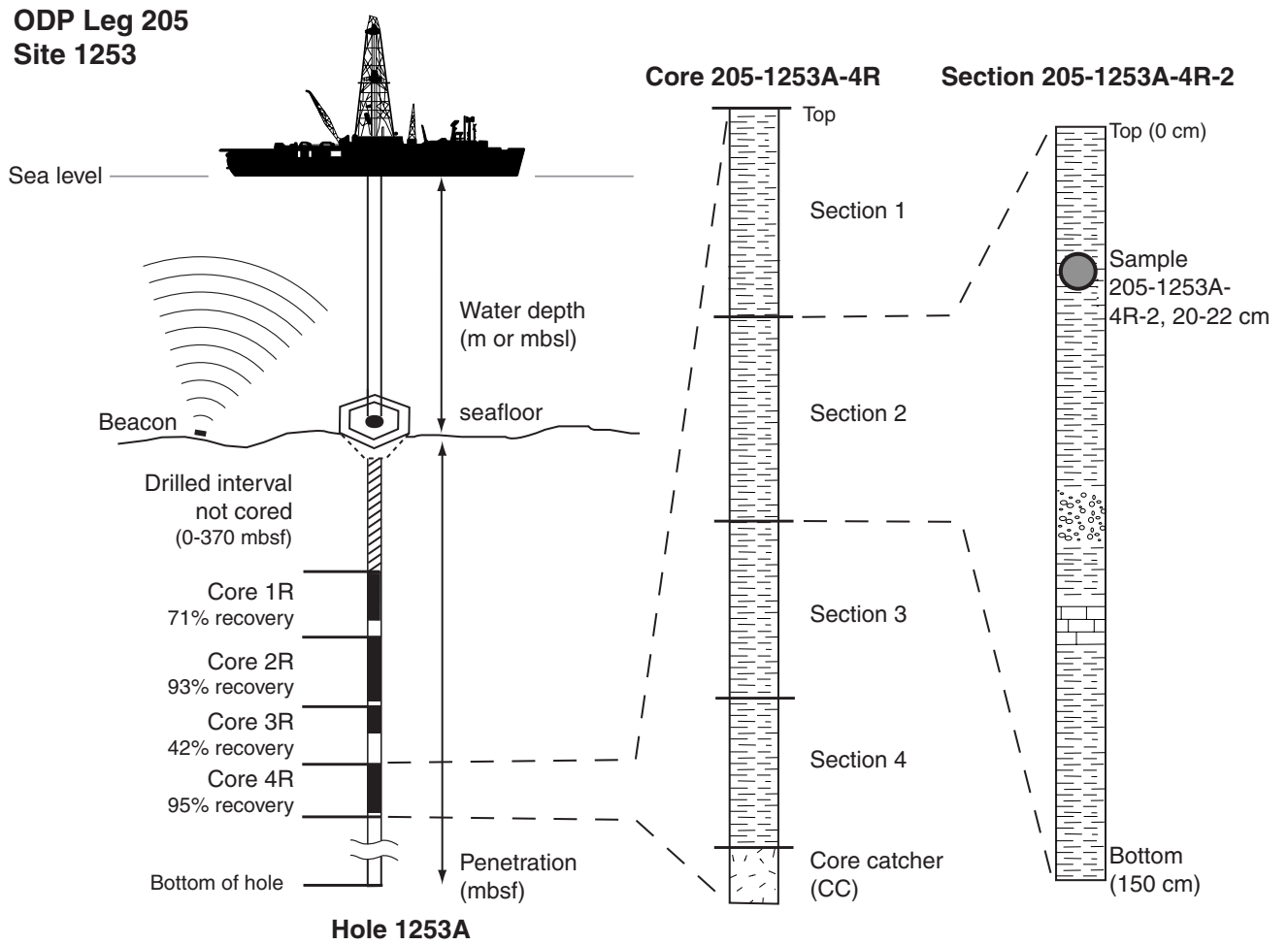
- Balsam, W.L., and Damuth, J.E., 2000. Further investigations of shipboard vs. shore-based spectral data: implications for interpreting Leg 164 sediment composition. *In* Paull, C.K., Matsumoto, R., Wallace, P., and Dillon, W.P. (Eds.), *Proc. ODP, Sci. Results*, 164: College Station, TX (Ocean Drilling Program), 313–324.
- Balsam, W.L., Damuth, J.E., and Schneider, R.R., 1997. Comparison of shipboard vs. shore-based spectral data from Amazon-Fan cores: implications for interpreting sediment composition. *In* Flood, R.D., Piper, D.J.W., Klaus, A., and Peterson, L.C. (Eds.), *Proc. ODP, Sci. Results*, 155: College Station, TX (Ocean Drilling Program), 193–215.
- Balsam, W.L., Deaton, B.C., and Damuth, J.E., 1998. The effects of water content on diffuse reflectance measurements of deep-sea core samples: an example from ODP Leg 164 sediments. *Mar. Geol.*, 149:177–189.
- Berggren, W.A., Hilgen, F.J., Langereis, C.G., Kent, D.V., Obradovich, J.D., Raffi, I., Raymo, M.E., and Shackleton, N.J., 1995a. Late Neogene chronology: new perspectives in high-resolution stratigraphy. *Geol. Soc. Am. Bull.*, 107:1272–1287.
- Berggren, W.A., Kent, D.V., Swisher, C.C., III, and Aubry, M.-P., 1995b. A revised Cenozoic geochronology and chronostratigraphy. *In* Berggren, W.A., Kent, D.V., Aubry, M.-P., and Hardenbol, J. (Eds.), *Geochronology, Time Scales and Global Stratigraphic Correlation*. Spec. Publ.—SEPM, 54:129–212.
- Blum, P., 1997. Physical properties handbook: a guide to the shipboard measurement of physical properties of deep-sea cores. *ODP Tech. Note*, 26 [Online]. Available from World Wide Web: <<http://www-odp.tamu.edu/publications/tnotes/tn26/INDEX.HTM>>. [Cited 2002-09-02]
- Boyce, R.E., 1976. Definitions and laboratory techniques of compressional sound velocity parameters and wet-water content, wet-bulk density, and porosity parameters by gravimetric and gamma-ray attenuation techniques. *In* Schlanger, S.O., Jackson, E.D., et al., *Init. Repts. DSDP*, 33: Washington (U.S. Govt. Printing Office), 931–958.
- Bullard, E.C., 1954. The flow of heat through the floor of the Atlantic Ocean. *Proc. R. Soc. London A*, 222:408–429.
- Christie, D.M., Pedersen, R.B., Miller, D.J., et al., 2001. *Proc. ODP, Init. Repts.*, 187 [CD-ROM]. Available from: Ocean Drilling Program, Texas A&M University, College Station TX 77845-9547, USA.
- Davis, E.E., Villinger, H., MacDonald, R.D., Meldrum, R.D., and Grigel, J., 1997. A robust rapid-response probe for measuring bottom-hole temperatures in deep-ocean boreholes. *Mar. Geophys. Res.*, 19:267–281.
- Edwards, K.J., Bond, P.L., and Banfield, J.F., 2000. Characteristics of attachment and growth of *Thiobacillus caldus* on sulphide minerals: a chemotactic response to sulphur minerals. *Environ. Microbiol.*, 2:324–332.
- Ellis, D.V., 1987. *Well Logging for Earth Scientists*: New York (Elsevier).
- Emeis, K.-C., and Kvenvolden, K.A., 1986. Shipboard organic geochemistry on *JOIDES Resolution*. *ODP Tech. Note*, 7.
- Espitalié, J., Deroo, G., and Marquis, F., 1986. La pyrolyse Rock-Eval et ses applications, Partie III. *Rev. Inst. Fr. Pet.*, 41:73–89.
- Fisher, A.T., and Underwood, M.B., 1995. Calibration of an X-ray diffraction method to determine relative mineral abundances in bulk powders using matrix singular value decomposition: a test from the Barbados accretionary complex. *In* Shipley, T.H., Ogawa, Y., Blum, P., et al., *Proc. ODP, Init. Repts.*, 156: College Station, TX (Ocean Drilling Program), 29–37.
- Fisk, M.R., Giovannoni, S.J., and Thorseth, I.H., 1998. Alteration of oceanic volcanic glass: textural evidence of microbial activity. *Science*, 281:978–980.

- Furnes, H., Muehlenbachs, K., Tumyr, O., Torsvik, T., and Thorseth, I.H., 1999. Depth of active bio-alteration in the ocean crust: Costa Rica rift (Hole 504B). *Terra Nova*, 11:228–233.
- Furnes, H., and Staudigel, H., 1999. Biological mediation in ocean crust alteration: how deep is the deep biosphere? *Earth Planet. Sci. Lett.*, 166:97–103.
- Gieskes, J., Gamo, T., and Brumsack, H.-J., 1991. Chemical methods for interstitial water analysis aboard *JOIDES Resolution*. *ODP Tech. Note*, 15 [Online]. Available from World Wide Web: <[http://www-odp.tamu.edu/publications/tnotes/tn15/f\\_chem1.htm](http://www-odp.tamu.edu/publications/tnotes/tn15/f_chem1.htm)>. [Cited 2002-09-21]
- Gladney, E.S., Jones, E.A., Nickell, E.J., and Roelandts, I., 1990. 1988 compilation of elemental concentration data for USGS basalt BCR-1. *Geostand. Newsl.*, 14:209–359.
- Gladney, E.S., and Roelandts, I., 1988. 1987 compilation of elemental concentration data from USGS BHOV-1, MAG-1, QLO-1, RGM-1, SCo-1, SDC-1, SGR-1 and STM-1. *Geostand. Newsl.*, 12:253–262.
- Goldberg, D., 1990. Test performance of the Ocean Drilling Program wireline heave motion compensator. *Sci. Drill.*, 1:206–209.
- , 1997. The role of downhole measurements in marine geology and geophysics. *Rev. Geophys.*, 35:315–342.
- Graber, K.K., Pollard, E., Jonasson, B., and Schulte, E. (Eds.), 2002. Overview of Ocean Drilling Program Engineering Tools and Hardware. *ODP Tech. Note*, 31 [Online]. Available from World Wide Web: <<http://www-odp.tamu.edu/publications/tnotes/tn31/INDEX.HTM>>. [Cited 2002-09-21]
- Hanert, H.H., 1992. The genus *Gallionella*. In Balows, A., Truper, H.F., Dworkin, M., Harder, W., and Schleifer, K.H. (Eds.), *The Prokaryotes* (2nd ed.) (Vol. 4): New York (Springer-Verlag), 4082–4088.
- Heesemann, M., 2002. Modeling and analysis of transient pressure measurements in ODP boreholes for undisturbed formation pressure estimation [M.S. thesis]. Univ. Bremen, Bremen, Germany.
- Hoppie, B.W., Blum, P., and the Shipboard Scientific Party, 1994. Natural gamma-ray measurements on ODP cores: introduction to procedures with examples from Leg 150. In Mountain, G.S., Miller, K.G., Blum, P., et al., *Proc. ODP, Init. Repts.*, 150: College Station, TX (Ocean Drilling Program), 51–59.
- Horai, K., and Von Herzen, R.P., 1985. Measurement of heat flow on Leg 86 of the Deep Sea Drilling Project. In Heath, G.R., Burckle, L.H., et al., *Init. Repts. DSDP*, 86: Washington (U.S. Govt. Printing Office), 759–777.
- Kimura, G., Silver, E.A., Blum, P., et al., 1997. *Proc. ODP, Init. Repts.*, 170: College Station, TX (Ocean Drilling Program).
- Lamont-Doherty Earth Observatory–Borehole Research Group, 2000. *ODP Logging Manual: An Electronic Guide to ODP Logging Services*, Version 2.0, [CD-ROM]. Available from: Lamont-Doherty Earth Observatory, Columbia University, Palisades NY 10964, USA.
- Lovell, M.A., Harvey, P.K., Brewer, T.S., Williams, C., Jackson, P.D., and Williamson, G., 1998. Application of FMS images in the Ocean Drilling Program: an overview. In Cramp, A., MacLeod, C.J., Lee, S.V., and Jones, E.J.W. (Eds.), *Geological Evolution of Ocean Basins: Results from the Ocean Drilling Program*. Spec. Publ.—Geol. Soc. London, 131:287–303.
- Lowrie, W., 1990. Identification of ferromagnetic minerals in a rock by coercivity and unblocking temperature properties. *Geophys. Res. Lett.*, 17:159–162.
- Lundberg, N., and Moore, J.C., 1986. Macroscopic structural features in Deep Sea Drilling Project cores from forearc regions. In Moore, J.C. (Ed.), *Structural Fabric in Deep Sea Drilling Project Cores From Forearcs*. Mem.—Geol. Soc. Am., 166:13–44.
- MacKenzie, W.S., Donaldson, C.H., and Guilford, C., 1982. *Atlas of Igneous Rocks and their Textures*: Harlow, England (Longman).

- Manheim, F.T., and Sayles, F.L., 1974. Composition and origin of interstitial waters of marine sediments, based on deep sea drill cores. *In* Goldberg, E.D. (Ed.), *The Sea* (Vol. 5): *Marine Chemistry: The Sedimentary Cycle*: New York (Wiley), 527–568.
- Mazzullo, J.M., Meyer, A., and Kidd, R.B., 1988. New sediment classification scheme for the Ocean Drilling Program. *In* Mazzullo, J., and Graham, A.G. (Eds.), *Handbook for Shipboard Sedimentologists*. *ODP Tech. Note*, 8:45–67.
- Moore, G.F., Taira, A., Klaus, A., et al., 2001. *Proc. ODP, Init. Repts.*, 190 [CD-ROM]. Available from: Ocean Drilling Program, Texas A&M University, College Station TX 77845-9547, USA.
- Murray, R.W., Miller, D.J., and Kryc, K.A., 2000. Analysis of major and trace elements in rocks, sediments, and interstitial waters by inductively coupled plasma–atomic emission spectrometry (ICP–AES). *ODP Tech. Note*, 29 [Online]. Available from World Wide Web: <<http://www-odp.tamu.edu/publications/tnotes/tn29/INDEX.HTM>>. [Cited 2002-09-21]
- Parkes, R.J., Cragg, B.A., Bale, S.J., Getliff, J.M., Goodman, K., Rochelle, P.A., Fry, J.C., Weightman, A.J., and Harvey, S.M., 1994. A deep bacterial biosphere in Pacific Ocean sediments. *Nature*, 371:410–413.
- Pfender, M., and Villinger, H., 2002. Miniaturized data loggers for deep sea sediment temperature gradient measurements. *Mar. Geol.*, 186:557–570.
- Pimmel, A., and Claypool, G., 2001. Introduction to shipboard organic geochemistry on the *JOIDES Resolution*. *ODP Tech. Note*, 30 [Online]. Available from World Wide Web: <<http://www-odp.tamu.edu/publications/tnotes/tn30/INDEX.HTM>>. [Cited 2002-09-21]
- Plank, T., Ludden, J.N., Escutia, C., et al., 2000. *Proc. ODP, Init. Repts.*, 185 [CD-ROM]. Available from: Ocean Drilling Program, Texas A&M University, College Station TX 77845-9547, USA.
- Pribnow, D.F.C., Kinoshita, M., and Stein, C.A., 2000. Thermal data collection and heat flow recalculations for ODP Legs 101–180. Institute for Joint Geoscientific Research, GGA, Hanover, Germany, 0120432. Available from World Wide Web: <<http://www-odp.tamu.edu/publications/heatflow/ODPreprt.pdf>>. [Cited 2002-09-21]
- Rider, M.H., 1996. *The Geological Interpretation of Well Logs* (2nd ed.): Caithness (Whittles Publishing).
- Rothwell, R.G., 1989. *Identification of Minerals and Mineraloids in Marine Sediments*: London and New York (Elsevier Appl. Sci.).
- Schlumberger, 1989. *Log Interpretation Principles/Applications*: Houston (Schlumberger Educ. Services), SMP-7017.
- , 1994. *IPL Integrated Porosity Lithology*: Houston (Schlumberger Wireline and Testing), SMP-9270.
- Schlumberger, C., Schlumberger, M., and Leonardon, E.G., 1934. Electric coring: a method of determining bottom-hole data by electrical measurement. *Trans. AIME*, 110:237–272.
- Serra, O., 1984. *Fundamentals of Well-Log Interpretation* (Vol. 1): *The Acquisition of Logging Data*. Dev. Pet. Sci., 15A.
- , 1986. *Fundamentals of Well-Log Interpretation* (Vol. 2): *The Interpretation of Logging Data*. Dev. Pet. Sci., 15B.
- , 1989. *Formation MicroScanner Image Interpretation*: Houston (Schlumberger Educ. Services), SMP-7028.
- Shepard, F.P., 1954. Nomenclature based on sand-silt-clay ratios. *J. Sediment. Petrol.*, 24:151–158.
- Shipboard Scientific Party, 1998. Introduction. *In* Becker, K., Malone, M.J., et al., *Proc. ODP, Init. Repts.*, 174B: College Station, TX (Ocean Drilling Program), 3–9.
- , 2001. Explanatory notes. *In* Christie, D.M., Pedersen, R.B., Miller, D.J., et al., *Proc. ODP, Init. Repts.*, 187, 1–42 [CD-ROM]. Available from: Ocean Drilling Program, Texas A&M University, College Station TX 77845-9547, USA.

- , 2003. Explanatory Notes. *In* Tréhu, A., Bohrmann, G., and Rack, F., et al., *Proc. ODP, Init. Repts.*, 204, 1–102 [CD-ROM]. Available from: Ocean Drilling Program, Texas A&M University, College Station TX 77845-9547, USA.
- Smith, D.C., Spivack, A.J., Fisk, M.R., Haveman, S.A., Staudigel, H., and ODP Leg 185 Shipboard Scientific Party, 2000a. Methods for quantifying potential microbial contamination during deep ocean coring. *ODP Tech. Note*, 28 [Online]. Available from the World Wide Web: <<http://www-odp.tamu.edu/publications/tnotes/tn28/INDEX.HTM>>. [Cited 2002-09-21]
- , 2000b. Tracer-based estimates of drilling-induced microbial contamination of deep sea crust. *Geomicrobiol. J.*, 17:207–219.
- Taira, A., Hill, I., Firth, J.V., et al., 1991. *Proc. ODP, Init. Repts.*, 131: College Station, TX (Ocean Drilling Program).
- Terry, R.D., and Chilingar, G.V., 1955. Summary of “Concerning some additional aids in studying sedimentary formations” by M.S. Shvetsov. *J. Sediment. Petrol.*, 25:229–234.
- Tissot, B.P., and Welte, D.H., 1984. *Petroleum Formation and Occurrence* (2nd ed.): Heidelberg (Springer-Verlag).
- Von Herzen, R.P., and Maxwell, A.E., 1959. The measurement of thermal conductivity of deep-sea sediments by a needle-probe method. *J. Geophys. Res.*, 64:1557–1563.
- Wellsbury, P., Goodman, K., Barth, T., Cragg, B.A., Barnes, S.P., and Parkes, R.J., 1997. Deep marine biosphere fueled by increasing organic matter availability during burial and heating. *Nature*, 388:573–576.
- Wentworth, C.K., 1922. A scale of grade and class terms of clastic sediments. *J. Geol.*, 30:377–392.
- Whitman, W.B., Coleman, D.C., and Wiebe, W.J., 1998. Prokaryotes: the unseen majority. *Proc. Nat. Acad. Sci. U.S.A.*, 95:6578–6583.
- Whittle, A.J., Sutabutr, T., Germaine, J.T., and Varney, A., 2001. Prediction and measurement of pore pressure dissipation for a tapered piezocone. *Offshore Technol. Conf.*, Pap. 13155.

Figure F1. Diagram illustrating core, section, and sample numbering.



**Figure F2.** Graphic patterns used on AppleCORE barrel sheets to indicate lithologies encountered during Leg 205. Also shown are symbols for sedimentary structures, deformation features, samples, and coring/drilling disturbance in soft sediment and hard sedimentary rock.

**Legend**


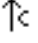






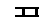


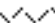






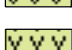


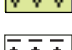














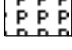


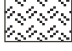




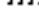



















<b>Lithologies</b>	<b>Physical structures</b>	<b>Lithologic accessories</b>
 Conglomerate	 Coarsening upward	 Shale lamina
 Gravel	 Fining upward	 Thin siliceous layer
 Sand or sandstone	 Normal graded bedding	 Thin calcareous layer
 Silt or siltstone	 Reverse graded bedding	 Thin ash layer
 Clay or claystone	 Planar tabular bedding	 Pebbles/granules
 Diatomite	 Planar laminae	 Patch of minor lithology
 Spiculite	 High-angle tabular bedding	 Lithoclast
 Siliceous claystone	 Low-angle tabular bedding	 Pumice
 Nannofossil chalk	 Wavy parallel bedding	 Wood fragments
 Foraminiferal chalk	 Ripple cross-laminae	 General nodule/concretion
 Limestone	 Lenticular bedding	 Pyrite nodule
 Packstone	 Convolute bedding	 Calcite cement
 Volcanic ash or tuff	 Isolated lamina, color band	 Black band
 Gabbro	 Silt lamina	 Green clay
 Extracted core sample (e.g., whole-round sample)	 Sand lamina	 Chalcedony/chert concretion
	 Chaotic bedding	 Breccia horizon
	 Slump folds	 Mottled
	 Pebbles/granules/sand	
	 Macrofault (normal)	
	 Macrofault (reverse)	
	<b>Ichnofossils</b>	<b>Core disturbance</b>
	 <i>Zoophycos</i>	 Disturbed
	 <i>Chondrites</i>	 Soupy
	 <i>Planolites</i>	 Biscuit
	 <i>Ophiomorpha</i>	 Fractured
	 Undefined burrow	 Slurry
		 Highly fragmented
		 Drilling breccia

Figure F3. Classification scheme for sediments showing the broad divisions between clastic, volcanoclastic, and carbonates of both neritic and pelagic types. Sediments with no clear dominant component are classified as “mixed sediments.”

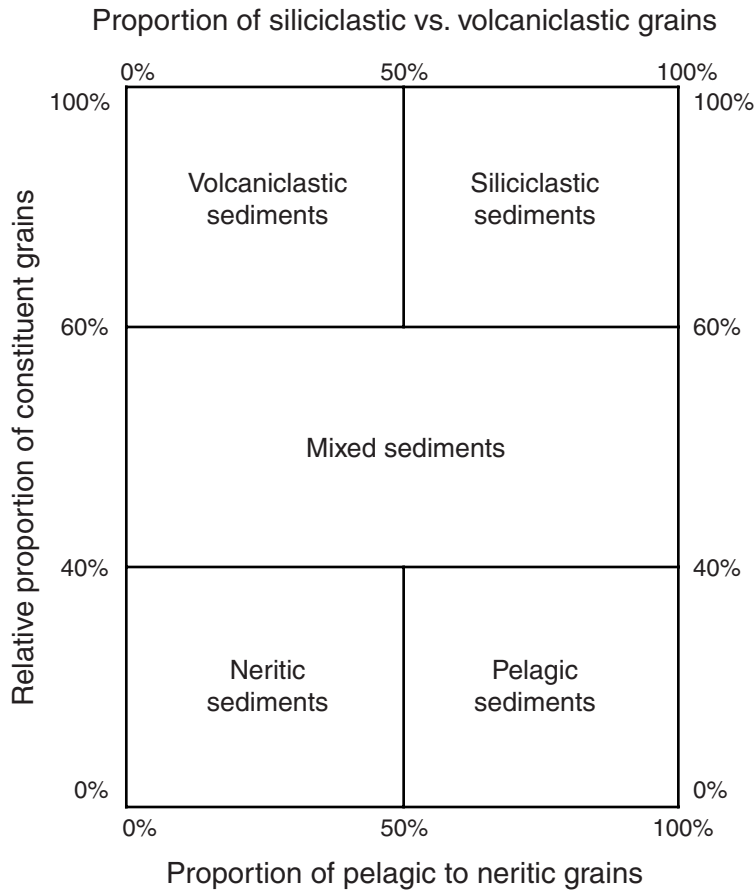
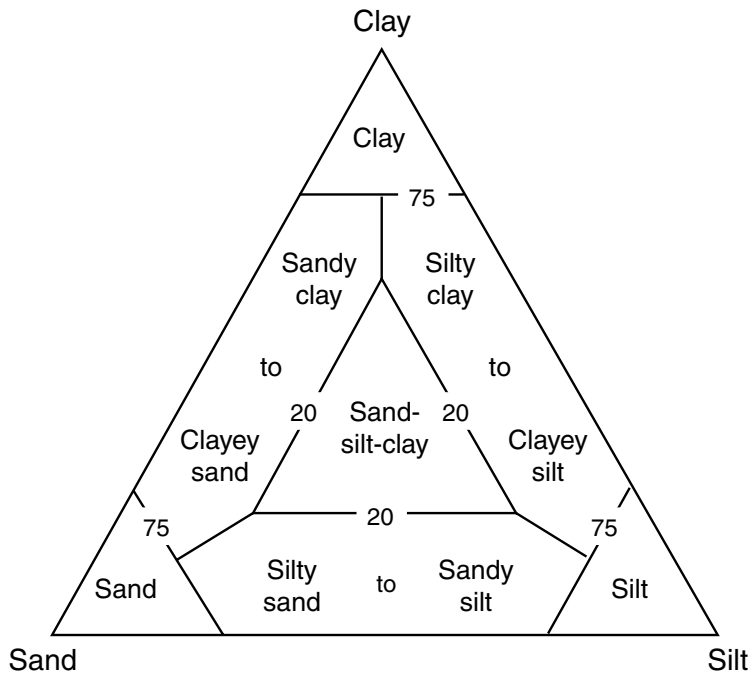




Figure F4. Ternary plot showing the naming scheme for clastic and volcaniclastic sediments based on the grain size distribution.





**Figure F6.** Example of a Leg 205 igneous rock visual core description (VCD). See Figure F7, p. 52, for definitions of abbreviations used in the igneous rock VCDs.

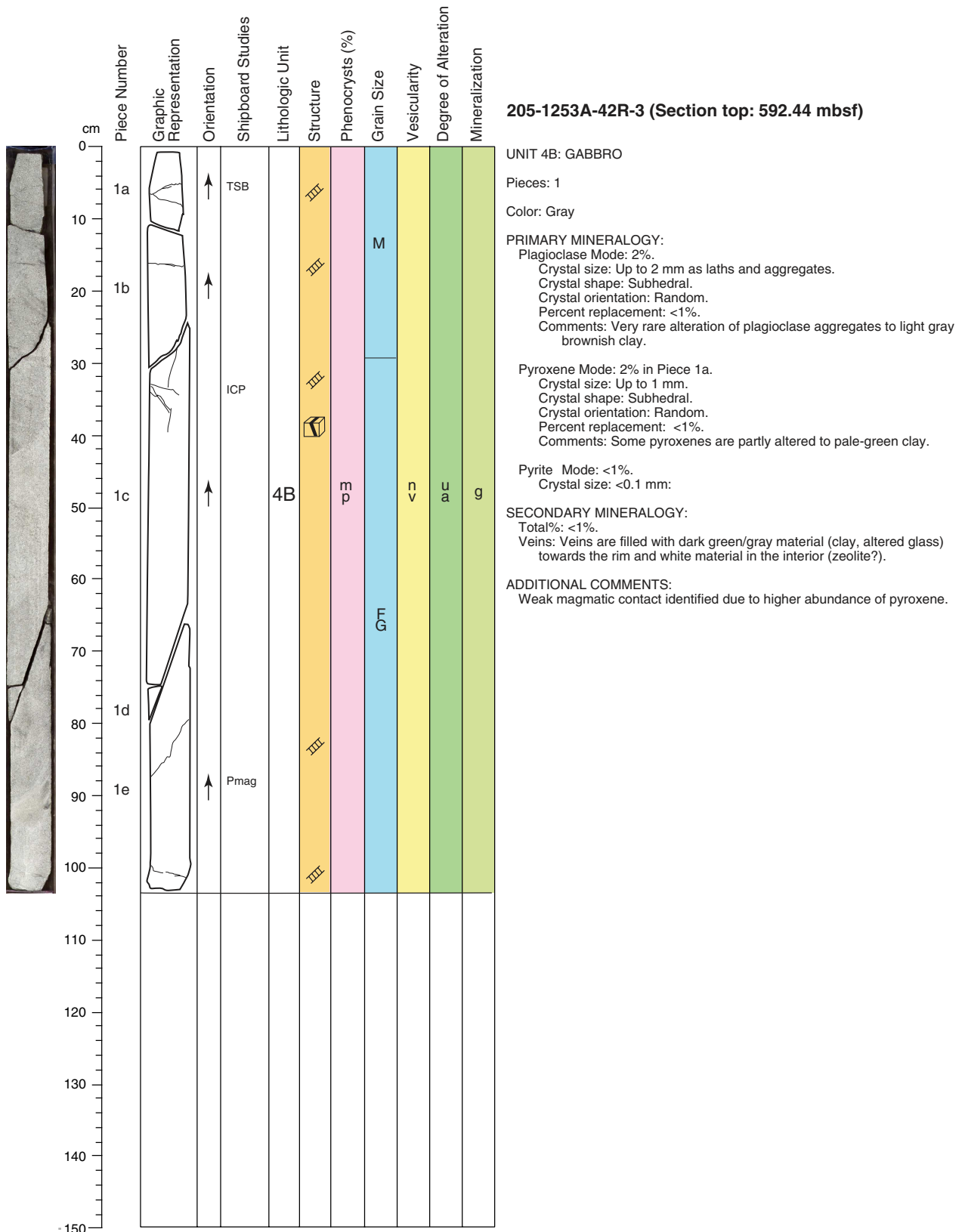


Figure F7. Igneous texture/structure definitions and abbreviations used for the visual core description.

Igneous texture/structure definitions and abbreviations

Structure						
Phenocryst	a Aphyric (<1%)	s p Sparsely phyric (1%-2%)	m p Moderately phyric (2%-10%)	h p Highly phyric (>10%)		
Grain size	G Glass	a p Aphanitic (<1 mm)	F G Fine grained (1-2 mm)	M G Medium grained (2-5 mm)	M Microcrystalline groundmass	C Cryptocrystalline groundmass
Vesicularity	n v Nonvesicular (<1%)	s p v Sparsely vesicular (1%-5%)	m o v Moderately vesicular (5%-20%)	h i v Highly vesicular (>20%)		
Degree of alteration	u a Unaltered (<2%)	s Slight (2%-10%)	m Moderate (10%-40%)	h High (40%-80%)	vh Very high (80%-95%)	c Complete (95%-100%)
Mineralization	p y r g Pyrite in the groundmass					

Figure F8. Thin section description form used during Leg 205.

<b>THIN SECTION:</b> 205-1253A-8R-1, 24-27 cm		<b>Piece No.:</b> 2B		<b>Unit:</b> 4A		<b>ODP TSP#:</b> 13		<b>OBSERVER:</b> BS, VC, JM	
<b>ROCK NAME:</b> Gabbro		<b>SHIPBOARD STUDIES</b>							
<b>WHERE SAMPLED:</b>									
<b>GRAIN SIZE:</b> Fine-grained gabbro.									
<b>TEXTURE:</b>									
PRIMARY MINERALOGY	% OBSERVED	% ALTERED	SIZE (mm)			MORPHOLOGY	COMMENTS		
			min.	max.	av.				
Plagioclase	10	5	0.6	1.8	0.8	Subhedral	An65; altered along cracks		
Clinopyroxene	3	2	0.4	0.8	0.5	Subhedral	Slightly altered along cracks		
Opakes	3		0.1	0.4	0.2				
Ilmenite	3		0.4	1	0.6				
Olivine	<1	80					Only remnants of olivine		
Orthopyroxene	<1	2	0.2	0.4	0.2	Subhedral			
GROUNDMASS	% OBSERVED		SIZE (mm)			MORPHOLOGY	COMMENTS		
			min.	max.	av.				
Plagioclase	60		0.1	0.8	0.5	Euhedral to subhedral			
Clinopyroxene	20		0.1	0.3	0.2	Subhedral			
Glass	2						Associated with clay in replacement of olivine		
SECONDARY MINERALOGY	% OBSERVED		SIZE (mm)			REPLACING / FILLING / COMMENTS			
			min.	max.	av.				
Clay	13					Within groundmass; replacing glass (palagonite?); replacement of olivine			
VEINS	FILLING		SIZE (mm)			COMMENTS			
			min.	max.	av.				
VOIDS	% OBSERVED	FILLING	SIZE (mm)			LOCATION / MORPHOLOGY / COMMENTS			
			min.	max.	av.				
<b>AVAILABLE PHOTOMICROGRAPHS</b>									
<b>OVERVIEW</b>		<b>CLOSE UP</b>							
IMAGE # (TSP-CLOSE UP #)	COMMENTS								
TS13-A	Altered clinopyroxene (PPL, 20x, 1.25mm)								
TS13-B	Ilmenite and palagonite clay (PPL, 20x, 1.25mm)								
TS13-C	Replaced olivine by clay (PPL, 40x, 0.625mm)								
TS13-D	Replaced olivine and ilmenite (PPL, 5x, 5mm)								
TS13-E	Replacement of primary mineral (probably plagioclase in this case) by glass and palagonite (PPL, 20x, 1.25mm)								
TS13-F	Partly replaced olivine (XPL, 5x, 5mm)								
TS13-G	Microcrystalline gabbro (XPL, 5x, 5mm)								

**Figure F9.** Symbols used for deformation structures on the computerized visual core description sheets.

	Normal fault		Clastic vein (vein type, dimensions, length, mineral)
	Reverse fault		Dike (dimension, type, mineral, zoning, reaction rim, reaction mineral, zonation)
	Fault		Ductile shear (sense)
	Foliated breccia		Brittle shear (sense)
	Scaly fabric		Slickensides (sense, habit, mineral)
	Stratal disruption		Disjunctive cleavage (orientation)
	Fracture, general		Crenulation cleavage (orientation)
	Conjugate fractures		Fold
	Fracture network		Crystal/plastic fabric (orientation, type, minerals)
	Fracture with brecciation		Crystal/mineral lineation (orientation, minerals)
	Sigmoidal vein		Magmatic fabric (orientation, type, minerals)
	Sediment-filled vein		Compositional/textural variation (orientation)
	Calcite vein		Compositional layering (orientation)
	Vein		Igneous contact (orientation, type)
	Boudin		Sedimentary bedding (orientation, type)
	Fissility		Lamination/color banding (orientation, type)
	Stylolite		Magmatic vein (orientation, dimension, type, mineral, zoning, reaction rim, reaction minerals, zonation)
	Deformation band		
	Foliation (sense)		
	Vesicles		

Figure F10. Structural geology visual description sheet.

**STRUCTURAL GEOLOGY DESCRIPTION**

Leg	Hole	Core	Section	Observer

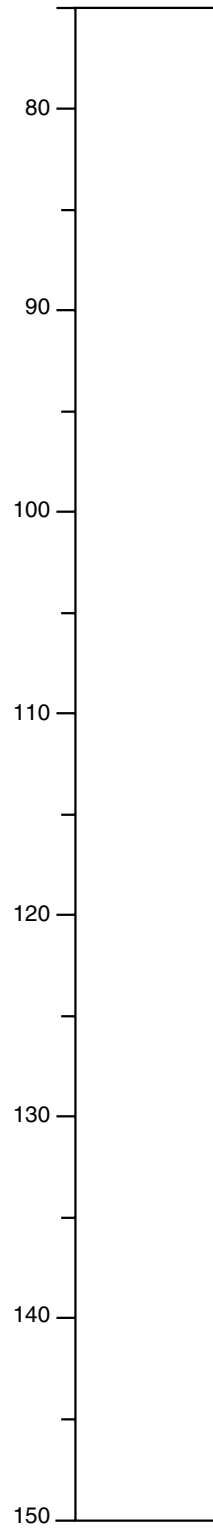
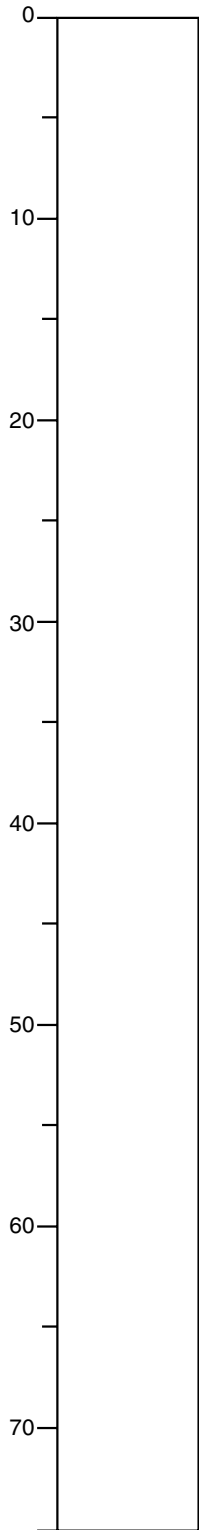






Figure F12. Protractor-goniometer used for measuring orientations of structures in the cores. (A) Drawing of device being used to (B) measure the dip of a structure on the face of a split core, (C) assess the dip of a structure as seen at right angles to the split-core face, and (D) measure the azimuth of a structure as seen on the upper surface of a core.

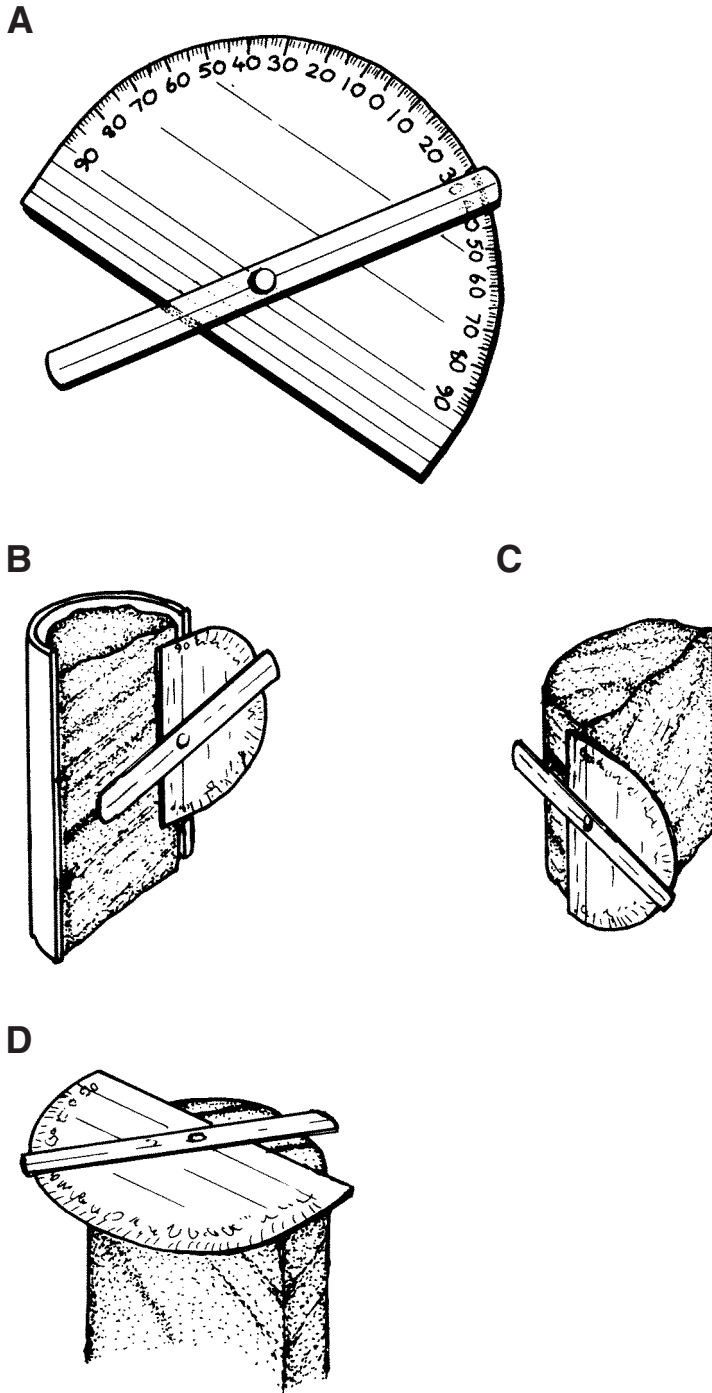


Figure F13. Core reference system used on Leg 205.

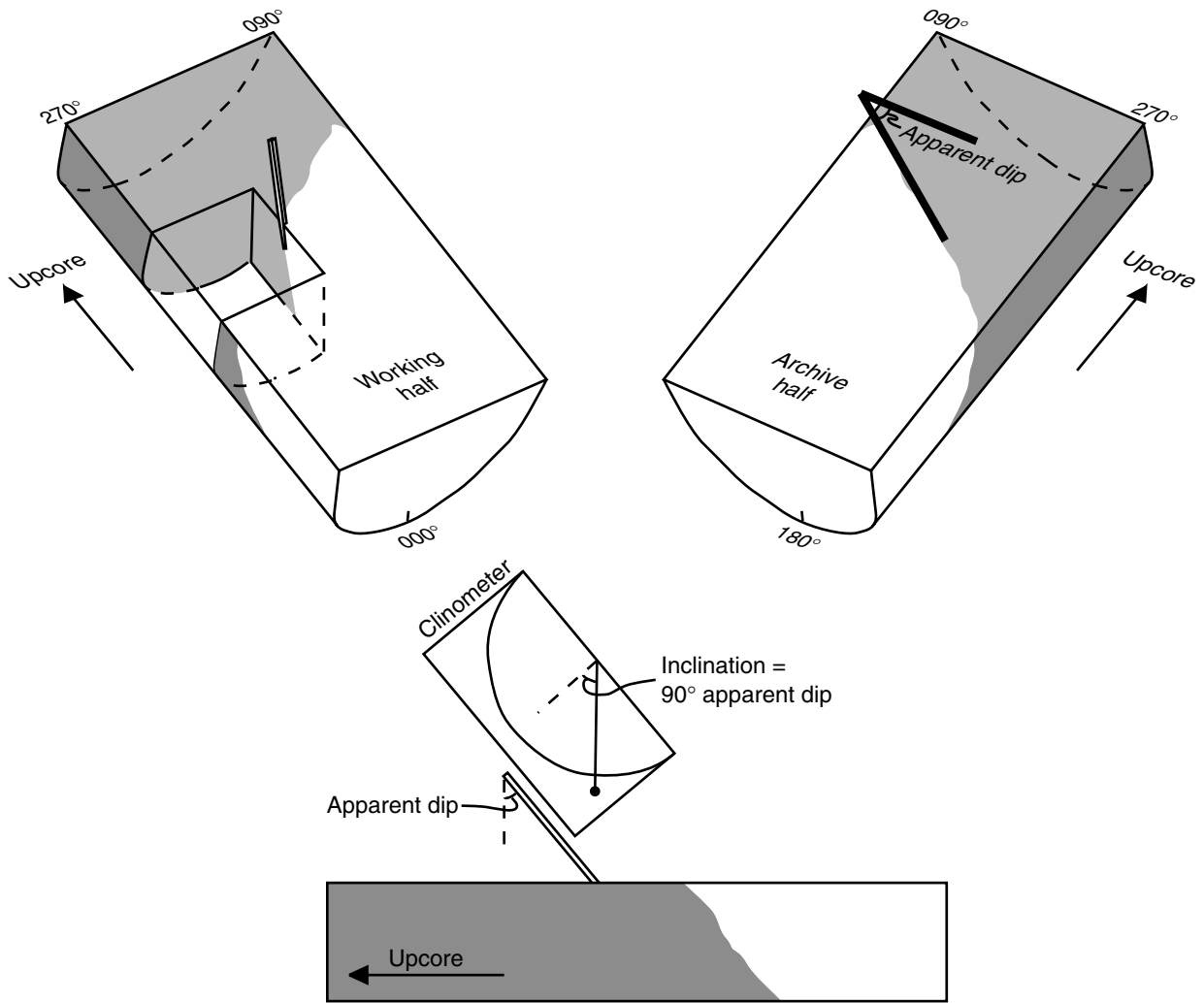
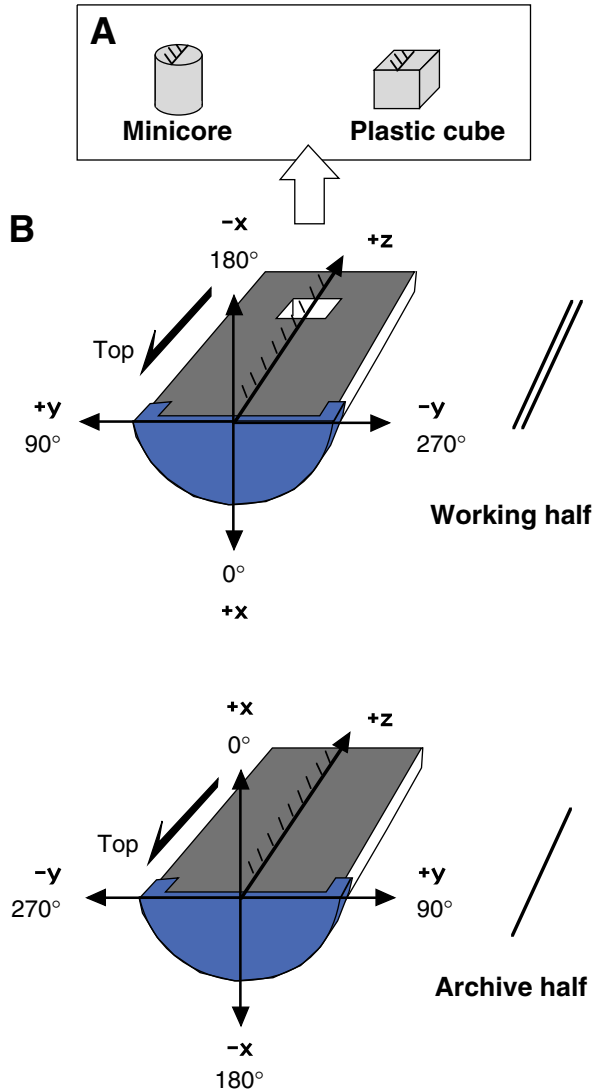
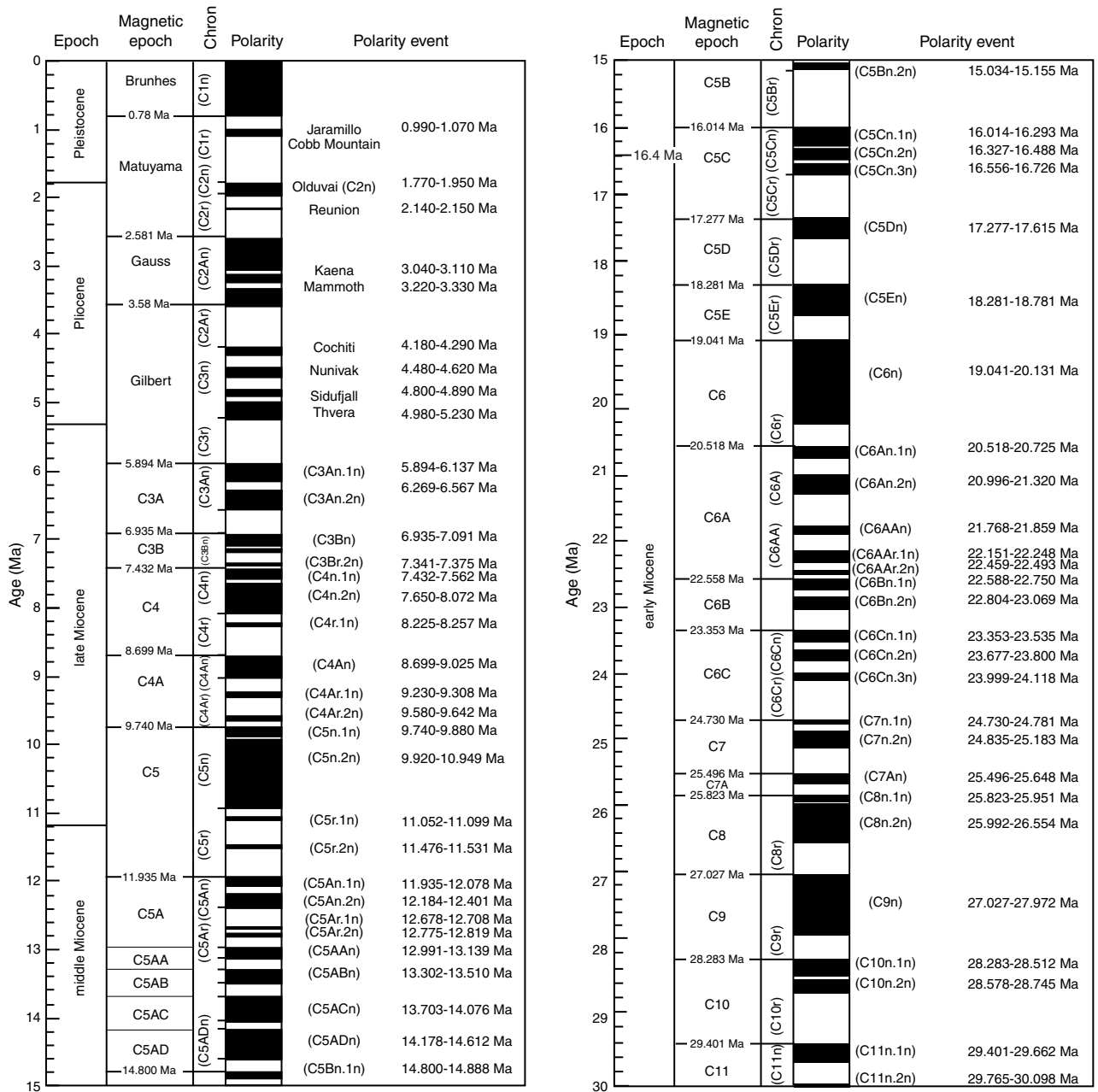


Figure F14. Coordinate systems of ODP cores and discrete samples. A. Orientation of the discrete samples. x- and y-axes of a plastic cube and minicore are opposite directions to those of archive halves. B. The coordinate systems for paleomagnetic measurements of archive- and working-half core sections.

**ODP magnetic direction convention**



**Figure F15.** Magnetostratigraphic timetable used during Leg 205 is based on Berggren et al. (1995a, 1995b).



**Figure F16.** Diagram showing inductively coupled plasma–atomic emission spectroscopy interstitial water sample preparation procedure. conc. = concentration.

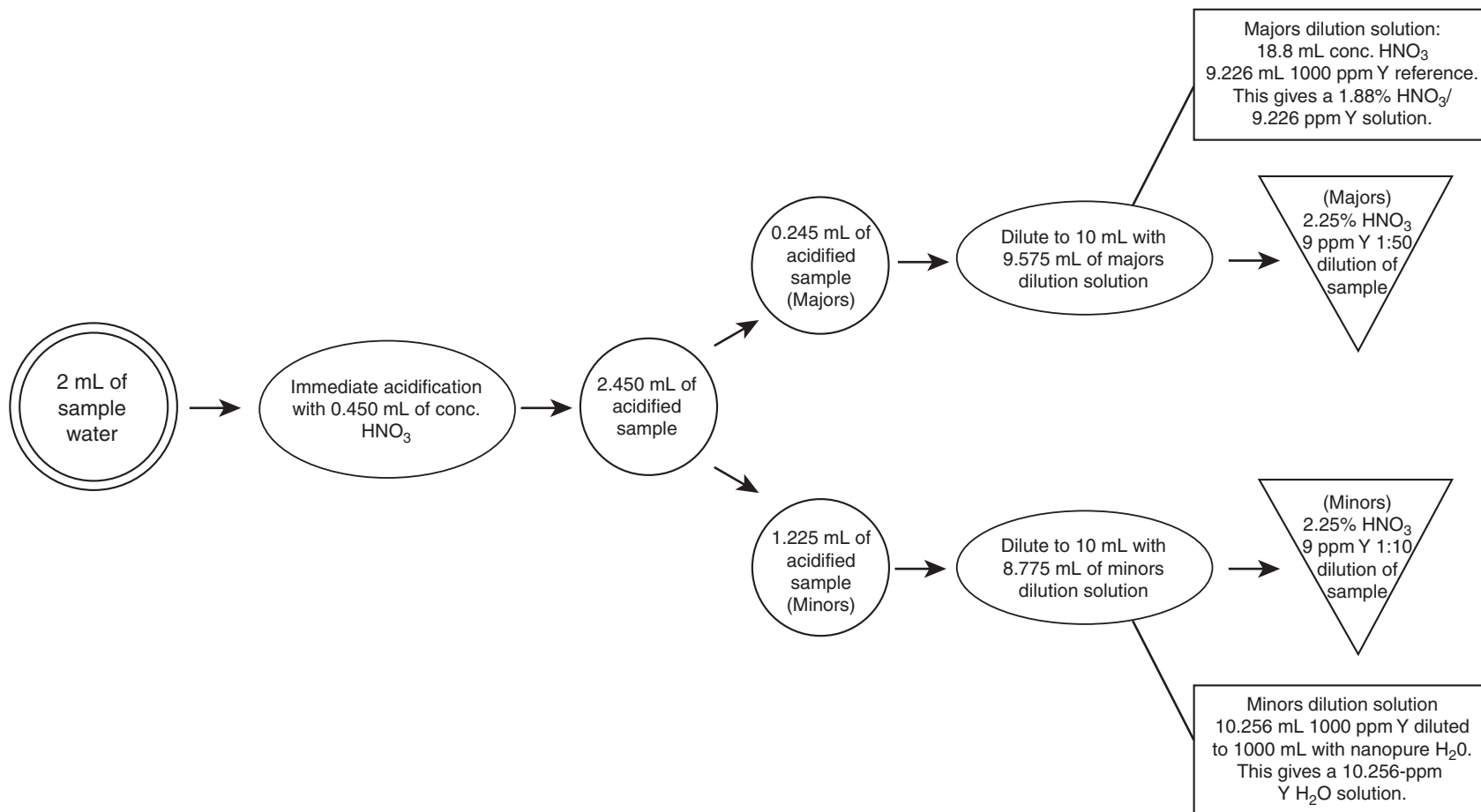
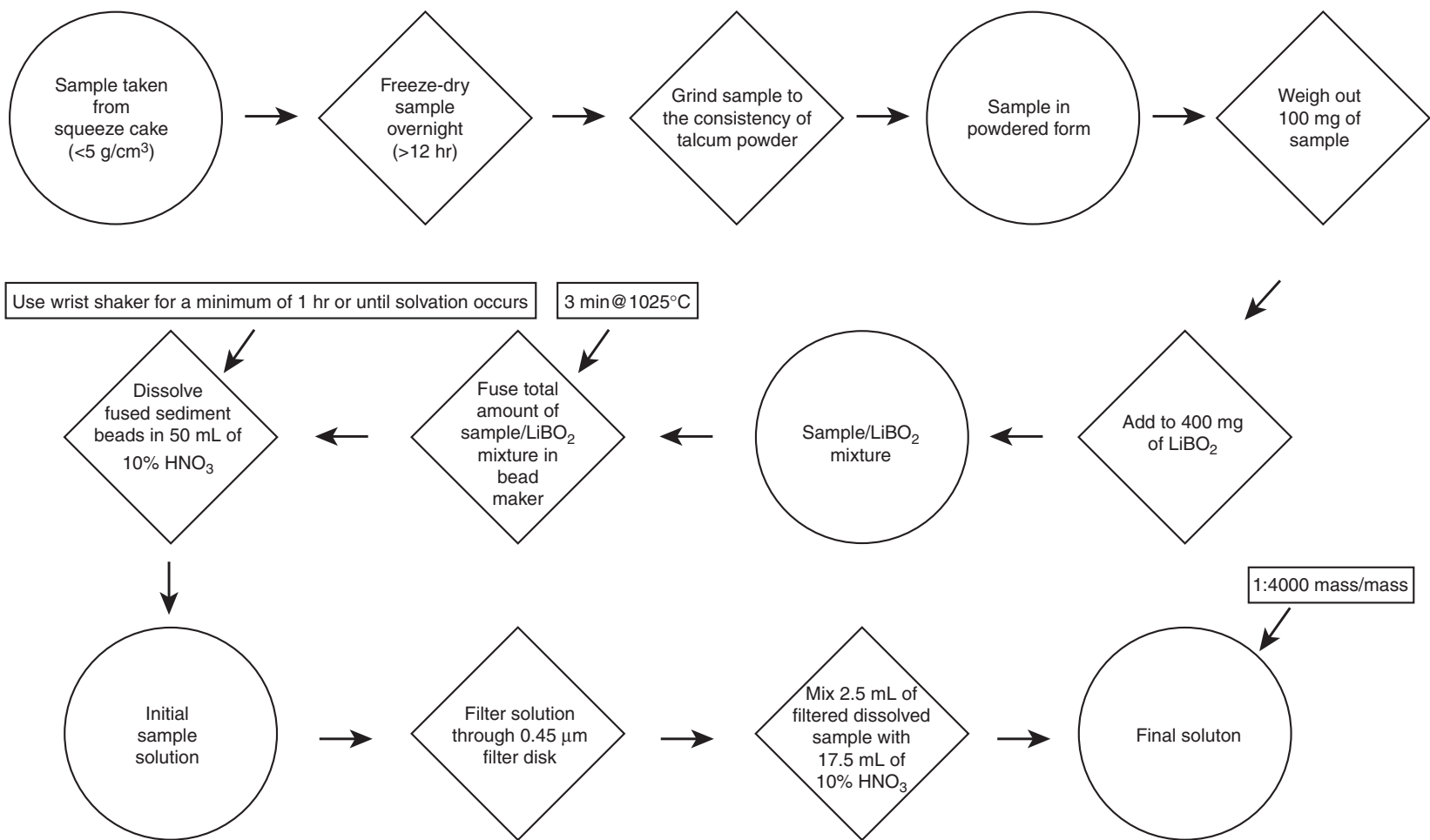


Figure F17. Diagram showing inductively coupled plasma–atomic emission spectroscopy sediment sample preparation procedure for sediment samples.



**Figure F18.** View of the Davis-Villinger Temperature-Pressure Probe tip. The thermistor is located 1 cm from the tip, and the pressure port is protected against invading sediments by the bronze filtering system. This consists of the outer screen lined inside with a 1- $\mu\text{m}$  filter sheet of polyester monofilament. The pressure port itself is protected with a porous polypropylene sheet.

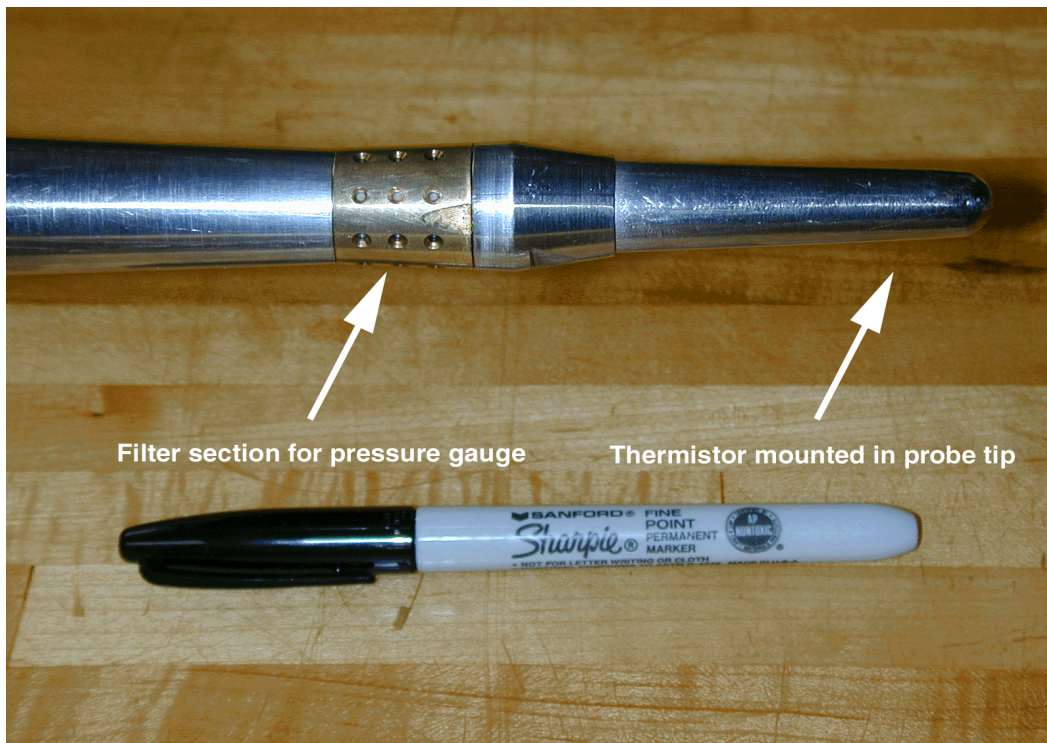
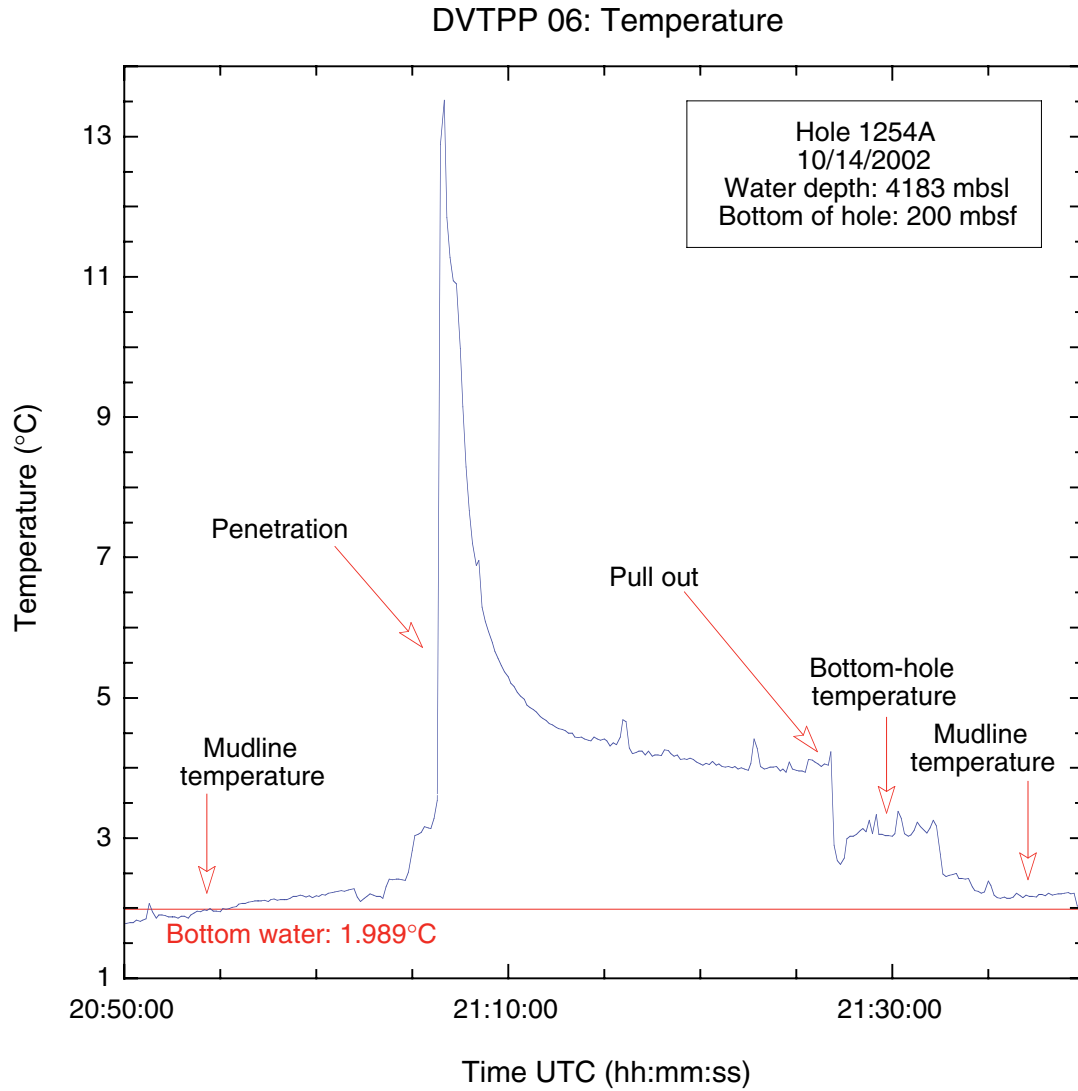


Figure F19. Typical data retrieved from a Davis-Villinger Temperature-Pressure Probe (DVTTP) deployment. The stops at the mudline and at the bottom of the borehole prior to penetration and the penetration in the sediment can be clearly seen in both temperature and pressure. UTC = Universal Time Coordinated.





**Figure F20.** View of a miniaturized temperature data logger. The thermistor is contained in the sensor tip on the left side; the cylindrical main body houses the electronics. The length scale is in centimeters.

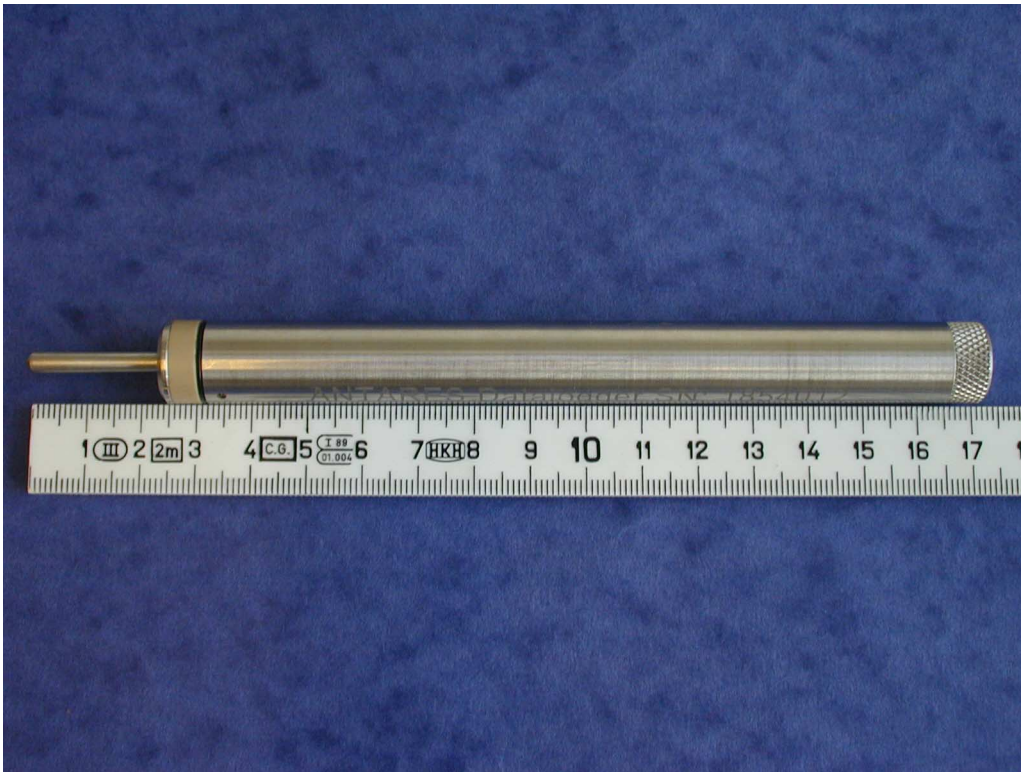
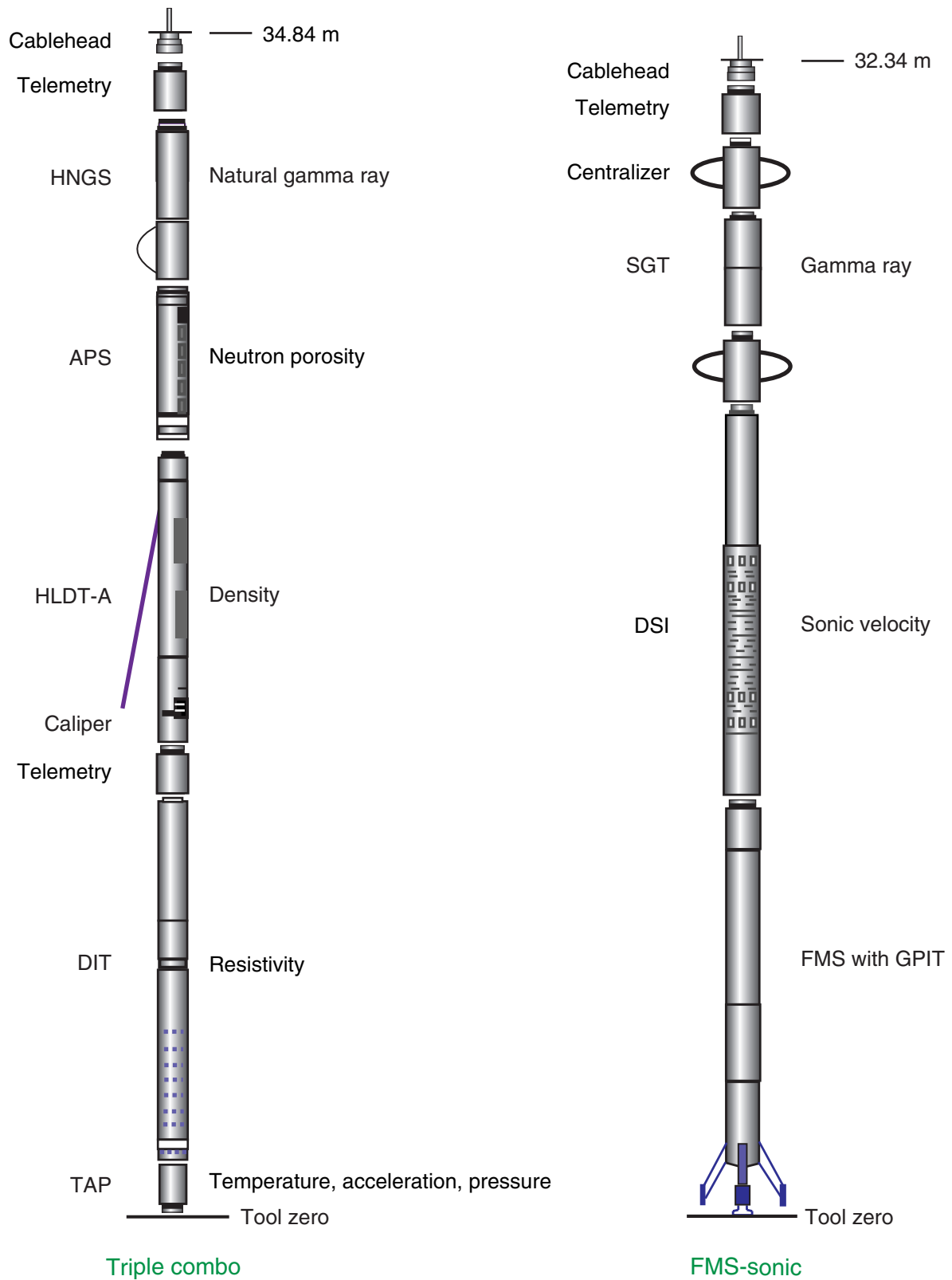


Figure F21. Wireline tool strings used during Leg 205. For tool abbreviations, see Table T7, p. 75.



**Table T1.** Normalization factors for bulk-powder samples, Leg 205.

Indicator mineral	Target mineral			
	Clay	Quartz	Plagioclase	Calcite
Clay	$1.3266639 \times 10^{-2}$	$-2.3594243 \times 10^{-4}$	$-4.3759623 \times 10^{-4}$	$-1.4851297 \times 10^{-3}$
Quartz	$3.8597998 \times 10^{-5}$	$7.9687272 \times 10^{-4}$	$5.2457042 \times 10^{-5}$	$-2.9641451 \times 10^{-6}$
Plagioclase	$2.1619760 \times 10^{-4}$	$-9.6193224 \times 10^{-5}$	$3.4794230 \times 10^{-3}$	$-5.4728327 \times 10^{-5}$
Calcite	$-5.4590277 \times 10^{-5}$	$6.9941205 \times 10^{-5}$	$8.5106571 \times 10^{-5}$	$1.7801351 \times 10^{-3}$

**Table T2.** Measured weight percentages of minerals in standard mineral mixtures and their calculated abundances.

Standard	Measured (wt%)				Calculated from X-ray diffraction (wt%)				Error (measured wt% – calculated wt%)			
	Clay	Quartz	Plagioclase	Calcite	Clay	Quartz	Plagioclase	Calcite	Clay	Quartz	Plagioclase	Calcite
1	78.9	6.9	7.0	7.2	84.76	6.99	4.06	4.19	5.86	0.09	-2.94	-3.01
2	54.7	26.8	8.3	10.2	51.33	27.65	10.06	10.96	-3.37	0.85	1.76	0.76
3	63.4	10.3	12.1	14.2	58.76	9.34	18.17	13.73	-4.64	-0.96	6.07	-0.47
4	49.7	5.6	26.8	18.0	50.95	6.60	21.65	20.80	1.25	1.00	-5.15	2.80
5	38.3	31.1	7.1	23.4	37.17	29.43	7.25	26.15	-1.13	-1.67	0.15	2.75
6	29.6	20.8	15.2	34.5	29.53	19.22	14.92	36.33	-0.07	-1.58	-0.28	1.83
7	19.9	15.3	12.0	52.8	19.59	15.13	10.29	54.99	-0.31	-0.17	-1.71	2.19
8	16.1	5.7	5.0	73.2	17.47	7.00	6.59	68.93	1.37	1.30	1.59	-4.27
9	10.6	49.5	39.9	0.0	11.40	48.96	39.64	0.00	0.80	-0.54	-0.26	0.00
10	15.8	59.1	19.8	5.2	16.61	60.13	18.96	4.30	0.81	1.03	-0.84	-0.90

Note: Calculated values are averages based on analyses of three repetitions per mineral mixture, using average peak areas from X-ray diffraction results and normalization factors determined with matrix singular value decomposition. Standards provided by Mike Underwood.

**Table T3.** Major and trace element concentrations for standards analyzed by ICP-AES. (See table note. Continued on next page.)

Standard	Major element oxide (wt%)										Trace element (ppm)								
	SiO <sub>2</sub>	TiO <sub>2</sub>	Al <sub>2</sub> O <sub>3</sub>	Fe <sub>2</sub> O <sub>3</sub>	K <sub>2</sub> O	MgO	MnO	CaO	Na <sub>2</sub> O	P <sub>2</sub> O <sub>5</sub>	Cr	Ni	Ba	Sr	V	Y	Zr	Sc	
BIR-1	44.91	0.97	14.68	11.52	0.04	9.46	0.17	13.08	1.75		364.73			105.51	318.05	15.45	18.04	39.13	
	46.68	0.92	14.92	11.11	0.04	9.58	0.17	13.05	1.74		378.00			108.37	315.08	15.41	21.91	40.60	
	46.75	0.97	16.58	11.14	0.01	9.51	0.17	12.67	1.85		380.60			107.53	319.88	15.73	21.03	42.97	
	46.76	0.96	16.28	11.48	0.01	9.53	0.17	12.68	1.78		346.58			106.13	322.19	15.62	15.24	36.76	
	46.80	1.01	15.07	11.65	0.03	9.50	0.17	14.09	1.78	0.04	372.24	175.07		105.10	314.40	16.29	20.63	43.11	
	45.98	0.84	14.58	11.19	0.03	9.48	0.17	13.88	1.75	0.02	372.66	163.98		104.11	313.57	15.82	16.32	40.83	
	Average:	46.31	0.95	15.35	11.35	0.03	9.51	0.17	13.24	1.77	0.03	369.14	169.53		106.12	317.20	15.72	18.86	40.57
	Certified concentration:	47.96	0.96	15.50	11.30	0.03	9.70	0.18	13.30	1.82	0.02	370.00	170.00	0.33	110.00	310.00	16.00	18.00	44.00
Standard deviation:	0.754	0.058	0.860	0.230	0.012	0.041	0.001	0.606	0.042	0.014	12.330	7.841		1.583	3.414	0.320	2.733	2.405	
Precision (%):	1.63	6.15	5.60	2.03	49.33	0.43	0.62	4.58	2.37	55.19	3.34	4.63		1.49	1.08	2.04	14.49	5.93	
Accuracy (%):	-3.43	-1.56	-0.95	0.43	-16.05	-1.98	-2.46	-0.45	-2.51	23.03	-0.23	-0.28		-3.52	2.32	-1.75	4.77	-7.8	
BHVO-2	48.86	2.79	13.66	12.48	0.53	7.23	0.17	11.43	2.22	0.29	277.27	120.81	116.14	387.86	321.82	26.99	170.07	30.01	
	49.84	2.72	13.49	12.09	0.51	7.30	0.17	11.53	2.16	0.25	279.43		126.77	386.12	316.01	26.61	167.47	32.17	
	49.54	2.76	15.05	12.31	0.54	7.47	0.17	11.41	2.38	0.28	285.35	138.64	127.31	384.11	329.54	25.61	178.27	32.82	
	50.50	2.79	14.89	12.59	0.52	7.47	0.17	11.36	2.29	0.37	288.59		129.39	384.37	334.54	26.88	175.27	31.52	
	49.30	2.80	13.55	12.28	0.51	7.14	0.17	12.64	2.26	0.31	268.69	118.65	121.41	389.07	318.68	26.29	171.64	33.55	
	48.91	2.60	13.26	12.01	0.51	7.14	0.17	12.24	2.18	0.20	284.70	119.45	121.79	388.52	315.10	25.14	169.30	31.64	
	Average:	49.49	2.74	13.98	12.29	0.52	7.29	0.17	11.77	2.25	0.28	280.67	124.39	123.80	386.67	322.61	26.25	172.00	31.95
	Certified concentration:	49.90	2.73	13.50	12.30	0.52	7.23	0.17	11.40	2.22	0.27	280.00	119.00	130.00	389.00	317.00	26.00	172.00	32.00
Standard deviation:	0.619	0.078	0.776	0.220	0.012	0.151	0.001	0.539	0.079	0.058	7.175	9.545	4.916	2.133	7.828	0.738	4.041	1.216	
Precision (%):	1.25	2.86	5.55	1.79	2.29	2.07	0.36	4.58	3.53	20.31	2.56	7.67	3.97	0.55	2.43	2.81	2.35	3.80	
Accuracy (%):	-0.82	0.54	3.57	-0.05	-0.55	0.86	2.73	3.22	1.28	4.94	0.24	4.53	-4.77	-0.6	1.77	0.97	0.00	-0.16	
JBG-1	43.72	1.60	17.74	14.39	0.24	8.17	0.18	12.12	1.29	0.08	59.82	27.16	56.19	327.25	647.70	10.98	33.24	35.25	
	44.77	1.69	17.68	14.98	0.23	7.94	0.18	12.14	1.28		52.03	18.61	60.25	330.42	642.78	10.78	30.84	35.66	
	44.16	1.67	19.24	15.40	0.25	8.49	0.19	11.92	1.33	0.10	66.21	27.92	57.80	331.08	656.33	12.14	35.53	36.32	
	44.36	1.65	18.90	14.13	0.23	8.19	0.18	11.73	1.27		52.28		54.31	320.55	658.48	10.32	28.84	33.04	
	44.11	1.60	16.82	14.66	0.24	8.00	0.18	12.75	1.28	0.02	55.54	26.81	52.39	325.72	627.52	10.58	33.81	35.12	
	44.56	1.45	17.54	14.99	0.24	8.27	0.19	13.01	1.28	0.06	57.30	26.81	69.31	331.98	642.82	10.66	35.35	33.56	
	Average:	44.28	1.61	17.99	14.76	0.24	8.18	0.18	12.28	1.29	0.07	57.20	25.46	58.37	327.83	645.94	10.91	32.94	34.82
	Certified concentration:	43.40	1.62	17.66	15.16	0.24	7.83	0.17	11.98	1.23	0.05	59.30	25.40	63.00	321.00	640.00	10.75	33.50	35.00
Standard deviation:	0.368	0.086	0.906	0.460	0.007	0.197	0.004	0.496	0.020	0.034	5.325	3.856	6.007	4.297	11.201	0.641	2.632	1.261	
Precision (%):	0.83	5.35	5.04	3.11	3.09	2.41	1.90	4.04	1.58	51.49	9.31	15.14	10.29	1.31	1.73	5.88	7.99	3.62	
Accuracy (%):	2.02	-0.7	1.84	-2.64	-0.12	4.43	8.70	2.50	4.84	30.82	-3.55	0.25	-7.34	2.13	0.93	1.49	-1.69	-0.5	
JB-2	52.89	1.20	14.55	14.28	0.42	4.64	0.20	9.94	2.05		27.80	18.36	216.77	180.82	574.51	24.51	53.64	53.03	
	53.53	1.23	15.00	14.37	0.42	4.54	0.20	10.06	2.06	0.08	25.70	18.06	227.95	181.96	572.42	25.86	49.03	54.48	
	53.62	1.21	16.24	14.12	0.45	4.89	0.20	10.29	2.19	0.12	29.65	22.25	233.18	183.63	596.12	25.87	53.71	54.23	
	53.22	1.19	16.22	13.80	0.43	4.59	0.20	9.98	2.12		22.99	23.87	219.46	178.60	566.44	23.14	51.69	45.33	
	54.63	1.29	15.07	14.69	0.45	4.83	0.20	11.41	2.19	0.09	31.10	15.39	224.95	191.07	594.06	25.63	49.87	55.41	
	52.63	1.37	14.85	14.46	0.42	4.74	0.20	11.02	2.04	0.13	28.49	20.72	219.44	182.39	574.49	25.23	50.10	52.60	
	Average:	53.42	1.25	15.32	14.29	0.43	4.70	0.20	10.45	2.11	0.10	27.62	19.78	223.63	183.08	579.67	25.04	51.34	52.51
	Certified concentration:	53.20	1.19	14.67	14.24	0.42	4.66	0.20	9.89	2.03	0.10	27.40	14.20	208.00	178.00	578.00	24.90	51.40	54.00
Standard deviation:	0.700	0.070	0.727	0.305	0.015	0.137	0.003	0.619	0.068	0.024	2.904	3.098	6.224	4.268	12.317	1.061	2.004	3.664	
Precision (%):	1.31	5.63	4.75	2.14	3.57	2.92	1.39	5.92	3.25	23.15	10.51	15.66	2.78	2.33	2.12	4.24	3.90	6.98	
Accuracy (%):	0.41	4.88	4.45	0.33	2.51	0.94	-0.12	5.66	3.80	3.78	0.80	39.27	7.51	2.85	0.29	0.55	-0.12	-2.75	

Table T3 (continued).

Standard	Major element oxide (wt%)										Trace element (ppm)							
	SiO <sub>2</sub>	TiO <sub>2</sub>	Al <sub>2</sub> O <sub>3</sub>	Fe <sub>2</sub> O <sub>3</sub>	K <sub>2</sub> O	MgO	MnO	CaO	Na <sub>2</sub> O	P <sub>2</sub> O <sub>5</sub>	Cr	Ni	Ba	Sr	V	Y	Zr	Sc
BCR-2	54.92	2.23	13.84	14.47	1.81	3.61	0.19	7.07	3.20	0.36	22.85	17.99	692.20	339.72	422.61	37.69	194.20	33.64
	53.95	2.17	13.37	12.38	1.77	3.55	0.19	6.98	3.16	0.33	21.77	18.53	667.63	339.98	391.02	35.02	187.38	33.76
	51.73	2.20	14.04	12.40	1.80	3.50	0.17	7.15	3.16	0.38	18.80	22.57	694.46	317.16	404.34	31.64	183.55	33.57
	50.40	2.13	13.89	12.75	1.77	3.40	0.18	6.93	3.00	0.21	18.36	26.04	660.00	311.36	386.93	34.58	182.68	33.52
	54.13	2.22	13.94	13.86	1.84	3.53	0.19	8.34	3.27	0.33	19.62	13.80	696.54	344.05	425.25	36.68	193.38	34.81
	52.10	2.34	13.24	13.27	1.73	3.40	0.18	8.06	3.06	0.36	19.06	16.51	662.45	325.99	396.12	33.41	185.39	32.20
Average:	52.87	2.21	13.72	13.19	1.79	3.50	0.18	7.42	3.14	0.33	20.08	19.24	678.88	329.71	404.38	34.84	187.76	33.59
Certified concentration:	54.10	2.26	13.50	13.80	1.79	3.59	0.24	7.12	3.16	0.35	18.00	20.00	683.00	346.00	416.00	37.00	188.00	33.00
Standard deviation:	1.730	0.071	0.330	0.844	0.039	0.085	0.007	0.612	0.098	0.064	1.809	4.392	17.232	13.558	16.243	2.187	4.947	0.832
Precision (%):	3.27	3.20	2.40	6.40	2.18	2.44	4.07	8.25	3.10	19.44	9.01	22.83	2.54	4.11	4.02	6.28	2.63	2.48
Accuracy (%):	-2.27	-2.05	1.63	-4.44	-0.14	-2.53	-23.69	4.24	-0.53	-5.98	11.53	-3.8	-0.6	-4.71	-2.79	-5.85	-0.13	1.77

Note: BIR-1 = United States Geological Survey Icelandic (Reykjannes) basalt, BHVO-2 = Basalt Hawaiian Volcano Observatory, JBG-1 = Geological Survey of Japan gabbro, JB-2 = Geological Survey of Japan basalt, BCR-2 = United States Geological Survey Columbia River basalt. Bold entries = average.

**Table T4.** Gabbro sample preparation procedure for fluorescence in situ hybridization analysis, Leg 205.

Solution	Components	Concentration	Comments
10× PBS solution	NaCl	40.0 g	Fill to 1000 mL with deionized water Adjust pH to 7.3 Autoclave
	KCl	1.0 g	
	KH <sub>2</sub> PO <sub>4</sub>	1.0 g	
	Na <sub>2</sub> HPO <sub>4</sub> ·2H <sub>2</sub> O	5.75 g	
4% Formaldehyde/ PBS buffer	Deionized H <sub>2</sub> O	90 mL	Heat to 60°C in fume cupboard
	2-M NaOH	2 drops	
	Paraformaldehyde	4 g	Stir 2 min
	10× PBS solution	10 mL	Cool on ice; adjust to pH 7.3 Filter through 0.45-µm filter

Notes: This solution must be prepared fresh or kept frozen. PBS = phosphate buffered saline.

**Table T5.** Media used for cultivation of microorganisms. (Continued on next page.)

Media	Component	Mass/Volume/ Concentration	Comments
Artificial seawater recipe (ASW)	Distilled water	1 L	
	NaCl	27.5 g	
	MgCl <sub>2</sub> ·6H <sub>2</sub> O	12.16 g	
	KCl	0.72 g	
	NaHCO <sub>3</sub>	0.2 g	
	Tris-HCl	3.2 g	
	CaCl <sub>2</sub> ·2H <sub>2</sub> O	1.4 g	
	NH <sub>4</sub> Cl	0.05 g	
	K <sub>2</sub> HPO <sub>4</sub> ·3H <sub>2</sub> O	0.05 g	
	Trace elements solution	1 mL	Adjust to pH 7.3; autoclave
Trace vitamins	1 mL		
Trace elements solution	Distilled water	1 L	
	Calcium pantothenate	10 mg	
	Niacin	10 mg	
	P-aminobenzoic acid	10 mg	
	Thiamine	10 mg	
	Riboflavin	10 mg	
	Pyridoxine	10 mg	
	Cobalamin	10 mg	
	Thioctic (a-lipoic acid)	10 mg	
	Folic acid	10 mg	
Biotin	10 mg	Filter sterilize; store in darkness at 4°C	
Trace vitamins solution	Distilled water	1 L	
	Nitritotriacetic acid	1.5 g	
	MgSO <sub>4</sub>	3 g	
	MnSO <sub>4</sub>	0.5 g	
	NaCl	1 g	
	FeSO <sub>4</sub>	0.1 g	
	CaCl <sub>2</sub>	0.1 g	
	CoCl <sub>2</sub>	0.1 g	
	ZnSO <sub>4</sub>	0.1 g	
	CuSO <sub>4</sub>	0.01 g	
	AlK(SO <sub>4</sub> ) <sub>2</sub>	0.01 g	
	H <sub>3</sub> BO <sub>3</sub>	0.01 g	
	NaMoO <sub>4</sub>	0.01 g	
Autotrophic sulfur oxidizing bacteria media (ASOB)	ASW		
	Na <sub>2</sub> S <sub>2</sub> O <sub>3</sub>	10 mM	
	Sodium sulfide	100 µM	Purge with N <sub>2</sub> mix prior to inoculating
Heterotrophic sulfur oxidizing bacteria media (HSOB)	ASOB		
	Dextrose	10 mM	
Autotrophic sulfate reducing bacteria media (ASRB)	ASW		
	Na <sub>2</sub> SO <sub>4</sub>	60 mM	
	Sodium sulfide	500 µM	Purge with N <sub>2</sub> mix prior to inoculating
Heterotrophic sulfate reducing bacteria media (HSRB)	ASRB		
	Lactate	10 mM	
	Acetate	10 mM	
Autotrophic methanogen media (ameth)	ASW		
	Autoclave		
	Sodium molybdate	5 mM	(filter sterilized solution)
	Sodium sulfide	100 µM	Purge with N <sub>2</sub> mix prior to inoculating
Heterotrophic methanogen media (hmeth)	Ameth		
	Methanol	10 mM	
Autotrophic iron(III) reducing bacteria media (AfeRB)	ASW		Autoclave
	Poorly crystalline iron oxides		Purge with N <sub>2</sub> mix prior to inoculating
Heterotrophic iron(III) reducing bacteria media (HfeRB)	AfeRB		
	Lactate	10 mM	
	Acetate	10 mM	
FeS gradient tubes for iron oxidizing bacteria Top layer:	ASW		Prepare FeS after Hanert, 1992
	Low melting agarose	0.15%	
	Sodium bicarbonate	5 mM	
	Trace elements solution	1 mL/L	Autoclave
	Trace vitamin solution	1 mL/L	



**Table T5 (continued).**

Media	Component	Mass/Volume/ Concentration	Comments
Bottom layer:	1:1 of FeS:ASW 1% high melting agarose		Autoclave After autoclaving, aliquot 0.75 mL of bottom layer while still hot into each gradient tube. Allow ~30 min to solidify. Aliquot 3.75 mL of the top solution and allow 3–4 hr to solidify before inoculating.
FeCO <sub>3</sub> gradient tubes for iron oxidizing bacteria			FeCO <sub>3</sub> stock solution was made in advance. Add 0.1-M FeCl <sub>2</sub> ·7H <sub>2</sub> O to 100 mL of sterile deionized water which had been boiled to remove O <sub>2</sub> . Subsequently, 0.1-M NaCO <sub>3</sub> was added to the FeCl <sub>2</sub> solution, the bottle was capped, and the headspace purged with nitrogen.
Top layer:	ASW Low melting agarose Sodium bicarbonate Trace vitamin solution	0.15% 5 mM 1 mL/L	Autoclave Bubble with filter-sterilized CO <sub>2</sub>
Bottom layer:	ASW High melting agarose Trace vitamins FeCO <sub>3</sub> stock solution	1% 1 mL/L 40 mL/L	Autoclave After autoclaving, aliquot 0.75 mL of bottom layer while still hot into each gradient tube but make sure to keep it anoxic. Let solidify on ice. Aliquot 3.75 mL of top solution and bubble with filter-sterilized CO <sub>2</sub> . Let solidify while capped.

**Table T6.** Procedure for DNA extractions from gabbro samples, Leg 205.

Reagent	Preparation	Storage
2× buffer A with EDTA	NaCl 200 mM Tris 200 mM Na Citrate 2 mM CaCl <sub>2</sub> 10 mM EDTA 50 mM Titrate to pH 8.0 with HCl, autoclave.	4°C
Poly A (10 mg/mL)	Make in 1.5-mL tubes with autoclaved water	-20°C
Pyrophosphate (10%)	10% sodium pyrophosphate, filter sterilize	Room temperature
Lysozyme (100 mg/mL)	Make in 1.5-mL tubes with autoclaved water	Make fresh
SDS 20%	Make with autoclaved water	Room temperature
Proteinase K (20 mg/mL)	Make in 1.5-mL tubes with autoclaved water	Fresh or -20°C
Phenol:chloroform: isoamyl-alcohol (24:24:1)	Saturate with pH 8.0 Tris	4°C
100% ethanol		Room temperature
3-M Na acetate	Titrate to pH 5.2 with acetic acid, autoclave	4°C
70% ethanol	Make with autoclaved water	4°C
TE buffer	10-mM Tris Cl, 1-mM EDTA; pH 8.0	

**Method**

**Lysis:**

- 1) Thaw the sample enough to remove a 0.5- to 1.0-g aliquot of sample (1 mL of liquid sample) into 1.5-mL tubes. Keep the tubes on ice. If it is a liquid sample, you may want to wash the sample initially, especially if it is something like AMD (i.e., pellet cells at 12,000 g for 5 min at 4°C), and then decant supernatant. Resuspend cells in 2× buffer A then pellet cells again and decant supernatant.
- 2) Add 500 µL of 2× buffer A, 20 µL of poly A, 20 µL of 10% pyrophosphate, and 30 µL of lysozyme in that order (~5 mg/mL concentration lysozyme). Mix by gentle inversion. Incubate for 40 min at 37°C. Poly A and pyrophosphate will coat surfaces to prevent sorption of nucleic acids.
- 3) Add 10 µL of 20% SDS and 60 µL of proteinase K. (Only 0.3% of the final concentration of SDS is added at this step to prevent inhibition of proteinase K; the approximate proteinase K concentration = 2 mg/mL.) Mix by gentle inversion. Incubate for 30 min at 50°C.
- 4) Add 200 µL of 20% SDS (~5% concentration) and conduct three cycles of freeze-thaw by placing tubes in a dry-ice ethanol bath for 3 min at -70°C, then in a 65°C water bath for 5 min.

**Extraction and precipitation:**

- 5) Add 1 volume (~700 µL) of phenol:CHCl<sub>3</sub>:IAA (24:24:1) and vortex to mix. Then spin at ~12,000 g at 4°C for 3 min to deposit sample debris. Pipette the aqueous supernatant (~600 µL of liquid) into a fresh 1.5-mL tube.
- 6) Extract samples with 1 volume phenol:CHCl<sub>3</sub>:IAA (24:24:1). Mix by inversion and spin at ~12,000 g for 2 min at room temperature. Remove aqueous upper layer and put in new tube.
- 7) Precipitate nucleic acids by adding an equal volume (~500 µL) of ethanol and 0.1 volume (~50 µL) 3-M Na acetate, pH 5.2. Put on ice for 20 min to overnight then spin at ~12,000 g for 20 min at 4°C.
- 8) Decant supernatant; the pellet should be visible and colored, depending on the sample. Rinse pellets with 500 µL of cold 70% ethanol. Invert tubes on KimWipes and air-dry for ~30 min. Resuspend pellets in 2–30 µL of TE.

**Purification:**

- 9) Combine the DNA from 2 to 4 extracts. Purify the DNA through Clonotech Chroma Spin+TE100 columns. These can take ~70–200 µL and up to 100 ng of DNA.
- 10) Load 5 µL of purified DNA with 2 µL of GLD onto 1% agarose gel. Also, load into separate wells: MWmarker III (4 µL) and 50 ng and 100 ng of Lamda DNA. Run gel at 70 V for 30–60 min.
- 11) Observe bands of chromosomal DNA in the samples; these should run with or slightly above the 21-kbp band of the marker. Estimate DNA concentration in sample extracts. If necessary, DNA can be concentrated by precipitation (see steps 7 and 8 above).
- 12) If further purification is required, it can be done by gel purification.

Notes: DNA = deoxyribonucleic acid. EDTA = ethylenediamine tetraacetic acid. SDS = sodium dodecyl sulfate. TE = Tris EDTA. AMD = Acid Mine Drainage. IAA = isoamyl alcohol. GLD = gel loading dye.

**Table T7.** Acronyms and units used for wireline logging tools.

Tool	Output	Tool name/explanation of output	Unit
APS		Accelerator Porosity Sonde	
	APLC	Near array porosity (limestone calibrated)	%
	SIGF	Formation capture cross section ( $\Sigma_f$ )	Capture units
	STOF	Tool standoff (computed distance from borehole wall)	in
DIT		Dual Induction Tool	
	IDPH	Deep induction resistivity	$\Omega\text{m}$
	IMPH	Medium induction resistivity	$\Omega\text{m}$
	SFLU	Spherically focused resistivity	$\Omega\text{m}$
DSI		Dipole Sonic Imager	
	DTCO	Compressional wave delay time ( $\Delta t$ )	ms/ft
	DTSM	Shear wave delay time ( $\Delta t$ )	ms/ft
	DTST	Stoneley wave delay time ( $\Delta t$ )	ms/ft
FMS		Formation MicroScanner	
	C1, C2	Orthogonal hole diameters	in
	P1AZ	Pad 1 azimuth	Degrees
		Spatially oriented resistivity images of borehole wall	
GPIT		General Purpose Inclinator Tool	
	DEVI	Hole deviation	Degrees
	HAZI	Hole azimuth	Degrees
	$F_x, F_y, F_z$	Earth's magnetic field (three orthogonal components)	Degrees
	$A_x, A_y, A_z$	Acceleration (three orthogonal components)	$\text{m/s}^2$
HLDT		Hostile Environment Litho-Density Tool	
	RHOM	Bulk density	$\text{g/cm}^3$
	PEFL	Photoelectric effect	b/e-
	LCAL	Caliper (measure of borehole diameter)	in
	DRH	Bulk density correction	$\text{g/cm}^3$
HNCS		Hostile Environment Gamma Ray Sonde	
	HSGR	Standard (total) gamma ray	gAPI
	HCGR	Computed gamma ray (HSGR minus uranium contribution)	gAPI
	HFK	Potassium	wt%
	HTHO	Thorium	ppm
	HURA	Uranium	ppm
SGT		Scintillation Gamma Ray Tool	
	SGR	Standard total gamma ray	gAPI
	CGR	Computed gamma ray (SGR minus uranium contribution)	gAPI
	POTA	Potassium	wt%
	THOR	Thorium	ppm
	URAN	Uranium	ppm
TAP		Temperature/Acceleration/Pressure tool	$^{\circ}\text{C}$ , $\text{m/s}^2$ , psi

Table T8. Measurements made by wireline tool strings.

Tool string	Tool	Measurement	Sampling interval (cm)	Approximate vertical resolution (cm)
Triple combination	HNGS	Spectral gamma ray	15	51
	APS	Porosity	5 and 15	43
	HLDS/HLDT	Bulk density	2.5 and 15	38/46
	DIT/DLL	Resistivity	15	200/150/76, 61 (DLL)
	TAP	Temperature	1 per s	NA
		Tool acceleration	4 per s	NA
		Pressure	1 per s	NA
Formation MicroScanner (FMS)-sonic combination	FMS	Microresistivity	0.25	0.5
	SGT	Total gamma ray	15	46
	GPIT	Tool orientation	0.25 and 15	NA
	DSI/SDT/LSS/BHC	Acoustic velocity	15	107/120/61/61

Notes: All tool and tool string names (except the TAP tool) are trademarks of Schlumberger. For additional information about tool physics and use consult ODP Logging Services at [www.ideo.columbia.edu/BRG/ODP](http://www.ideo.columbia.edu/BRG/ODP). See Table T7, p. 75, for explanations of acronyms used to describe tool strings and tools. NA = not applicable.